DIRECT USE OF PGV FOR ESTIMATING PEAK NONLINEAR OSCILLATOR DISPLACEMENTS

A THESIS SUBMITTED TO
THE GRADUATE SCHOOL OF NATURAL AND APPLIED SCIENCES
OF
MIDDLE EAST TECHNICAL UNIVERSITY

BY

BİLGE KÜÇÜKDOĞAN

IN PARTIAL FULFILLMENT OF THE REQUIREMENTS
FOR
THE DEGREE OF MASTER OF SCIENCE
IN
CIVIL ENGINEERING

NOVEMBER 2007

Approval of the Thesis;

DIRECT USE OF PGV FOR ESTIMATING PEAK NONLINEAR OSCILLATOR DISPLACEMENTS

Submitted by **BİLGE KÜÇÜKDOĞAN** in partial fulfillment of the requirements for the degree of **Master of Science in Civil Engineering, Middle East Technical University** by,

Prof. Dr. Canan Özgen
Dean, Graduate School of **Natural and Applied Sciences** _____

Prof. Dr. Güney Özcebe
Head of Department, **Dept. of Civil Engineering** _____

Assoc. Prof. Dr. Sinan Dede Akkar
Supervisor, **Dept. of Civil Engineering, METU** _____

Examining Committee Members:

Prof. Dr. Polat Gülkan (*)
Civil Engineering Dept., METU _____

Assoc. Prof. Dr. Sinan Dede Akkar (**)
Civil Engineering Dept., METU _____

Prof. Dr. Haluk Sucuoğlu
Civil Engineering Dept., METU _____

Assoc. Prof. Dr. Ahmet Yakut
Civil Engineering Dept., METU _____

Assist. Prof. Dr. Tolga Yılmaz
Engineering Sciene Dept., METU _____

Date: _____

(*) Head of Examining Committee

(**) Supervisor

I hereby declare that all information in this document has been obtained and presented in accordance with academic rules and ethical conduct. I also declare that, as required by these rules and conduct, I have fully cited and referenced all material and results that are not original to this work.

Name, Last name : Bilge Küçükdoğan

Signature :

ABSTRACT

DIRECT USE OF PGV FOR ESTIMATING PEAK NONLINEAR OSCILLATOR DISPLACEMENTS

KÜÇÜKDOĞAN, Bilge

M.S., Department of Civil Engineering

Supervisor: Assoc. Prof. Dr. Sinan AKKAR

Co-supervisor : Prof. Dr. M. Semih YÜCEMEN

November 2007, 129 pages

Recently established approximate methods for estimating the lateral deformation demands on structures are based on the prediction of nonlinear oscillator displacements ($S_{d,ie}$). In this study, a predictive model is proposed to estimate the inelastic spectral displacement as a function of peak ground velocity (*PGV*). Prior to the generation of the proposed model, nonlinear response history analysis is conducted on several building models of wide fundamental period range and hysteretic behavior to observe the performance of selected demands and the chosen ground-motion intensity measures (peak ground acceleration, *PGA*, peak ground velocity, *PGV* and elastic pseudo spectral acceleration at the fundamental period ($PS_a(T_1)$). Confined to

the building models used and ground motion dataset, the correlation studies revealed the superiority of *PGV* with respect to the other intensity measures while identifying the variation in global deformation demands of structural systems (i.e., maximum roof and maximum interstory drift ratio). This rational is the deriving force for proposing the *PGV* based prediction model. The proposed model accounts for the variation of $S_{d,ie}$ for bilinear hysteretic behavior under constant ductility (μ) and normalized strength ratio (R) associated with postyield stiffness ratios of α= 0% and α= 5%. Confined to the limitations imposed by the ground-motion database, the predictive model can estimate $S_{d,ie}$ by employing the *PGV* predictions obtained from the attenuation relationships. This way the influence of important seismological parameters can be incorporated to the variation of $S_{d,ie}$ in a fairly rationale manner. Various case studies are presented to show the consistent estimations of $S_{d,ie}$ by the proposed model using the *PGV* values obtained from recent ground motion prediction equations.

Keywords: Peak ground velocity; Inelastic spectral displacement; Ground-motion predictive models; Regression; Seismic design/ performance assessment

ÖZ

DOĞRUSAL OLMAYAN MAKSİMUM TEK DERECELİ SİSTEM DEPLASMANI TAHMİNİNDE MAKSİMUM YER HAREKETİ HIZININ KULLANILMASI

KÜÇÜKDOĞAN, Bilge
Yüksek Lisans, İnşaat Mühendisliği Bölümü
Tez Yöneticisi : Doç. Dr. Sinan AKKAR
Yardımcı Tez Yöneticisi : Prof. Dr. M. Semih YÜCEMEN

Kasım 2007, 129 sayfa

Bina sistemleri için yanal deformasyon taleplerini yaklaşık olarak tahmin eden metodların pek çoğu doğrusal olmayan tek dereceli sistem (osilatör) maksimum deplasmanlarını ($S_{d,ie}$) temel almaktadır. Bu çalışmada, doğrusal olmayan spektral deplasmanları maksimum yer hareketi hızının (*MYH*) bir fonksiyonu olarak hesaplayan bir model önerilmiştir. Modelin önerilmesinden önce, seçilen yer hareketi şiddet parametrelerinin (maksimum yer ivmesi (*MYİ*), maksimum yer hareketi hızı (*MYH*) ve temel periyottaki elastik spektral ivme ($PS_a(T_1)$) ile global deformasyon talepleri arasındaki ilişkiyi gözlemlemek üzere, geniş bir bantta değişim gösteren temel periyot ve histeretik davranım özelliklerine sahip bir grup çok serbestlik dereceli model elastik olmayan zaman mukabele hesaplarına tabii tutulmuştur. Global deformasyon

talepleri ile (maksimum kat arası ötelemesi ve maksimum deformasyon) yer hareketi şiddet parametreleri arasında yapılan korelasyon çalışmaları sonucunda *MYH* parametresinin diğer yer hareketi parametrelerine nazaran bina global deformasyon taleplerin ile daha uyumlu olduğu görülmüş ve önerilen model bu rasyonel ışığında geliştirilmiştir. Önerilen model, ve sabit süneklik (μ) ve normalize edilmiş mukavemet oranları (R) için doğrusal olmayan spektral deplasman değişimlerini akma sonrası yanal rijitlik oranı (α) α= %0 ve α= %5 çift doğrulu histeretik model için gösterebilmektedir. Seçilen yer hareketi veritabanının özelliklerine bağlı olarak, $S_{d,ie}$ değerlerini yer hareketi *MYH* değerlerine bağlı kalarak hesaplayabilmektedir. Böylelikle, model önemli sismolojik parametrelerin $S_{d,ie}$ üzerindeki etkisini de yansıtabilmektedir. Modelin yakın zamanlarda geliştirilen yer hareketi tahmin denklemlerinden elde edilmiş *MYH* değerleri kullanılarak $S_{d,ie}$ için tutarlı tahminler yaptığı çeşitli örneklerle gösterilmiştir.

Anahtar Kelimeler : Maksimum yer hareketi hızı; Elastik olmayan spektral deplasman; Yer hareketi tahmin modelleri; Regresyon; Sismik tasarım/performans değerlendirmesi

To,

Doç.Dr. Sinan D. AKKAR

ACKNOWLEDGEMENT

"Do something everyday that you don't want to do; this is the golden rule for acquiring the habit of doing your duty without pain."

Mark Twain

"Was ihn nicht umbringt, macht ihn stärker."

Friedrich Wilhelm Nietzsche

This study is particulary helpful to clearly define my interests and desires and a milestone only during which I was able to decide on the subject and the career that I want to pursue for the future. It is a pleasure to thank the many people who made this thesis possible.

It is difficult to overstate my gratitude to my supervisor, Assoc.Prof. Dr. Sinan Akkar, to whom I dedicated this study. Mr. Akkar, in every single stage of the work, has also been abundantly helpful, and has assisted me in numerous ways, including providing me the necessary articles and program codes to proceed the analyses, introducing patiently new softwares with a great effort to explain things clearly and simply.

This work would not have been possible without the support and encouragement of Erhan Karaesmen and Engin Karaesmen who have always been near me opening new perspectives in my mind and believing in me. Knowing this family has been the most precious gain that I had during my years in Middle East Technical University.

I would like to thank Assist.Prof. Dr Tolga Yılmaz, for his guidance in regression analysis and statistical evaluation of the results. I have also to thank my examinıng committee members for their invaluable advices and suggestions that improved the study considerably.

I offer my sincere thanks to: my beloved family my mother Emel Küçükdogan, my grandfather Adem Hablemitoglu, my sister İdil Belgin Küçükdogan and my dear aunt Efser Koçakoglu for their unique love and support throughout my life and their endless faith in me; my father Alaettin Küçükdoğan and my uncle Necip Hablemitoğlu for their determination of pursuing their believes even confronting the death without slightest hesitation and fear.

Sincere thanks to all my friends whom I found beside me whenever I needed and felt blue for their refreshing energy, their encouraging and calming words and their love. Many thanks to:

Chorists of J.S.Bach Choir: Duygu, Özgür, Gökçen, Derya, Öncü, Esra, Güçlü, Moldiyar, Janar, Hamdi, Can, Bülent and many others for their absolutely limitless joy and energy; The members of the Arinna Sailing Team, Tayfun, Serhan, Koray, Oguz and Semih for their willingness to share the mystery of the eternal blue with me; Tayfun Hız for offering me a big barrel of wine upon the completion of this study; Utku Kartal, for his sincere friendship and sense of humor; Semih Demirer, for his courage, emotional support and mostly for his patience to calm me down; Bekir Özer Ay, Sami Demiroluk, Zerrin Ardıç Eminağa, Hazım Yılmaz, for their friendship and their support during every stages of the study; Özge Göbelez, for being the indispensable company at the times when the things all went wrong; Tuba Eroğlu for her courage, her help in technical matters; Vanessa Rheinheimer for her understanding and feeding me for the last week before the exam.

Finally, and most importantly, I am profoundly grateful to Mustafa Kemal Atatürk. I owe him my being able to write this MS dissertation as a woman while other women in other parts of the world still fight for their gender rights.

TABLE OF CONTENTS

LIST OF FIGURES

FIGURES **PAGE**

LIST OF TABLES

CHAPTER 1

INTRODUCTION

1.1 General

Performance based approach in the field of earthquake engineering aims to envisage the performance of a structure under common or extreme loads with a quantifiable confidence responding the needs of users and society (Krawinkler, 1999). The key point in the performance assessment studies is the estimation of lateral deformation demands in buildings under seismic excitation. Seismic excitation is quantified through a ground-motion intensity measure (IM) while deformation demand is depicted in terms of demand measure (DM). The disposition of the intricate relationship between IM and DM has been the eventual aim of the studies in this field. Several different methods are employed to achieve this objective with a wide spectrum of complexity, accuracy and computational effort features. Among those, response history analyses, albeit give more accurate results, are demanding in input preparation, modeling and data evaluation processes which makes the approach impractical especially beyond the elastic capacity (Metin, 2006; Ruiz-Garcia and Miranda, 2006; Yılmaz, 2007). Therefore, a great deal of effort has been devoted by the researchers to simplify the procedures on the estimation of nonlinear deformation demands on structures. Various recommendations have been proposed and academic studies have been conducted for the evaluation and rehabilitation of existing structures by professional academic agencies and establishments that introduce simplified analysis methods based on the maximum displacements of single-degree-of-freedom-systems

(SDOF) (e.g. ATC-40 (ATC,1996); FEMA 273/274 (ATC, 1997); FEMA-356 (ASCE, 2000) ; Miranda, 1999; Miranda and Garcia, 2002; Farrow and Kurama, 2004).

The performance assessment studies have utilized a variety of ground motion parameters as intensity measures which, in a way, portray the fundamental features of the ground motion as amplitude, frequency content and duration (Kramer, 1996). Two ground acceleration related parameters peak ground acceleration (*PGA*) and pseudo spectral acceleration at the fundamental period ($PS_a(T_1)$) have been widely preferred among the several ground motion intensity parameters defined in the literature. Douglas (2003) concludes that this common use is due to the predominance of many earthquake resistant design methods that are based on the response spectrum of acceleration. There exist several prediction equations which promote *PGA* and $PS_a(T_1)$ as well-recognized IMs. On the other hand, although the relative scarcity of prediction equations for *PGV*, many researches have been conducted to scrutinize and reveal the properties of *PGV* and its adequacy as an intensity measure in the last decade details of which will be discussed in the succeeding section.

The main subject of this study is to propose a predictive model to estimate the peak oscillator displacements as a function of *PGV* for bilinear hysteretic behavior under constant ductility (μ) and normalized lateral strength ratios (R) associated with α= 0% and α= 5% post yield stiffness ratio with independent variables, magnitude (M) and period (T), respectively. The secondary objective is to observe the correlation between intensity measures (*PGA*, *PGV* and $PS_a(T_1)$ and global demand measures (*MIDR* and *MRDR*) in multi-degree of freedom systems as a result of which *PGV* is selected as the ground motion intensity parameter for the predictive model. As a part of the thesis, the

use of predictive model with ground motion prediction equations of Akkar and Bommer (2007a, 2007b) is presented. The study has made use of 60 ground motions in the MDOF analyses and 109 ground-motions in the regression study of the predictive model, 20 model frames with 3-to 9-story levels to achieve these objectives.

1.2 Previous Research

In the estimation of the expected peak inelastic oscillator displacements (inelastic spectral displacement, $S_{d,ie}$), approximate models have made use of elastic period (T) dependent empirical relationships for a given displacement ductility (μ) or normalized lateral strength (R). Studies conducted by Velestos and Newmark (1960) and Newmark and Hall (1973, 1982) have been the pioneer studies that are based on R_μ - μ - T relationships within the context of force-based design to approximate the oscillator yield-strength (F_y) that would limit a predefined μ value. During the following decades many useful period-dependent empirical regression equations for direct estimation of $S_{d,ie}$ as a function of R (Ruiz-García and Miranda, 2003; Chopra and Chintanapakdee, 2004) or μ (e.g. Miranda, 2000; MacRae and Tagava, 2002; Chopra and Chintanapakdee, 2004; Ruiz-García and Miranda, 2004) have been proposed. These studies used ground motion datasets to establish the empirical relationships based on the quantity and quality of accumulated strong-motion records at the time when they were conducted. Different features of ground motion parameters have been stood out depending on the objective of the study. For the definition of ground-motion frequency content, the studies that followed the Velestos and Newmark approach have made use of peak ground motion values. They then derived their empirical relationships to relate elastic to inelastic oscillator response for the spectral period ranges described by the peak ground motion ratios. In these studies datasets were classified

according to ground-motion duration, moderate- to large-magnitude events, pulse-dominant signals or severe events produced by a particular fault type (e.g. Vidic et al., 1994; Cuesta et al., 2003; Riddell et al., 2002). The studies conducted by Elghadamsi and Mohraz (1987), Sewel (1989), Nassar and Krawinkler (1991), Miranda (1993, 2000), Ruiz-García and Miranda (2003, 2004), Arroyo and Teran (2003) mostly emphasized the influence of different site classes on the estimation of $S_{d,ie}$ using small- to large-size ground-motion datasets. Different magnitude-distance bins as well as different site classes were used for ground motions in the studies of Chopra and Chintanapakdee (2003, 2004). Researchers such as MacRae and Roeder (1999), Baéz and Miranda (2000), MacRae et al. (2001) and Chopra and Chintanapakdee (2001) shaped their $S_{d,ie}$ predictive expressions on the differences between near- and far-fault ground-motion records. These studies revealed significant insight about the nonlinear oscillator behavior under different load-deformation rules. The studies by Miranda and Bertero (1994) and Mahin and Bertero (1981) may also be referred for a detailed review on nonlinear oscillator response studies for the estimation of $S_{d,ie}$.

Regardless of the approximate model proposed, the major concept used in the estimation of $S_{d,ie}$ is

$$S_{d,ie} = \frac{\mu}{R} S_{d,e} = \frac{\mu}{R}\left(\frac{T}{2\pi}\right)^2 PS_{a,e} \tag{1.1}$$

In the case of R_μ - μ - T relations, $S_{d,ie}$ can be estimated using the expected R_μ for a given μ - T pair from its elastic counterpart $S_{d,e}$ (or equivalently utilizing elastic pseudo-spectral acceleration, $PS_{a,e}$ that can be related to $S_{d,e}$ through the constant $(T/2\pi)^2$ as shown in Eq. (1.1)). For the direct empirical relationships, $S_{d,ie}$ is related to $S_{d,e}$ by using the

regression equations that mimic the expected variation of μ/R either for a constant ductility level or normalized lateral strength ratio with the inclusion of a period-dependent modification factor (C_x) either for constant μ or for constant R. Thus, an alternative way of expressing Eq. (1.1) is given below

$$S_{d,ie} = C_x S_{d,e} = C_x \left(\frac{T}{2\pi} \right)^2 P S_{a,e} \tag{2}$$

The expressions presented in Eqs. (1.1) and (1.2) establish a linear relationship between inelastic and elastic spectral displacements (or equivalently a linear variation between $S_{d,ie}$ and $S_{a,e}$) for a given elastic period, T. As a matter of fact this approach is one of the current methods used in the simplified nonlinear static procedures (e.g., FEMA, 1997; ASCE, 2000; FEMA, 2003; ATC, 2005). Note that the ongoing research efforts for the estimation of $S_{d,ie}$ continuously result in new predictive models. In a recent study, Tothong and Cornell (2006) proposed an attenuation relationship for estimating $S_{d,ie}$ as a function of oscillator yield-strength and magnitude.

The attention received by peak ground velocity (*PGV*) in the technical literature is much less than that of peak ground acceleration and spectral ordinates (Bommer and Alarcón, 2006). However, *PGV* has various applications in earthquake engineering field as a damage potential indicator of ground motion to structural damage. The study of Wu et al (1999) revealed that *PGV* correlates better than *PGA* with Modified Mercalli Intensity (*MMI*) for higher values of intensity. The similar results were observed from the derived relationships of Kaka and Atkinson (2004) that estimated *MMI* from *PGV* for eastern North America. In their study that focused on the damage potential of earthquake ground motions based on inelastic dynamic response of

equivalent single degree of freedom structures, Sucuoğlu et al (1999) concluded that *PGV* is a promising seismic hazard parameter. Researchers like Miyakoshi et al (1998) and Yamazaki and Murao (2000) used *PGV* to derive vulnerability functions using the damage data from the 1995 Hyogo-ken Nanbu earthquake in Japan. *PGV* was used as a parameter that measures the potential of earthquake ground motions to cause damage in structures of intermediate periods of vibration by Fajfar et al (1990). A more recent study conducted by Akkar and Özen (2005) investigated the effect of peak ground velocity on deformation demands for SDOF systems using 60 near fault records of moderate to large magnitude. The correlations of *PGV*, *PGA*, spectral acceleration (S_a) and *PGV*/*PGA* as intensity measures with inelastic deformation demands of oscillators were compared between the period range of 0 to 4 seconds and the results revealed that *PGV* correlates better than the other intensity measures. The authors suggested *PGV* "*as a stable candidate for ground motion intensity measure in simplified seismic assessment methods".* As observed by many researchers (e.g., Bommer and Alarcón, 2006; Akkar and Bommer, 2007a; Douglas, 2003) there is a wide range of applications for *PGV* in the field of earthquake engineering however the prediction equations for this ground motion parameter are few in number when compared with those of *PGA* and spectral ordinates. An overview of published prediction equations by various researchers for *PGV* was presented by Bommer and Alarcón (2006) covering the equations from North America, Europe, Middle East, Japan and stable continental regions like Australia and Eastern North America (e.g. Campbell, 1997; Sadigh and Egan, 1998; Gregor et al, 2002; Tromans and Bommer, 2002; Frisenda et al (2005); Molas and Yamazaki, 1995; Singh et al, 2003; Atkinson and Boore, 1995; Pankow and Pechmann, 2004). In a more recent study, an alternative empirical prediction equation for *PGV* was derived by Akkar and Bommer (2007a) derived from the strong ground motions of Europe

and the Middle East to estimate both the larger horizontal component and the horizontal geometric mean component while only the former definition is taken into account generally in European prediction equations. The prediction equation has a quadratic term in magnitude and magnitude dependent geometric attenuation including the influence of style of faulting and site class. Another recent prediction equation developed for *PGV* is the prediction equation of Boore and Atkinson (2007) which is derived from a worldwide ground motion dataset that is compiled for the Next Generation Attenuation (NGA) project. The equation considers the soil nonlinearity effects by including the shear wave velocity in the upper 30 m of soil profile ($V_{s,30}$) while having the magnitude, distance and fault type as independent variables. The prediction equations for *PGV* of Akkar and Bommer (2007a) and Boore and Atkinson (2007) will be used to exemplify the application of the predictive model developed in this study.

1.3 Disposition of the study

The study consists of four chapters and three appendices. Introductory remarks on the estimation of inelastic deformation demands of single degree of freedom systems and ground motion intensity measures used and related previous studies are presented in Chapter 1.

Chapter 2 starts with the selection and grouping of the strong-ground motion records with some relevant descriptions about their important seismological features. The information regarding to the model buildings used and their dynamic characteristics are also provided in a detailed way. Chapter 2 also reports the results of response history and pushover analyses under three different hysteretic behaviors: nondegrading, stiffness degrading and stiffness and strength degrading, respectively. The relationships between global deformation demands

(maximum interstory drift ratio, *MIDR* and maximum roof drift ratio, *MRDR*) and the selected ground-motion intensity measures (peak ground acceleration, *PGA*, peak ground velocity, *PGV* and the elastic pseudospectral acceleration at the fundamental period, $PS_a(T_1)$) are investigated in Chapter 2. The results of the correlation studies between the demand measures and intensity measures are also summarized within the context of this chapter. The observations highlighted in Chapter 2 motivated the selection of *PGV* as the ground-motion intensity measure for the predictive model derived in Chapter 3.

Chapter 3 contains the regression analyses for the proposed predictive model for the estimation of the peak oscillator displacements as a function of *PGV*. Sensitivity analysis is conducted to observe the influence of independent ground-motion parameters (i.e. magnitude, site class, distance and style of faulting) on the predicted dimensionless parameter before deciding on the final functional form of the predictive equation. The results of the regression analyses are provided in this chapter together with the relevant residual plots. Normal distribution assumption for residuals is verified as well as their unbiased relationship with magnitude and the dependent parameter. Generic expressions are derived for standard deviations as a function of T and R (or μ). Within the context of this chapter, the application of the proposed model using the *PGV* values obtained from ground motion prediction equations is also provided as case studies.

Chapter 4 summarizes the conclusions of this study and presents complementary suggestions for future studies on this subject.

CHAPTER 2

GROUND-MOTIONS AND MDOF ANALYSIS

2.1 Description of ground-motions

This study used two sets of ground-motions that are compiled by Akkar and Özen (2005) and Akkar and Bommer (2007). The first database is directly taken from Akkar and Özen (2005) and it is used to observe the variation of global deformation demands on building systems with some certain ground-motion intensity parameters. Maximum interstory drift and maximum roof drift ratios (*MIDR* and *MRDR*, respectively) are chosen as the global deformation demands for the multi degree of freedom systems. The maximum interstory drift refers to the maximum absolute difference between the lateral displacements of two consecutive stories along the building height. When this lateral displacement parameter is normalized by the story height it is called as *MIDR*. The maximum roof drift ratio (*MRDR*) is the maximum absolute roof displacement normalized by the total building height. These demand parameters are the most frequently used global deformation indicators for the seismic performance assessment of MDOF systems. Peak ground acceleration and peak ground velocity (*PGA* and *PGV*, respectively) and the elastic pseudo spectral acceleration at the fundamental period ($PS_a(T_1)$) are the ground-motion intensities used while comparing their relation with the global deformation demands. As indicated in the introductory chapter, the purpose of this limited study is to verify the single degree of freedom (SDOF) results reported in Akkar and Özen (2005) for MDOF deformation demands. The second ground-motion set is the extended version of the database used in Akkar and

Özen (2005). Several records from the recently compiled European ground-motion database (Akkar and Bommer, 2007) are added to the first ground-motion database.These new records have fairly the same seismological features as of the first ground-motion set. The larger dataset is used for the regression analysis to estimate inelastic spectral displacements where details are given in Chapter 3.

In the selection of the records, strong pulse effects that are caused by forward directivity or any other complexity are avoided to hinder the probable bias in response estimations.

The first suite of records is composed of 60 ground-motion records and they are downloaded from the COSMOS Virtual Data Center (www.cosmos-eq.org). The selected ground-motions represent moderate to large near-fault events having moment magnitudes (M_w) and source to site distances (R_{jb}) varying between $5.7 \leq M_w \leq 7.6$ and $2 \leq R_{jb} \leq 24$ km, respectively. R_{jb} designates the shortest distance from the surface projection of the fault rupture to the accelerometric data (Joyner and Boore, 1981). The records are classified under three bins according to their *PGV* values. First bin contains records having *PGV* values less than 20 cm/s whereas the second bin consists of the records with *PGV* values ranging between 20 cm/s and 40 cm/s. The last sub-group comprises of records having values between 40 cm/s and 60 cm/s for *PGV*. The ground-motions are recorded on NEHRP C and NEHRP D site classes (FEMA, 2003). The average shear wave velocity in the upper 30 m of soil profile ($V_{s,30}$) ranges between 360 m/s $< V_{s,30} <$ 750 m/s for NEHRP C site classes. The variation of $V_{s,30}$ is in between 180 m/s and 360 m/s for NEHRP D sites. The ground-motions of first database are presented in Tables 2.1 to 2.3 along with their major seismological parameters: M_w, R_{jb}, site characteristics, *PGA*, *PGV* and *PGD*. *PGV* and magnitude distributions can be seen in Figure 2.1.

Table 2.1 Bin 1 of the first ground-motion dataset (0< *PGV*<20 cm/s)

Earthquakes	Station	Comp.	Mw	R_{jb} (km)	PGV (cm/s)	PGA (cm/s^2)	PGD (cm)	Site*
Whittier Narrows, 10/01/87	7420 Jaboneria, Bell Gardens	S27W	6.1	16.4	2.67	89.80	0.40	Q-Qof
Morgan Hill, 04/24/84	Gilroy-Gavilan College	67	6.1	13.2	3.39	95.00	0.50	Alluvium
Coyote Lake, 08/06/79	SJB Overpass, Bent 3	67	5.7	20.4	4.74	84.60	0.70	Terrace deposit over sandstone
Morgan Hill, 04/24/84	Gilroy #2	0	6.1	11.8	4.99	153.70	1.10	Alluvium
Morgan Hill, 04/24/84	Gilroy #7	90	6.1	7.9	5.76	111.50	0.60	Alluvium
North Palm Springs, 07/08/86	Fun Valley	45	6.2	12.7	6.12	123.50	1.00	Alluvium over sandstone
Whittier Narrows, 10/01/87	200 S. Flower, Brea, CA	N20E	6.1	22.2	7.07	109.40	1.30	Alluvium
North Palm Springs, 07/08/86	Fun Valley	135	6.2	12.7	9.47	123.00	1.40	Q
Imperial Valley, 10/15/79	Borchard Ranch, El Centro Array #1	S50W	6.5	19.8	10.36	121.10	7.40	Class C
Livermore, 01/27/80	Morgan Territory Park	265	5.8	10.3	11.04	242.70	1.40	Q
Morgan Hill, 04/24/84	Gilroy #6	0	6.1	6.1	11.26	214.80	1.80	Alluvium (Q)
Morgan Hill, 04/24/84	Gilroy #3	90	6.1	10.3	11.88	189.80	2.60	Silty clayover sandstone
Loma Prieta, 10/18/89	Gilroy #6 - San Ysidoro	0	7.0	17.9	13.09	112.20	5.00	Silty clayover sandstone
Loma Prieta, 10/18/89	Gilroy #6 - San Ysidoro	90	7.0	17.9	13.92	166.90	3.40	Alluvium
Coyote Lake, 08/06/79	Gilroy Array N0. 3 Sewage Treatment	50	5.7	6.8	16.89	252.40	3.70	Alluvium (Q-Qym)
Imperial Valley, 10/15/79	Parachute Test Facility,El Centro	N45W	6.5	12.7	17.27	197.60	10.90	Silty clayover sandstone
Livermore, 01/24/80	Livermore VA Hospital	128	5.5	100.0	17.39	121.70	3.40	Q
Livermore, 01/24/80	Livermore VA Hospital	38	5.5	100.0	17.87	180.30	2.30	Alluvium;600m;Sandstone
Imperial Valley, 10/15/79	Calexico Fire Station	N45W	6.5	10.5	18.95	197.60	15.20	Alluvium;600m;Sandstone
Imperial Valley, 10/15/79	Casa Flores, Mexicali	0	6.5	9.8	19.29	236.80	7.20	Alluvium (Q)

Abbreviations for site conditions : Q :quaternary(Vs=333m/s),Class C : 360 m/s<Vs < 750 m/s, Class D: 180 m/s < Vs < 360 m/s, T : Tertiary (Vs=406 m/s), Qym : Holocone, medium-grained sediment, Qyc : Holocone,coarse-grained sediment, Qof : Pleistocene,fine-grained sediment, Qom: Pleistocone, medium-grained sediment

Table 2.2 Bin 2 of the first ground-motion dataset (20< *PGV*<40 cm/s)

Earthquakes	Station	Comp.	Mw	R_{jb} (km)	PGV (cm/s)	PGA (cm/s^2)	PGD (cm)	Site*
Whittier Narrows, 10/01/87	Los Angeles Obrega Park	360	6.1	14.2	21.783	420.1	2.8	Alluvium (Q-Qom)
Northridge, 01/17/94	Los Angeles - UCLA Grounds	360	6.7	22.9	21.882	464.6	7.3	Alluvium (Q-Qom)
Northridge, 01/17/94	Los Angeles - UCLA Grounds	90	6.7	22.9	21.995	272.4	4	Alluvium (Q-Qom)
Imperial Valley, 10/15/79	Community Hospital, Keystone Rd., El C	S50W	6.5	6.2	22.948	117.3	13.3	Alluvium;more than 300m
Loma Prieta, 10/18/89	Gilroy - Gavilan Coll	337	7	9.2	22.954	310	4.8	Terrace deposit over sandstone
Northridge, 01/17/94	6850 Coldwater Canyon Ave.,	S00W	6.7	12.5	23.066	296	10	Alluvium(Q-Qyc)
Imperial Valley, 10/15/79	Aeropuerto Mexicali	315	6.5	0.0	23.85	249.9	5.4	Deep Alluvium
Northridge, 01/17/94	Los Angeles, Brentwood V.A. Ho	195	6.7	23.1	24.01	182.1	5.4	Alluvium (Q-Qom)
Parkfield, 06/27/66	Cholame,Shandon, Array No. 5	N85E	6.1	7.1	25.437	425.7	71	Alluvium;Sandstone(Q)
Whittier Narrows, 10/01/87	7420 Jaboneria,Bell Gardens	N63W	6.1	16.4	28	215.9	50	Alluvium(Q-Qym)
Loma Prieta, 10/18/89	Gilroy - Gavilan Coll	67	7	9.2	28.925	349.1	5.8	Terrace deposit over sandstone
Imperial Valley, 10/15/79	Casa Flores, Mexicali	270	6.5	9.8	31.51	414.7	7.7	Alluvium
Coyote Lake, 08/06/79	Gilroy Array No. 2	140	5.7	8.5	31.88	248.9	5.3	Alluvium
Imperial Valley, 10/15/79	Keystone Rd., El Centro Array #2	S40E	6.5	13.3	32.712	309.4	15	Alluvium (Q)
Loma Prieta, 10/18/89	Gilroy #2 - Hwy 101/Bolsa Rd	0	7	10.4	33.339	344.2	6.7	Alluvium
Loma Prieta, 10/18/89	Gilroy #3 - Gilroy Sewage Plant	0	7	12.2	34.476	531.7	7.4	Alluvium
Loma Prieta, 10/18/89	Saratoga - 1-Story School Gym	270	7	8.5	37.192	347.3	7.8	Alluvium
Imperial Valley, 10/15/79	Anderson Rd., El Centro Array #4	S40E	6.5	4.9	38.1	480.8	22	Alluvium;more than 300m
Loma Prieta, 10/18/89	Gilroy #2 - Hwy 101/Bolsa Rd	90	7	10.4	39.229	316.3	10.9	Alluvium
Morgan Hill, 04/24/84	Halls Valley	240	6.1	2.5	39.573	305.8	6.6	Alluvium

Abbreviations for site conditions : Q :quaternary(Vs=333m/s),Class C : 360 m/s<Vs < 750 m/s, Class D: 180 m/s < Vs < 360 m/s, T : Tertiary (Vs=406 m/s), Qym : Holocone, medium-grained sediment, Qyc : Holocone,coarse-grained sediment, Qof : Pleistocene,fine-grained sediment, Qom: Pleistocone, medium-grained sediment

Table 2.3 Bin 3 of the first ground-motion dataset (40< *PGV*<60 cm/s)

Earthquakes	Station	Comp.	Mw	R_{jb} (km)	PGV (cm/s)	PGA (cm/s^2)	PGD (cm)	Site*
Chi-Chi, Taiwan, 09/20/99	Taichung - Chungming School, TCU051	360	7.6	7	40.58	230	42.5	Class D
Chi-Chi, Taiwan, 09/20/99	Taichung - Taichung City, TCU082	360	7.6	4.5	41.03	182.1	39.3	Class D
Imperial Valley, 10/15/79	Dogwood Rd., Diff. Array, El Centro	NS	6.5	5.1	41.145	473.6	16.3	Alluvium (Q)
Imperial Valley, 10/15/79	Aeropuerto Mexicali	45	6.5	0.0	42.03	284.9	10.1	Deep Alluvium
Chi-Chi, Taiwan, 09/20/99	Chiayi - Meishan School, CHY006	360	7.6	14.5	42.089	351.8	16.4	Class D
Cape Mendocino, 04/25/92	Rio Dell - 101/Painter St. Overseas	360	7	18.5	42.629	538.5	13.4	Class C
Landers, 06/28/92	Joshua Tree - Fire Station	90	7.3	11.0	42.71	278.4	15.7	Shallow Alluvium over granite (Q)
Imperial Valley, 10/15/79	Bonds Corner	140	6.5	0.5	44.33	578	15	Alluvium (Q)
Imperial Valley, 10/15/79	Bonds Corner	230	6.5	0.5	44.95	762.4	15.1	Alluvium (Q)
Imperial Valley, 10/15/79	McCabe School, El Centro Array #11	S50W	6.5	12.5	45.24	362.5	22.3	Alluvium (Q)
Imperial Valley, 10/15/79	Community Hospital, Keystone Rd.,	N40W	6.5	6.2	45.958	226.6	26.7	Alluvium;more than 300m
Cape Mendocino, 04/25/92	Petrolia	0	7	9.5	48.304	578.1	15.2	Alluvium
Imperial Valley, 10/15/79	James Rd., El Centro Array #5	S40E	6.5	1.8	49.713	539.8	40.8	Alluvium;more than 300m
Kocaeli 8/18/99	Duzce	SN	7.4	13.6	50.7	307.8	35.8	Alluvium
Northridge, 01/17/94	Pacoima - Kagel Canyon	360	6.7	10.6	50.877	424.,2	6.6	Sandstone (T)
Duzce, 11/12/99	Bolu	NS	7.1	12.0	55.17	722.,1	2.4	Alluvium
Loma Prieta, 10/18/89	Corralitos - Eureka Canyon Rd	0	7	0.2	55.196	617.7	9.5	Landslide Deposits
Northridge, 01/17/94	14145 Mulholland Dr.,Beverly Hills, CA	N09E	6.7	19.6	57.936	419.3	15	Landslide Deposits
Northridge, 01/17/94	17645 Saticoy St.	S00E	6.7	13.3	59.821	428.7	17.6	Class D
Northridge, 01/17/94	7769 Topanga Canyon Blvd.,Canoga Par	S16W	6.7	15.7	59.836	381	12.4	Alluvium(Q-Qym)

Abbreviations for site conditions : Q :quaternary(Vs=333m/s),Class C : 360 m/s<Vs < 750 m/s, Class D: 180 m/s < Vs < 360 m/s, T : Tertiary (Vs=406 m/s), Qym : Holocone, medium-grained sediment, Qyc : Holocone,coarse-grained sediment, Qof : Pleistocene,fine-grained sediment, Qom: Pleistocone, medium-grained sediment

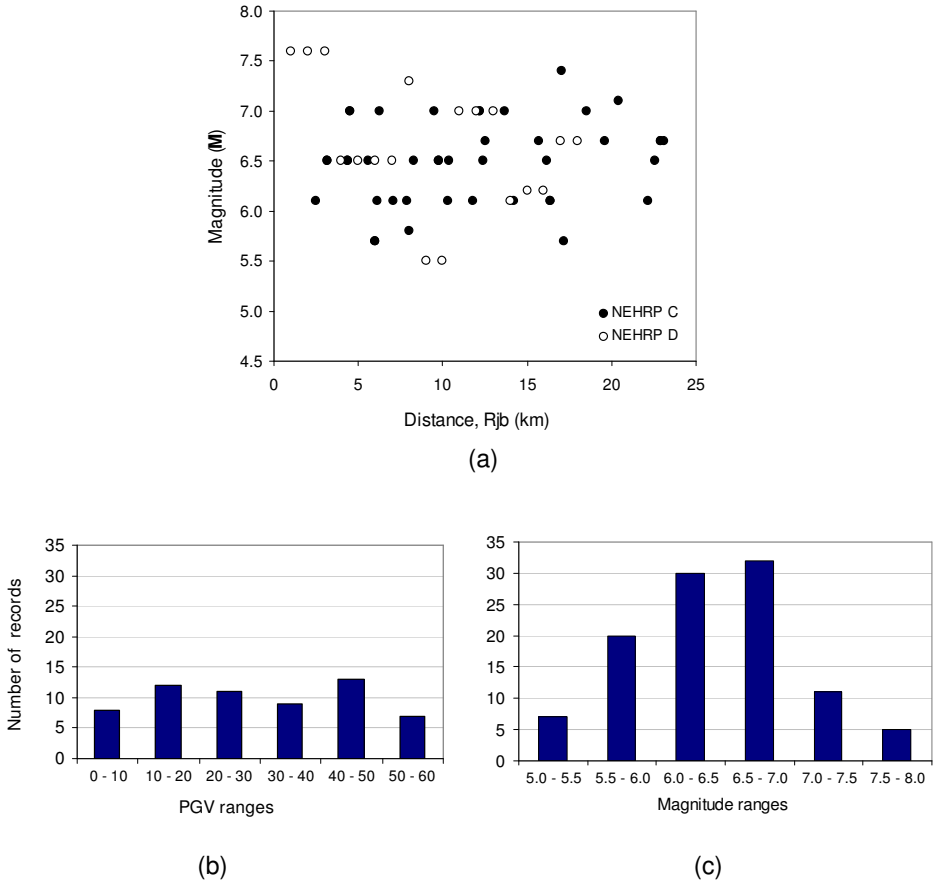

Figure 2.1. Magnitude distance, *PGV* range and magnitude range distribution of the ground motion dataset 1

The second ground-motion dataset (the expanded version of the first set) consists of 105 ground-motion records. A total of 56 records are taken from the European dataset presented in Akkar and Bommer (2007). The rest of the records is from the first ground-motion dataset. The second ground-motion database mimics the random component effect for the selected records: one horizontal component is selected arbitrarily from each accelogram. This is not the case for the first database since it contains both horizontal components of some of the accelograms. In terms of data number and the specific horizontal

component definition the second database is more suitable for conducting regression analyses. The relevant seismological information for the larger database is presented in Table 2.4. The magnitude of the records varies between 5.2 ≤ M_w ≤ 7.6. Majority of the records (66 out of 109) are classified as NEHRP class D (180 m/s < $V_{s,30}$ < 360 m/s). The site class of the rest of the ground-motions is NEHRP class C (360 m/s ≤ $V_{s,30}$ < 750 m/s). The magnitude- distance distribution of the larger dataset along with the *PGV* and magnitude histograms are presented in Figure 2.2. The distribution indicates that the database is dominated by the near fault events. Note that similar to the first database, the selected records do not contain pulse dominant signals in their waveforms.

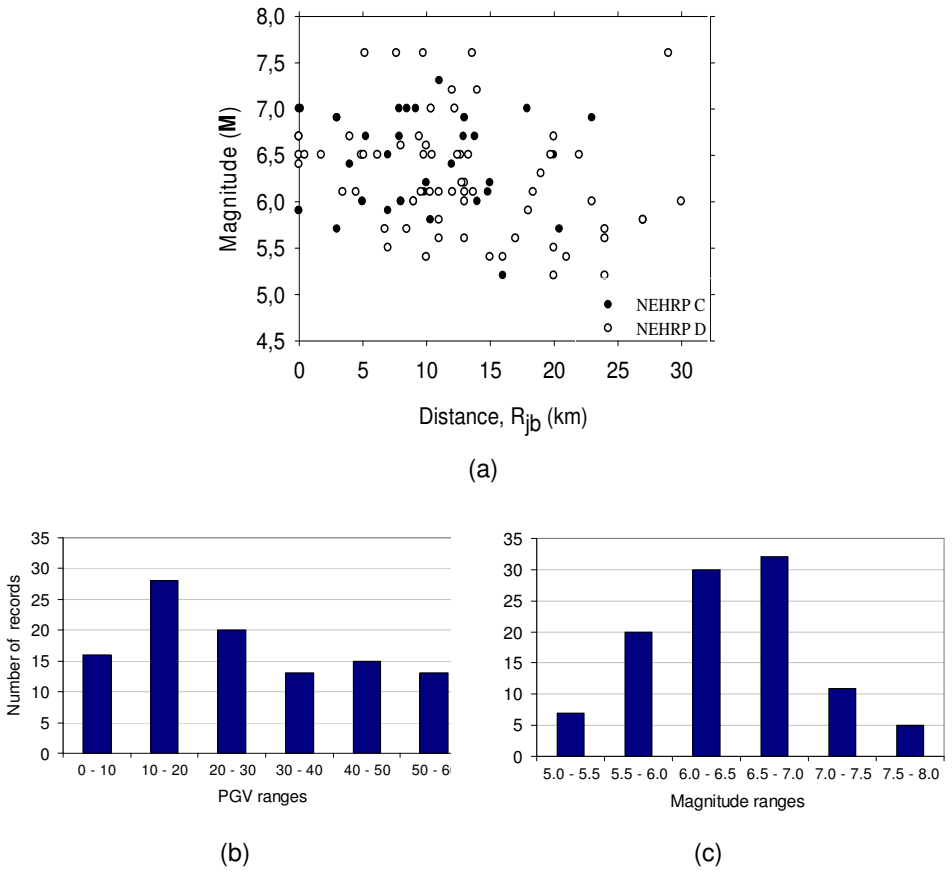

Figure 2.2. Magnitude distance, *PGV* range and magnitude range distribution of the ground motion dataset 2

Table 2.4 Important seismological features of suite of ground-motion records

Earthquake	Station	M_w	R_{jb} (km)	NEHRP	PGV (cm/s)	PGA (cm/s²)	PGD (cm)	F*
Kozani, 19/5/1995	Karpero-Town Hall	5.2	16.0	C	14.85	262.50	1.39	N
Umbria Marche,12/10/1997	Foligno Santa Maria Infraportas-Base	5.2	20.0	D	1.07	29.71	0.10	N
Manesion , 07/06/1989	Patra-OTE Building	5.2	24.0	D	2.34	24.35	0.85	S
Pyrgos , 26/03/1993	Pyrgos-Agriculture Bank	5.4	10.0	D	19.02	436.90	1.75	S
Komilion,25/2/1994	Lefkada-Hospital	5.4	15.0	D	12.08	134.10	1.11	S
Komilion, 25/2/1994	Lefkada-OTE Building	5.4	16.0	D	14.53	197.70	1.36	S
Preveza, 10/3/1981	Lefkada-OTE Building	5.4	21.0	D	5.94	97.73	0.84	R
Friuli, 11/09/1976	Buia	5.5	7.0	D	21.71	227.40	2.52	R
Umbria Marche,6/10/1997	Castelnuovo-Assisi	5.5	20.0	D	7.55	109.10	1.81	N
Livermore, 01/24/80	Livermore VA Hospital	5.5	100.0	D	17.39	121.70	3.39	S
Racha, 03/05/1991	Ambrolauri	5.6	11.0	D	25.10	347.50	2.78	R
Cerkes,14/8/1996	Merzifon-Meteoroloji Mudurlugu	5.6	13.0	D	5.02	101.30	1.26	S
Racha, 03/05/1991	Oni-Base Camp	5.6	17.0	D	1.97	51.14	0.17	R
Sicilia-Orientale, 13/12/1990	Catania-Piana	5.6	24.0	D	10.78	174.00	1.66	S
Umbria Marche, 26/09/1997	Colfiorito	5.7	3.0	C	23.01	461.90	4.10	N
Coyote Lake, 08/06/79	Gilroy Array No. 3 Sewage Treatment	5.7	6.8	D	16.89	252.37	3.68	S
Coyote Lake, 08/06/79	Gilroy Array No. 2	5.7	8.5	D	31.88	248.94	5.34	S
Coyote Lake, 08/06/79	SJB Overpass, Bent 3	5.7	20.4	C	4.74	84.58	0.74	S
Umbria Marche,26/09/1997	Castelnuovo-Assisi	5.7	24.0	D	6.44	99.11	1.86	N
Livermore, 01/27/80	Morgan Territory Park	5.8	10.3	C	11.04	242.66	1.36	S
Ionian , 04/11/1973	Lefkada-OTE Building	5.8	11.0	D	56.90	523.30	18.29	R
Izmit,13/9/1999	Adapazari Kadin D. Cocuk B. Evi	5.8	27.0	D	7.02	69.51	3.03	S
Izmit,13/9/1999	Yarimca-Petkim	5.8	27.0	D	8.07	91.48	2.25	S
Kalamata, 13/9/1986	Kalamata-OTE Building	5.9	0.0	C	34.61	234.20	9.71	N
Kalamata, 13/9/1986	Kalamata-Prefecture	5.9	0.0	C	33.10	234.50	7.91	N
Firuzabad, 20/6/1994	Zanjiran (Iran)	5.9	7.0	C	40.44	963.00	2.63	S
Lazio Abruzzo, 07/05/1984	Cassino-Sant' Elia	5.9	18.0	D	11.12	143.60	1.86	N
Ano Liosia, 07/09/1999	Athens-Sepolia Metro Station	6.0	5.0	C	17.84	245.00	1.37	N
Ano Liosia, 07/09/1999	Athens-Sepolia Garage	6.0	5.0	C	21.32	346.40	2.74	N
Ano Liosia ,07/09/1999	Athens-Syntagma 1st lower level	6.0	8.0	C	12.99	233.60	1.71	N
Ano Liosia, 07/09/1999	Athens 3 Kallithea District	6.0	8.0	C	15.70	259.40	2.35	N
Friuli, 15/9/1976	Forgaria-Cornio	6.0	9.0	C	23.97	344.32	3.36	R
Friuli, 15/9/1976	San Rocco	6.0	9.0	C	19.40	232.04	4.90	R
Friuli,15/9/1976	Buia	6.0	9.0	D	12.53	93.79	2.39	R
Basso Tirreno, 15/4/1978	Patti-Cabina Prima	6.0	13.0	D	15.21	160.70	2.88	S
Friuli, 15/9/1976	Breginj-Fabrika IGLI	6.0	14.0	C	27.74	478.70	2.37	R
Umbria Marche, 26/09/1997	Castelnuovo-Assisi	6.0	23.0	D	13.06	169.10	3.06	N
Umbria Marche,26/09/1997	Gubbio-Piana	6.0	30.0	D	17.72	94.25	5.80	N
Morgan Hill, 04/24/84	Halls Valley	6.1	3.5	D	39.57	305.77	6.56	S
Whittier Narrows, 10/01/87	Los Angeles Obregon Park	6.1	4.5	D	21.78	420.11	2.82	R
Parkfield, 06/27/66	Cholame,Shandon, Array No. 5	6.1	9.6	D	25.44	425.68	7.11	S
Morgan Hill, 04/24/84	Gilroy #6	6.1	9.9	C	11.26	214.81	1.81	S
Whittier Narrows, 10/01/87	7420 Jaboneria,Bell Gardens	6.1	10.3	D	28.00	215.93	4.96	R
Faial, 09/07/1998	Horta	6.1	11.0	D	34.37	368.50	3.88	S
Morgan Hill, 04/24/84	Gilroy #7	6.1	12.1	D	5.76	111.54	0.61	S
Morgan Hill, 04/24/84	Gilroy #3	6.1	13.0	D	11.88	189.84	2.58	S
Morgan Hill, 04/24/84	Gilroy #2	6.1	13.7	D	4.99	153.67	1.12	S
Morgan Hill, 04/24/84	Gilroy-Gavilan College	6.1	14.8	C	3.39	94.98	0.47	S
Whittier Narrows, 10/01/87	200 S. Flower, Brea, CA	6.1	18.4	D	7.07	109.39	1.32	R
Montenegro, 24/5/1979	Budva-PTT	6.2	10.0	C	27.73	265.70	4.16	R
North Palm Springs, 07/08/86	Fun Valley	6.2	12.8	D	6.12	123.50	0.99	S
Volvi, 20/6/1978	Thessaloniki-City Hotel	6.2	13.0	D	16.08	144.10	3.01	N
Montenegro, 24/5/1979	Bar-Skupstina Opstine	6.2	15.0	C	16.54	261.60	1.69	R
Alkion, 25/2/1981	Korinthos-OTE Building	6.3	19.0	D	13.67	115.20	5.93	N
Dinar, 01/10/1995	Dinar-Meteoroloji Mudurlugu	6.4	0.0	D	43.99	317.20	9.75	N
South Iceland, 21/6/2000	Solheimar	6.4	4.0	C	40.95	432.10	24.42	S
South Iceland, 21/6/2000	Kaldarholt	6.4	12.0	C	26.62	389.90	10.64	S
Imperial Valley, 10/15/79	Aeropuerto Mexicali	6.5	0.0	D	42.03	284.90	10.08	S
Imperial Valley, 10/15/79	Bonds Corner	6.5	0.5	D	44.33	578.00	14.95	S
Imperial Valley, 10/15/79	James Rd., El Centro Array #5	6.5	1.8	D	49.71	539.78	40.77	S
Imperial Valley, 10/15/79	Anderson Rd., El Centro Array #4	6.5	4.9	D	38.10	480.76	21.99	S
South Iceland, 17/6/2000	Hella	6.5	5.0	C	55.26	463.30	13.48	S
Imperial Valley, 10/15/79	Dogwood Rd., Diff. Array, El Centro	6.5	5.1	D	41.15	473.64	16.33	S
Imperial Valley, 10/15/79	Community Hospital,El Centro Array #10	6.5	6.2	D	45.96	226.58	26.74	S
Aigion, 15/6/1995	Aigio-OTE Building	6.5	7.0	C	52.36	531.18	8.53	N

Table 2.4 (continued)

Earthquake	Station	M_w	R_{jb} (km)	NEHRP	PGV (cm/s)	PGA (cm/s²)	PGD (cm)	F*
Imperial Valley, 10/15/79	Casa Flores, Mexicali	6.5	9.8	D	31.51	414.70	7.67	S
Imperial Valley, 10/15/79	Calexico Fire Station	6.5	10.5	D	18.95	197.56	15.20	S
Imperial Valley, 10/15/79	McCabe School, El Centro Array #11	6.5	12.5	D	45.24	362.52	22.34	S
Imperial Valley, 10/15/79	Parachute Test Facility,El Centro	6.5	12.7	D	17.27	197.63	10.92	S
Imperial Valley, 10/15/79	Keystone Rd., El Centro Array #2	6.5	13.3	D	32.71	309.40	15.02	S
Imperial Valley, 10/15/79	Borchard Ranch, El Centro Array #1	6.5	19.8	D	10.36	121.06	7.35	S
South Iceland, 17/6/2000	Selsund	6.5	20.0	C	22.06	220.50	7.87	S
Aigion,15/6/1995	Amfissa-OTE Building	6.5	22.0	D	9.72	188.56	1.93	N
Alkion, 24/2/1981	Xilokastro-OTE Building	6.6	8.0	D	28.04	300.40	13.74	N
Alkion, 24/2/1981	Korinthos-OTE Building	6.6	10.0	D	23.62	304.90	6.13	N
Northridge, 01/17/94	17645 Saticoy St.	6.7	0.0	D	59.82	428.70	17.57	R
Northridge, 01/17/94	7769 Topanga Canyon Blvd.,Canoga Park	6.7	0.0	D	59.84	380.98	12.39	R
Gazli, 17/5/1976	Karakyr Point	6.7	4.0	D	54.75	618.80	16.62	R
Northridge, 01/17/94	Pacoima - Kagel Canyon	6.7	5.3	C	50.88	424.21	6.59	R
Northridge, 01/17/94	6850 Coldwater Canyon Ave.,	6.7	7.9	C	23.07	296.04	9.98	R
Northridge, 01/17/94	14145 Mulholland Dr.,Beverly Hills, CA	6.7	9.4	D	57.94	419.28	15.01	R
Northridge, 01/17/94	Los Angeles, Brentwood V.A. Ho	6.7	12.9	C	24.01	182.10	5.44	R
Northridge, 01/17/94	Los Angeles - UCLA Grounds	6.7	13.8	C	21.88	464.55	7.33	R
Spitak, 07/12/1988	Gukasian	6.7	20.0	D	30.09	180.20	19.56	R
Montenegro, 15/4/1979	Petrovac-Hotel Oliva	6.9	3.0	C	39.96	454.30	12.75	R
Montenegro, 15/4/1979	Bar-Skupstina Opstine	6.9	3.0	C	52.81	364.50	16.25	R
Campano Lucano, 23/11/1980	Calitri	6.9	13.0	C	29.36	170.95	9.19	N
Montenegro, 15/4/1979	Ulcinj-Hotel Olimpic	6.9	13.0	C	51.70	243.60	15.15	R
Campano Lucano,23/11/1980	Brienza	6.9	23.0	C	11.50	220.92	3.22	N
Cape Mendocino, 04/25/92	Petrolia	7.0	0.0	C	48.30	578.14	15.24	R
Loma Prieta, 10/18/89	Corralitos - Eureka Canyon Rd	7.0	0.2	C	55.20	617.70	9.54	RO
Cape Mendocino, 04/25/92	Rio Dell - 101/Painter St. Overseas	7.0	7.9	C	42.63	538.52	13.37	R
Loma Prieta, 10/18/89	Saratoga - 1-Story School Gym	7.0	8.5	C	37.19	347.35	7.79	RO
Loma Prieta, 10/18/89	Gilroy - Gavilan Coll	7.0	9.2	C	28.93	349.14	5.81	RO
Loma Prieta, 10/18/89	Gilroy #2 - Hwy 101/Bolsa Rd	7.0	10.4	D	39.23	316.31	10.89	R
Loma Prieta, 10/18/89	Gilroy #3 - Gilroy Sewage Plant	7.0	12.2	D	34.48	531.66	7.37	RO
Loma Prieta, 10/18/89	Gilroy #6 - San Ysidoro	7.0	17.9	C	13.92	166.93	3.35	OR
Duzce, 11/12/99	Bolu	7.2	12.0	D	55.17	722.10	24.36	S
Duzce 1,12/11/1999	LDEO Station No. C1062 FI	7.2	14.0	D	18.25	254.00	8.99	S
Landers, 06/28/92	Joshua Tree - Fire Station	7.3	11.0	C	42.71	278.38	15.73	S
Chi-Chi, Taiwan, 09/20/99	Taichung - Taichung City, TCU082	7.6	5.2	D	41.03	182.10	39.30	R
Chi-Chi, Taiwan, 09/20/99	Taichung - Chungming School, TCU051	7.6	7.7	D	40.58	230.00	42.46	R
Chi-Chi, Taiwan, 09/20/99	Chiayi - Meishan School, CHY006	7.6	9.8	D	42.09	351.84	16.35	R
Kocaeli 8/18/99	Duzce	7.6	13.6	D	50.70	307.80	35.78	S
Izmit, 17/08/1999	Iznik-Karayollari Sefligi Muracaati	7.6	29.0	D	26.82	121.20	26.02	S

F - Style of Faulting Strike-slip(S), Normal(N), Reverse (R), Reverse Oblique (RO), Oblique(O)*

2.2 Building models used for the first ground-motion database

Moment resisting frames (MRFs) are designed to observe the relationships between the global deformation demands and ground-motion parameters chosen in this study. The basic objective of this investigation is to verify the remarks made by Akkar and Özen (2005) for the nonlinear MDOF behavior. Based on the nonlinear oscillator response, the aforementioned study indicated the superior correlation of *PGV* with the oscillator displacement demands. The building models would give an opportunity to see whether this observation holds for

model systems. The frame models are designed for the median design spectra of the 3 bins that are assembled according to different *PGV* ranges as described in Section 2.1. The median spectrum of each bin assembled from the first ground-motion database as well as the corresponding design spectra are presented in Figure 2.3. The smooth design spectrum for each bin is obtained by following the procedure in the FEMA 356 document. Five groups of reinforced concrete MRFs are designed by making use of the three smoothed design spectra described above. Each group contains 3, 5, 7 and 9 story regular frames in compliance with the Turkish standards for Design and Construction of RC structures, TS500 (TSE, 2000) and Turkish Seismic Code (Bayındırlık ve İskan Bakanlığı, 1998).

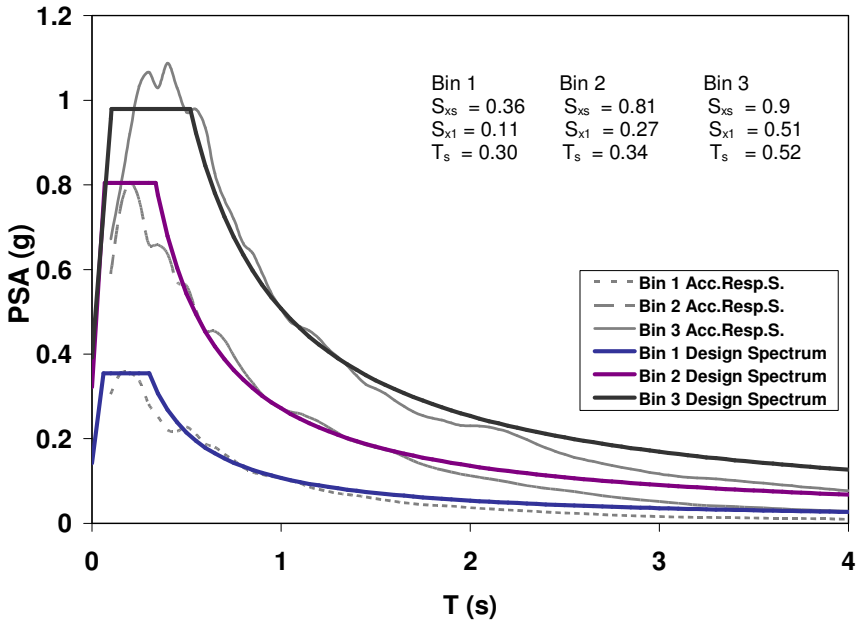

Figure 2.3 Median response and smoothed design spectra of the ground-motions assembled from the first ground-motion dataset. The abbreviations S_{xs}, S_{x1} and T_s are the parameters used in the FEMA 356 document (ASCE, 2000) for the smoothed design spectrum.(S_{xs} and S_{x1} represents the pseudo spectral acceleration at short and long periods,respectively. The variable T_s is the corner period that separates constant acceleration plateau from the descending branch)

In all models, the story height and bay width are 3m and 5 m, respectively. The compressive strength of concrete is 20MPa and the yield strength of steel bars is 420 MPa. Rigid diaphragm assumption was made and floor masses were lumped at the beam-column joints at each story level. The Design Loads for Buildings, TS498 (TSE, ACI1997) was used in the calculation of gravity loads (dead and live loads). Design loads were calculated by using the provisions of the aforementioned codes and the designed spectra presented in Figure 2.3. The dimensions of structural members are calculated by the constraints imposed by the design spectrum and the design loads. The column and beam dimensions were reduced with increasing height in order to reflect the common design and construction practice. For 3 story models the column and beam dimensions remain constant throughout the building height. In the case of 5 story models, the column dimensions reduce after the 4^{th} story and the beam dimensions are kept constant. For 7 story models, both beam and column cross sections reduce simultaneously at the 4^{th} and 6^{th} stories. The beam and column dimensions are reduced at the 4^{th} and 7^{th} story levels for 9 story models. The reduction in structural member dimensions is in accordance with the Turkish seismic design code (TEC, 1998). The reinforcement detailing of the frames are determined by using the commercial software program SAP 2000 v.8.2.3 (CSI, 2000) and therefore conformed to the provisions of ACI-318 (AC:I, 1999). A list presenting the main properties of the analytical models is provided in Table 2.5.

The model abbreviations in Table 2.5 describe the specific design spectrum used in design of the buildings. For instance, e2 refers to the design spectrum obtained from the second bin of the first ground-motion database. The suit of building models e1' and e2' are obtained by redesigning the corresponding e1 and e2 models for the design

spectrum of the third ground-motion bin. During the design of e1' and e2', the geometric properties of e1 and e2 models were used whereas the reinforcement detailing was modified according to the design spectrum of the third ground-motion bin. This table contains the sections, beam and column dimensions of each model as well as the first mode periods and the post-yield stiffness ratios obtained from the idealized pushover curves. Details of the frame models are provided in Appendix A. Figure 2.4 shows a typical sketch of one of the 9 story building models.

Table 2.5 Different properties of models

# of story	Model	T1	α	Section	Story	h (cm)	b (cm)
3	e1	0.8203	0.0556	BEAM3	1-2-3	45.0	25.0
				COL3	1-2-3	30.0	30.0
	e2	0.8156	0.0337	BEAM3	1-2-3	45.0	30.0
				COL3	1-2-3	35.0	35.0
	e3	0.8052	0.0274	BEAM3	1-2-3	50.0	30.0
				COL3	1-2-3	45.0	45.0
	e1'	0.6740	0.0598	BEAM3	1-2-3	45.0	25.0
				COL3	1-2-3	30.0	30.0
	e2'	0.5667	0.0382	BEAM3	1-2-3	45.0	30.0
				COL3	1-2-3	35.0	35.0
5	e1	1.0427	0.0558	BEAM2	1-2-3	45.0	25.0
				BEAM3	4-5	45.0	25.0
				COL2	1-2-3	35.0	35.0
				COL3	4-5	30.0	30.0
	e2	0.7867	0.0394	BEAM2	1-2-3	50.0	30.0
				BEAM3	4-5	50.0	30.0
				COL2	1-2-3	40.0	40.0
				COL3	4-5	35.0	35.0
	e3	0.6985	0.0274	BEAM2	1-2-3	50.0	30.0
				BEAM3	4-5	50.0	30.0
				COL2	1-2-3	45.0	45.0
				COL3	4-5	40.0	40.0
	e1'	1.0163	0.0425	BEAM2	1-2-3	45.0	25.0
				BEAM3	4-5	45.0	25.0
				COL2	1-2-3	35.0	35.0
				COL3	4-5	30.0	30.0
	e2'	0.7788	0.0343	BEAM2	1-2-3	50.0	30.0
				BEAM3	4-5	50.0	30.0
				COL2	1-2-3	40.0	40.0
				COL3	4-5	35.0	35.0
7	e1	1.1516	0.0978	BEAM1	1-2-3	50.0	30.0
				BEAM2	4-5	50.0	30.0
				BEAM3	6-7	45.0	30.0
				COL1	1-2-3	40.0	40.0
				COL2	4-5	35.0	35.0
				COL3	6-7	30.0	30.0
	e2	0.9575	0.0531	BEAM1	1-2-3	55.0	30.0
				BEAM2	4-5	50.0	30.0
				BEAM3	6-7	50.0	30.0
				COL1	1-2-3	45.0	45.0
				COL2	4-5	40.0	40.0
				COL3	6-7	35.0	35.0
	e3	0.8715	0.0342	BEAM1	1-2-3	55.0	30.0
				BEAM2	4-5	50.0	30.0
				BEAM3	6-7	50.0	30.0
				COL1	1-2-3	50.0	50.0
				COL2	4-5	45.0	45.0
				COL3	6-7	40.0	40.0
	e1'	1.1400	0.0416	BEAM1	1-2-3	50.0	30.0
				BEAM2	4-5	50.0	30.0
				BEAM3	6-7	45.0	30.0
7				COL1	1-2-3	40.0	40.0
				COL2	4-5	35.0	35.0
				COL3	6-7	30.0	30.0
	e2'	0.9513	0.0424	BEAM1	1-2-3	55.0	30.0
				BEAM2	4-5	50.0	30.0
				BEAM3	6-7	50.0	30.0
				COL1	1-2-3	45.0	45.0
				COL2	4-5	40.0	40.0
				COL3	6-7	35.0	35.0
9	e1	1.2964	0.0589	BEAM1	1-2-3	55.0	30.0
				BEAM2	4-5-6	50.0	30.0
				BEAM3	7-8-9	45.0	30.0
				COL1	1-2-3	45.0	45.0
				COL2	4-5-6	40.0	40.0
				COL3	7-8-9	35.0	35.0
	e2	1.1213	0.0581	BEAM1	1-2-3	55.0	30.0
				BEAM2	4-5-6	55.0	30.0
				BEAM3	7-8-9	50.0	30.0
				COL1	1-2-3	50.0	50.0
				COL2	4-5-6	45.0	45.0
				COL3	7-8-9	40.0	40.0
	e3	0.9895	0.0373	BEAM1	1-2-3	60.0	30.0
				BEAM2	4-5-6	55.0	30.0
				BEAM3	7-8-9	50.0	30.0
				COL1	1-2-3	55.0	55.0
				COL2	4-5-6	50.0	50.0
				COL3	7-8-9	45.0	45.0
	e1'	1.2827	0.0530	BEAM1	1-2-3	55.0	30.0
				BEAM2	4-5-6	50.0	30.0
				BEAM3	7-8-9	45.0	30.0
				COL1	1-2-3	45.0	45.0
				COL2	4-5-6	40.0	40.0
				COL3	7-8-9	35.0	35.0
	e2'	1.1130	0.0435	BEAM1	1-2-3	55.0	30.0
				BEAM2	4-5-6	55.0	30.0
				BEAM3	7-8-9	50.0	30.0
				COL1	1-2-3	50.0	50.0
				COL2	4-5-6	45.0	45.0
				COL3	7-8-9	40.0	40.0

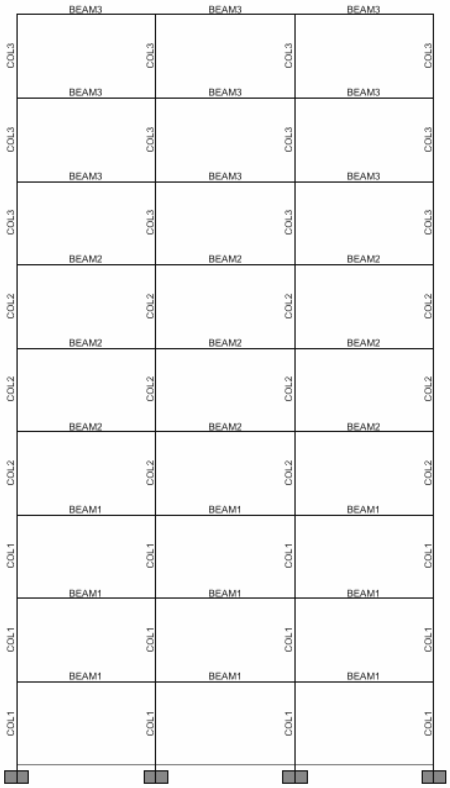

Figure 2.4 Typical sketch of 9 story analytical model. Note that column dimensions are reduced at the 4th and 7th story levels. The beam dimensions are also reduced at the same story levels

2.3 Nonlinear Response History Analyses of Frame Models Using First Ground-Motion Dataset

As indicated in the previous section the relationship between some well known ground-motion intensity measures and global deformation demands of MDOF systems are investigated via nonlinear response history analyses. The records in the first ground-motion database and frames are used to achieve this objective. The details of the ground-motions and building models are described in the previous section. IDARC 2D (Valles et al, 1996) analysis program is used for running the nonlinear response history analysis. The damage analysis model of Modified Park-Ang-Wen is utilized by the program on single element

level and global structure level for the determination of inelastic response. The program calculates the behavior of macro models in the inelastic range by the distributed flexibility models that are suitable for RC concrete elements and includes new hysteretic models upon which the validation tests were conducted. The assumption of floor diaphragms behaving as rigid horizontal links reduces the total computational effort. For more information about the program IDARC-2D capabilities and assumptions, the reader may refer to the technical report NCEER-96-0010 (Valles et al., 1996).

Table 2.6 briefs the response history analysis conducted in this study. The relationships between the global deformation demands (*MRDR* and *MIDR*) and the ground-motion intensity measures *(PGA, PGV* and $PS_a(T_1)$) are evaluated for 3 levels of nonlinear structural behavior: non-degrading, stiffness degrading and stiffness and strength degrading. Number of failures that occurred due to numerical stabilities in the solution algorithm or structural collapses within each level of nonlinear behavior and each model are also listed in the table. The built in tri-linear hysteretic model of IDARC is modified to simulate these nonlinear hysteretic behavior. The control parameters provided by IDARC-2D was used for this purpose. Table 2.7 lists the control parameters used for simulating various stiffness and strength degradation levels. The designated values of stiffness degradation (α), ductility and energy based strength degradation parameters (β_1 and β_2) as well as the slip control parameter (γ) are suggested by the IDARC manual that are verified by the test results of various structural members. As can be depicted from these tabulated values the strength degradation is governed by the energy dissipated during the cyclic excursions whereas the role of slip in the reinforcing bars is disregarded in the cyclic strength degradation of structural members.

Table 2.6 Response history analysis conducted in the study

3 STORY				5 STORY				7 STORY				9 STORY			
Model	**GM Used**	**Structural behavior**	**Failure in R.H.A.**	**Model**	**GM Used**	**Structural behavior**	**Failure in R.H.A.**	**Model**	**GM Used**	**Structural behavior**	**Failure in R.H.A.**	**Model**	**GM Used**	**Structural behavior**	**Failure in R.H.A.**
e1	Bin 1	ND	0 / 20	e1	Bin 1	ND	0 / 20	e1	Bin 1	ND	0 / 20	e1	Bin 1	ND	0 / 20
		SD	0 / 20			SD	0 / 20			SD	0 / 20			SD	0 / 20
		SSD	2 / 20			SSD	0 / 20			SSD	0 / 20			SSD	1 / 20
e2	Bin 2	ND	0 / 20	e2	Bin 2	ND	0 / 20	e2	Bin 2	ND	0 / 20	e2	Bin 2	ND	0 / 20
		SD	3 / 20			SD	4 / 20			SD	2 / 20			SD	0 / 20
		SSD	5 / 20			SSD	3 / 20			SSD	6 / 20			SSD	7 / 20
e3	Bin 1	ND	0 / 20	e3	Bin 1	ND	0 / 20	e3	Bin 1	ND	0 / 20	e3	Bin 1	ND	0 / 20
		SD	0 / 20			SD	0 / 20			SD	0 / 20			SD	0 / 20
		SSD	0 / 20			SSD	0 / 20			SSD	0 / 20			SSD	0 / 20
	Bin 2	ND	0 / 20		Bin 2	ND	0 / 20		Bin 2	ND	0 / 20		Bin 2	ND	0 / 20
		SD	1 / 20			SD	2 / 20			SD	1 / 20			SD	1 / 20
		SSD	2 / 20			SSD	1 / 20			SSD	5 / 20			SSD	7 / 20
	Bin 3	ND	0 / 20		Bin 3	ND	0 / 20		Bin 3	ND	0 / 20		Bin 3	ND	0 / 20
		SD	3 / 20			SD	8 / 20			SD	5 / 20			SD	3 / 20
		SSD	10 / 20			SSD	11 / 20			SSD	11 / 20			SSD	12 / 20
e1'	Bin 1	ND	0 / 20	e1'	Bin 1	ND	0 / 20	e1'	Bin 1	ND	0 / 20	e1'	Bin 1	ND	0 / 20
		SD	0 / 20			SD	0 / 20			SD	0 / 20			SD	0 / 20
		SSD	0 / 20			SSD	0 / 20			SSD	0 / 20			SSD	0 / 20
e2'	Bin 2	ND	1 / 20	e2'	Bin 2	ND	0 / 20	e2'	Bin 2	ND	0 / 20	e2'	Bin 2	ND	0 / 20
		SD	0 / 20			SD	1 / 20			SD	2 / 20			SD	0 / 20
		SSD	5 / 20			SSD	7 / 20			SSD	4 / 20			SSD	7 / 20

Abbreviations : ND - Nondegrading, SD - Stiffness degrading, SSD - Stiffness and strength degrading, GM - Ground motions
R.H.A - Response history analysis

Table 2.7 Hysteretic model parameters used in the analysis

Hysteretic Model Parameter	Non degrading (ND)	Stiffness Degrading (SD)	Stiffness and Strength Degrading (SSD)
α	200	4	4
β_1	0.01	0.01	0.6
β_2	0.01	0.01	0.01
γ	1	1	1

Pushover curves obtained from the inverse triangular lateral loading and their bilinear idealizations in compliance with the methodology presented in ATC 40 document (ATC, 1996) are presented for each model in Appendix B (Figures B1-B15). The pushover curve of each model is displayed both in terms of base shear coefficient (η) vs. roof displacement (Δ_{roof}) and acceleration vs displacement response spectrum (ADRS) formats. The expressions used for the ADRS format are also presented in ATC-40 (ATC, 1996). The maximum observed base shear and roof displacement pairs are compiled from response analysis are also superimposed on these plots to investigate whether the model buildings are mostly deformed under the first mode dominant structural behavior. Note that the response history analysis results that are superimposed in the global capacity curves (pushover curves) suggest that the building models are generally subjected to moderate to large lateral deformation demands except for the e1' building models. The deformation demands computed from the response history analysis of e1' model buildings are mostly within the elastic limits (Figures B.4, B.9 and B.14). This is quite expected because e1' model buildings are subjected to the records that contain the lowest *PGV*s (i.e. they mirror relatively the lowest hazard level). Contradictory to the e1, they are designed for the design spectrum that relatively represents the highest hazard level (i.e. for the ground motion bin with the highest *PGV* values. Although the existence of some significant differences between the pushover curves and maximum absolute η-Δ_{roof} pairs obtained from

response history analysis, the buildings seem to predominantly under the fundamental mode. The reason behind the conclusion is that for most cases as displayed in Appendix B, the maximum absolute η-Δ_{roof} scatter points follow the pushover curve patterns closely that are computed from the inverse triangular loading pretending to mimic fundamental mode global capacity. Thus, the succeeding discussion for the relationships between the chosen ground-motion intensity parameters and global deformation demands are confined to the building behavior deforming primarily under first mode response.

It should be noted that the influence of p-delta effect is not considered in the nonlinear response history analyses since a series of pushover analyses with different hysteretic behaviors resulted in a very similar global response curves with and without p-delta effects. This observation may also suggest that the IDARC-2D does not incorporate p-delta effects in the nonlinear structural response although the software seems to provide an option for the consideration of second order effects in nonlinear structural response.

The variation of three ground-motion intensity parameters (*PGA, PGV* and $PS_a(T_1)$) with global deformation demands (*MIDR* and *MRDR*) is presented in Figures 2.5 - 2.10 for frame type building behavior having fundamental periods between $0.60<T_1<1.3$ s. The scatter diagrams in Figure 2.5 and 2.6 display the performance of chosen ground-motion intensity parameters for non-degrading building behavior as a function of *MRDR* and *MIDR*, respectively. Figures 2.7 to 2.8 and 2.9 to 2.10 present similar comparisons for stiffness degrading and stiffness and strength degrading structural behavior, respectively. Each scatter diagram contains the nonlinear response history results of five different models (e1, e2, e3, e1' and e2') between the chosen IM's and demand parameters for frame buildings subjected to records associated with low-to-high amplitude peak motions and spectral quantities of their

fundamental periods. Note that the scatter plots do not present the nonlinear response history results when the model buildings showed collapse behavior or when IDARC-2D experienced numerical problems during the analysis stage. In each figure, the panels in the 1st, 2nd, 3rd and 4th rows display the scatter plots for 3, 5, 7 and 9 story models, respectively. Similarly, the three columns from left to right display the relationship between the chosen demand parameters with *PGA*, *PGV* and $PS_a(T_1)$, respectively. In general, the increase in intensity measures results in an increase in demand parameters. However the scatter (or dispersion) in the increasing trends is significant for some cases. Therefore, an unbiased statistical index is required to measure the correlation between the chosen IMs and the demand parameters. This is discussed in the next paragraph.

Spearman's non-parametric coefficient (ρ) is used to assess the correlation between the intensity measures and demand parameters (Equation 2.1). This correlation index does not assume a linear relationship between the variables. It also does not require any assumption about he frequency distribution of the variables (Press et al, 1989). These features make Spearman's coefficient more versatile then the conventional correlation coefficient parameter since the latter is only valid for normally distributed variables. High ρ values suggest higher correlation on the linearity between the variables under investigation. The Spearman's non-parametric coefficients are displayed on each panel in Figures 2.5 to 2.10.

$$\rho = 1 - \frac{6\sum d_i^2}{n(n^2 - 1)} \qquad (2.1)$$

d_i : the difference between each rank of corresponding values of x and y

n : number of pairs of values

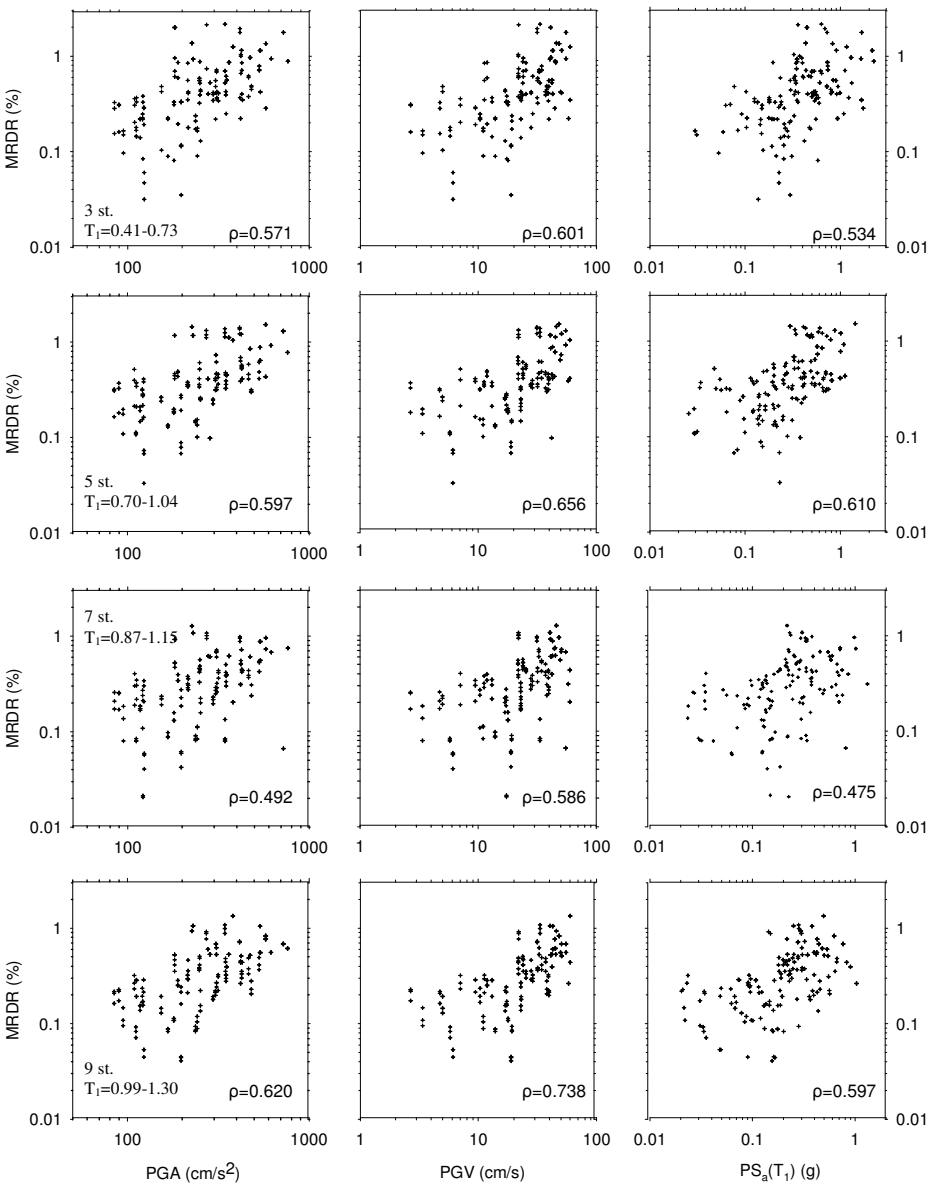

Figure 2.5 Variation of *MRDR* with *PGA*, *PGV* and $PS_a(T_1)$ for nondegrading building models

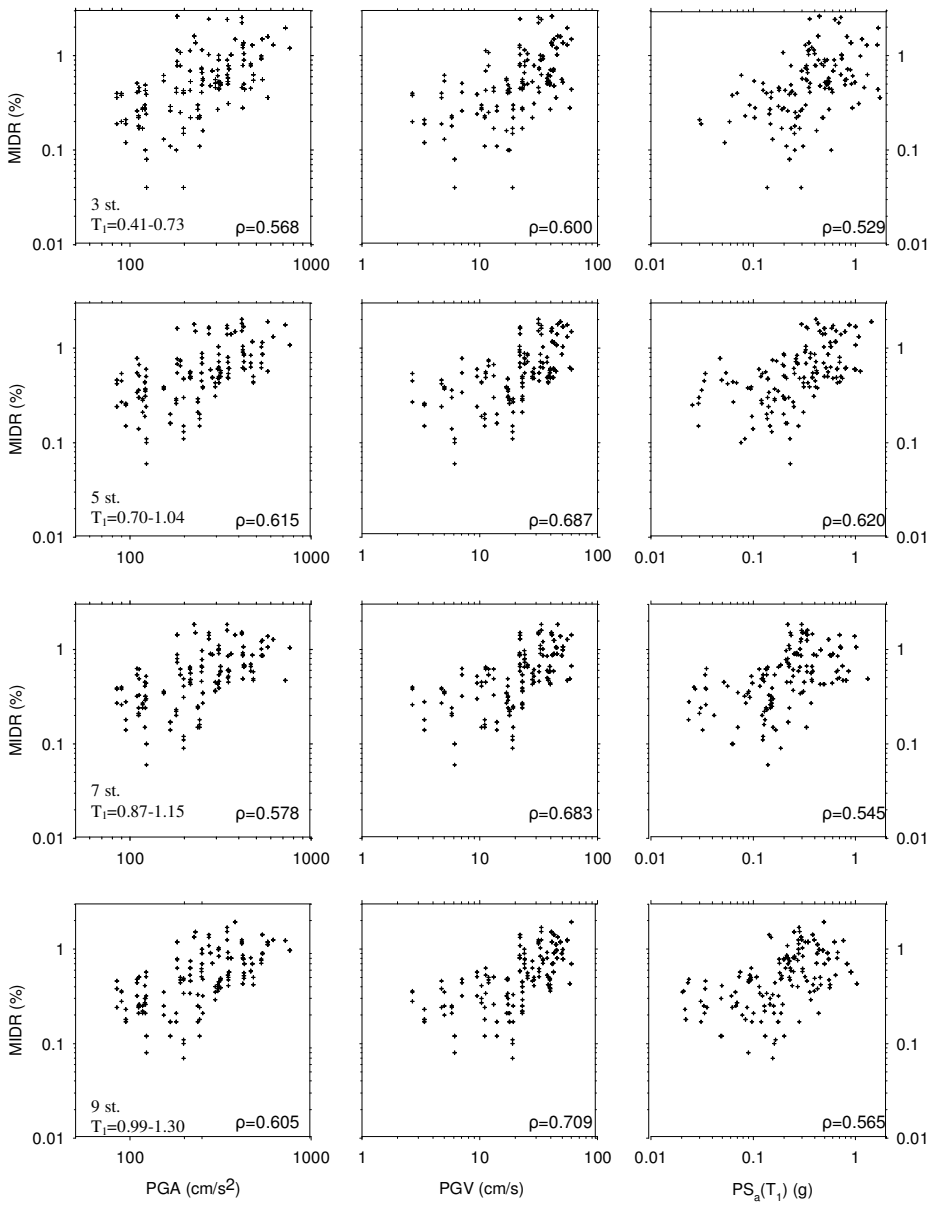

Figure 2.6 Variation of *MIDR* with *PGA*, *PGV* and $PS_a(T_1)$ for Nondegrading building models

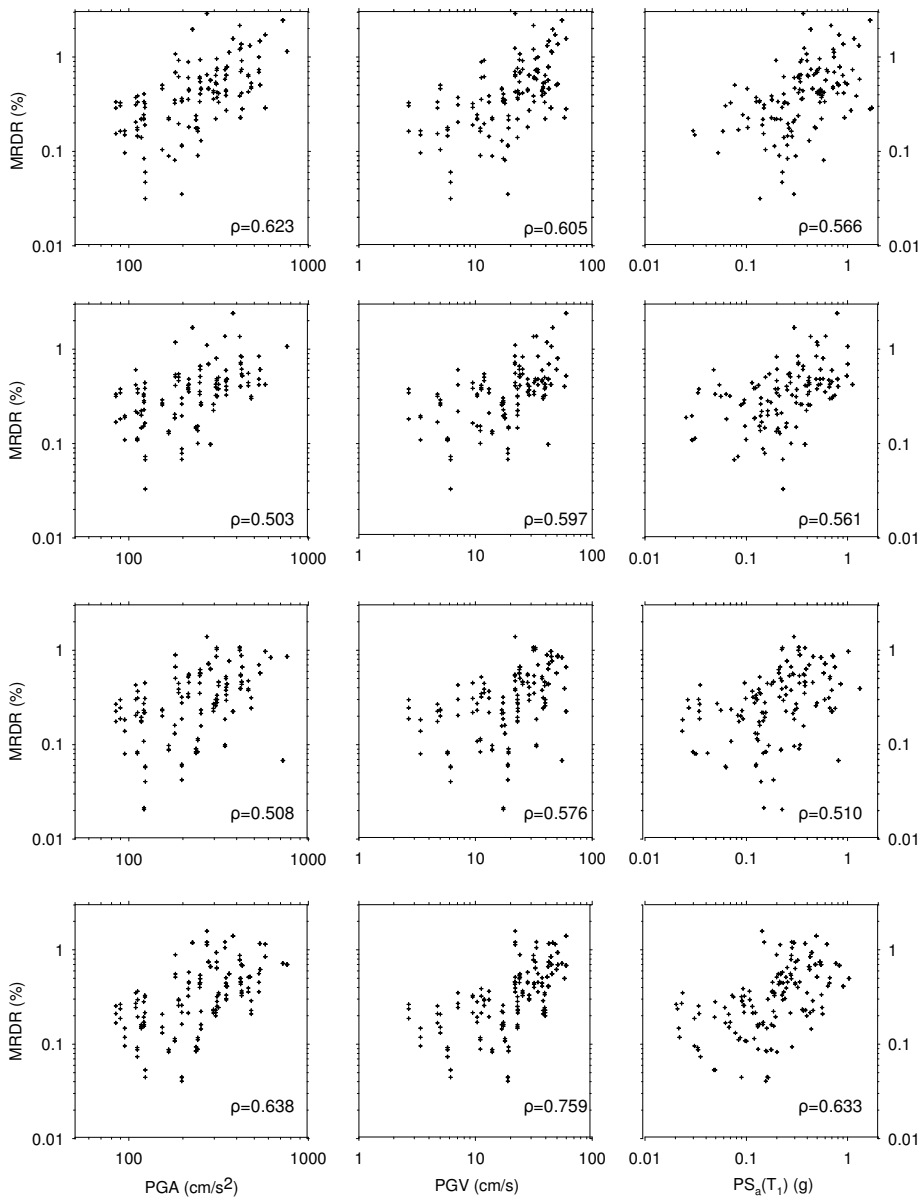

Figure 2.7 Variation of *MRDR* with *PGA*, *PGV* and $PS_a(T_1)$ in Stiffness degrading building models

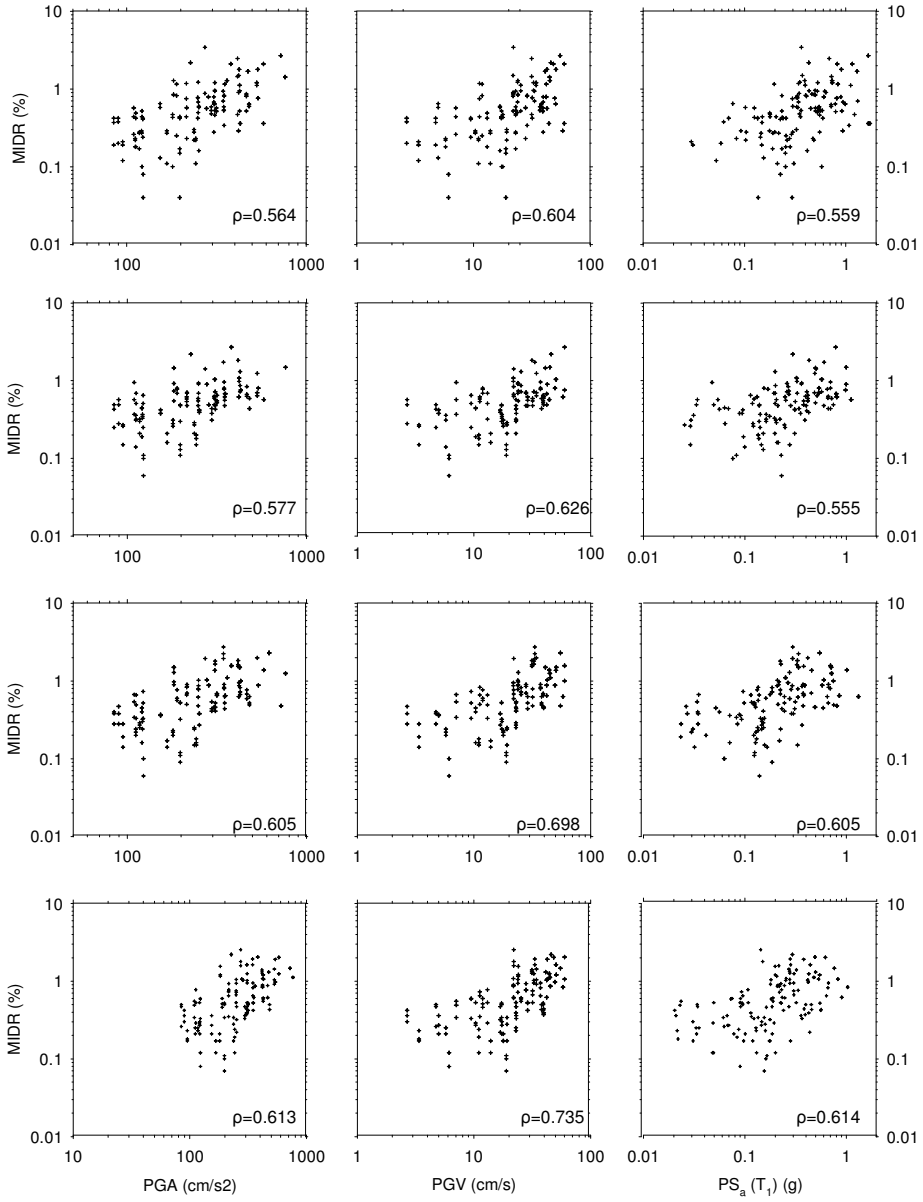

Figure 2.8 Variation of *MIDR* with *PGA, PGV* and $PS_a(T_1)$ for Stiffness degrading building models

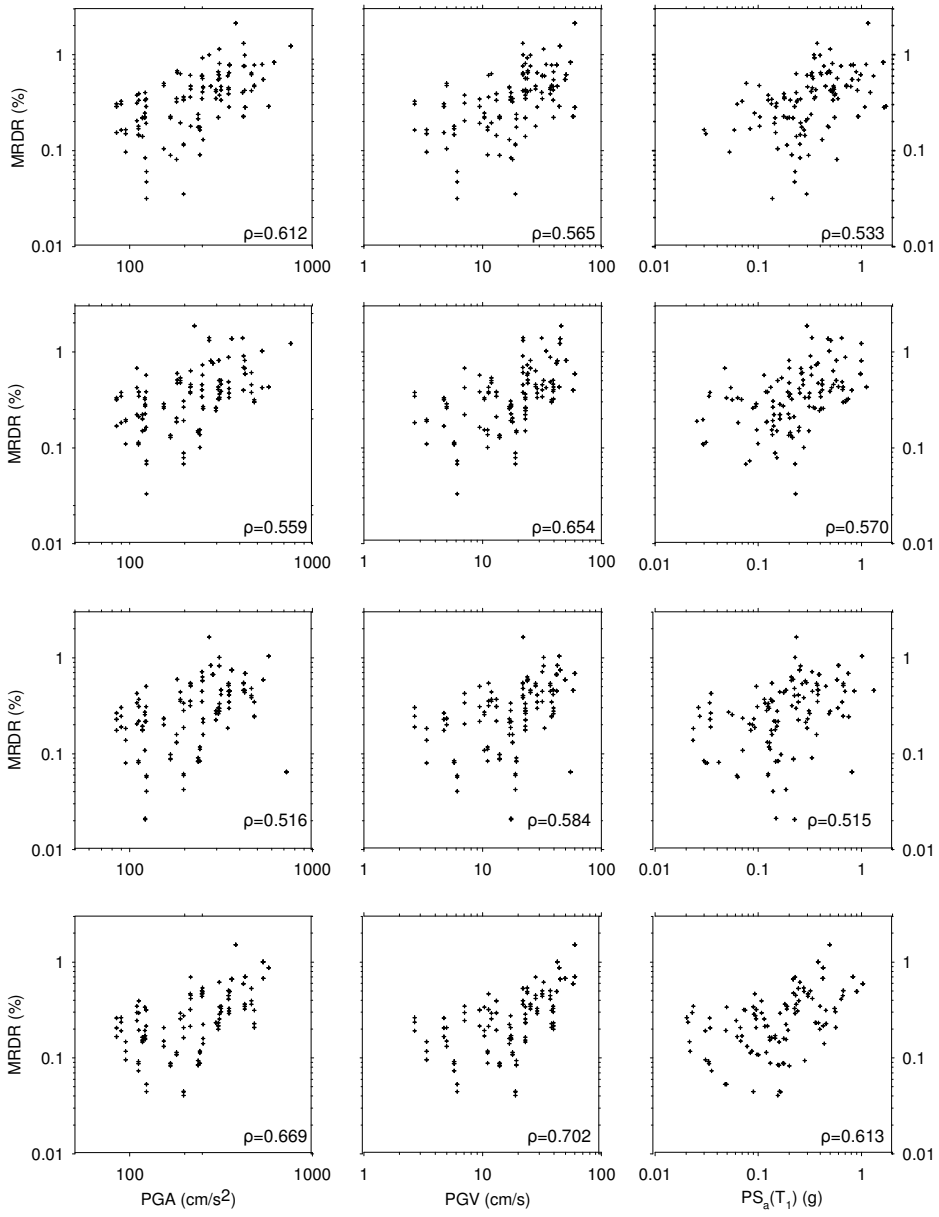

Figure 2.9 Variation of *MRDR* with *PGA*, *PGV* and $PS_a(T_1)$ for Stiffness and strength degrading building models

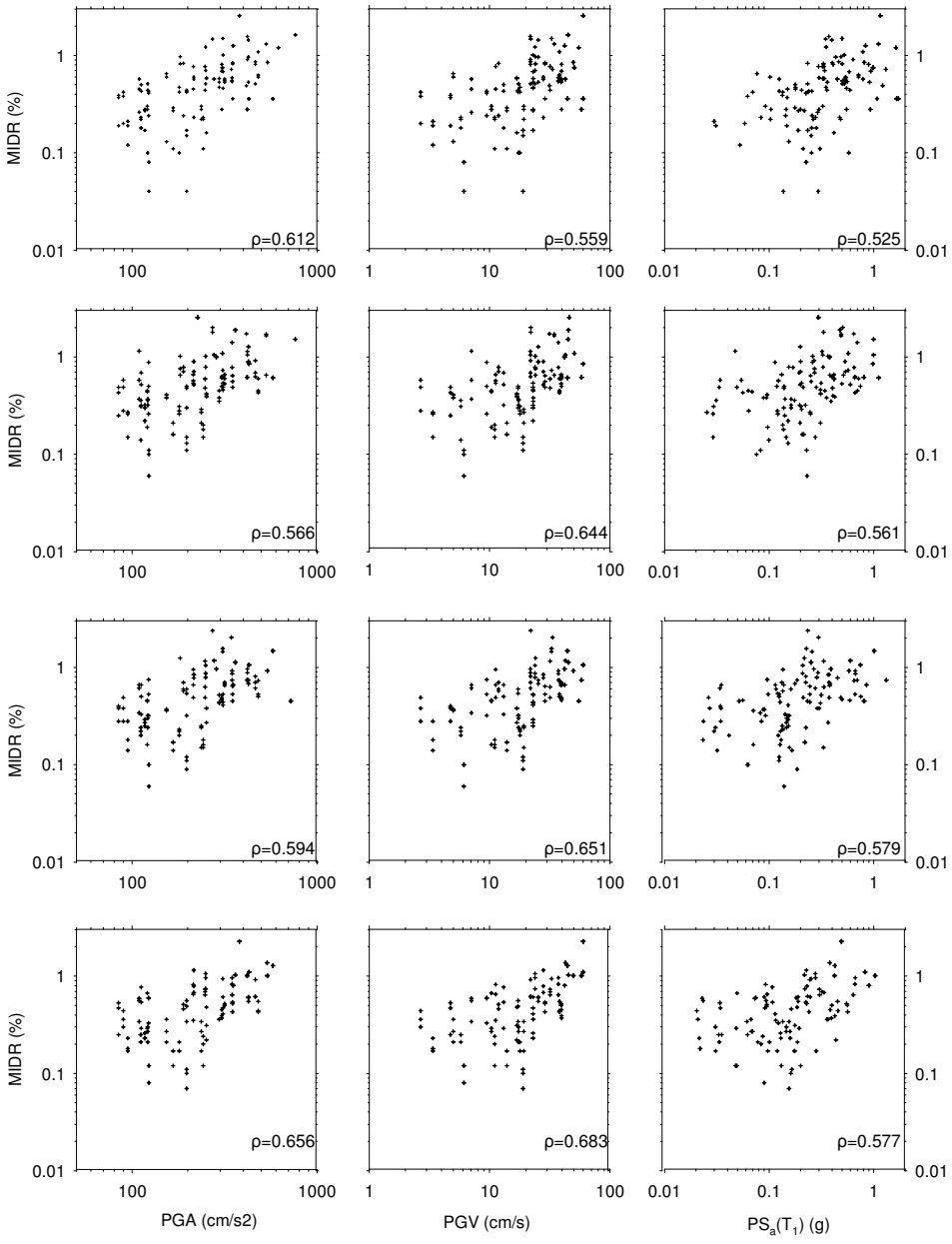

Figure 2.10 Variation of *MIDR* with *PGA, PGV* and $PS_a(T_1)$ for Stiffness and strength degrading building models

Table 2.8 and Figure 2.11 also display the computed ρ values to summarize the relationship between the chosen IMs and demand parameters in terms of this statistical index.

Table 2.8 Spearman's coefficient values (ρ) between intensity measures and global demand parameters under three different structural behavior

Structural Behavior	Intensity Measure	MRDR				MIDR			
		3 story	5 story	7 story	9 story	3 story	5 story	7 story	9 story
ND	PGA	0.571	0.597	0.492	0.620	0.568	0.615	0.578	0.605
	PGV	0.601	0.656	0.586	0.738	0.600	0.687	0.683	0.709
	PSA	0.534	0.610	0.475	0.597	0.529	0.620	0.545	0.565
SD	PGA	0.623	0.503	0.508	0.638	0.564	0.577	0.605	0.613
	PGV	0.605	0.597	0.576	0.759	0.604	0.626	0.698	0.735
	PSA	0.566	0.561	0.510	0.633	0.559	0.555	0.605	0.614
SSD	PGA	0.612	0.559	0.516	0.669	0.612	0.566	0.594	0.656
	PGV	0.565	0.654	0.584	0.702	0.559	0.644	0.651	0.683
	PSA	0.533	0.570	0.515	0.613	0.525	0.561	0.579	0.577

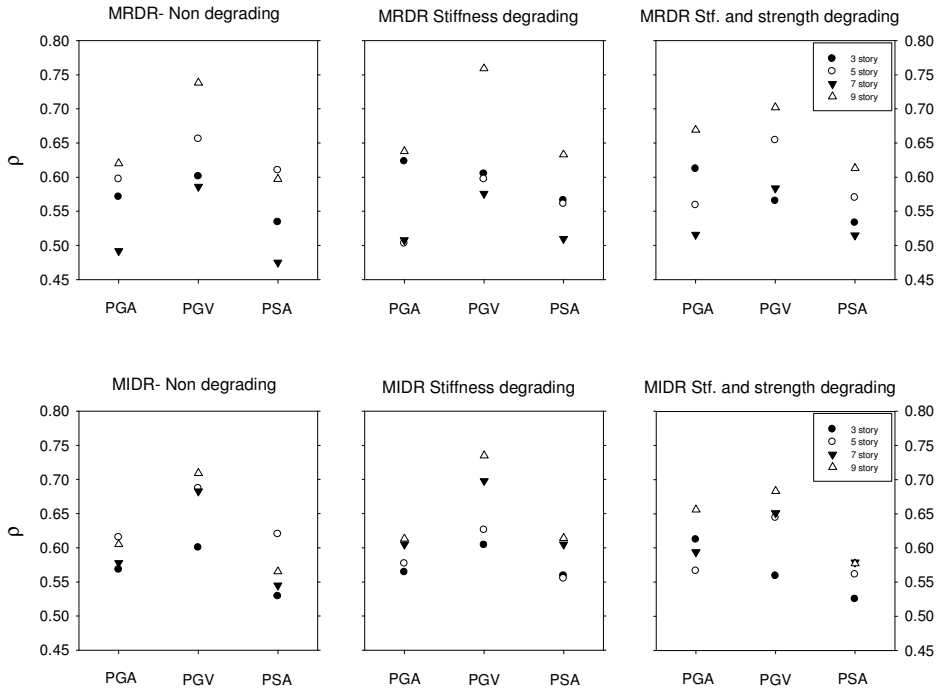

Figure 2.11 Comparison of the Spearman' s correlation coefficient values of ground motion intensity measures with global demand measures

The observations drawn from these figures and Table 2.8 are written below:

1. Regardless of the hysteretic behavior *ρ* values for *PGV* vs. *MRDR* and *PGV* vs. *MIDR* tend to increase with increasing story number.

2. When *ρ* values computed for all three ground-motion intensity measures are considered, those associated with *PGV* are larger than those computed for *PGA* and $PS_a(T_1)$.

3. When *PGA* vs. *MRDR* and *PGA* vs. *MIDR* relationships are of concern, there is no clear relationship between the associated ρ values and the story number.

4. There seems to be a consistent trend between ρ and story number when $PS_a(T_1)$ vs. *MRDR* and $PS_a(T_1)$ vs. *MIDR* relationships are evaluated. However, the associated ρ values generally attain smaller values with respect to those computed for *PGV* and *PGA*. For this particular *IM*, the consistent increase in *ρ* with the increasing story number may advocate that the building models predominantly behave under the fundamental mode influence. This is because many researchers (e.g. Curballa et al, 2002) stated that $PS_a(T_1)$ is not a good indicator of damage for studies that are dominated by higher mode effects.

The general tendency of increase in the correlation values of *PGA* and *MRDR* is distinguishable with the increasing story numbers except for 5 story model. Similar observation is valid for *PGA* and *MIDR* relation. However, the relation of *PGV* with *MRDR* reveals a clear decrease in stiffness degrading case for 5 and 7 story models when the different

degrading situations are considered whereas higher values are seen for 3 and 9 stories. A different situation is noted for *PGV-MIDR* relation. The value of 5 story is lower in stiffness degrading case, while those of the other story models are higher than ρ values of other degradation situations. The variation of $PS_a(T_1)$ with *MRDR* and *MIDR* exhibits similarities. For 3, 5 and 9 story models, ρ value increases in general sense and highest correlation values among different structural behaviors are observed in stiffness degrading case.

Note that some of the observations indicated above are open to further discussion. In general, *PGA* is generally referred to as a poor indicator of structural damage that is closely related to *MRDR* and *MIDR*. However, the results presented in this study show that there seems to be no appreciable differences between the performance of *PGA* and $PS_a(T_1)$ when establishing relationships with these *IM*s and the demand parameters considered. Moreover, the analyses presented here indicate that *PGV* is a better indicator of the deformation demand than *PGA* and $PS_a(T_1)$ that is also questioned by some recent studies (e.g. Yılmaz, 2007; Riddell, 2007).

The conclusions made in this chapter are confined to the ground-motion database used by Akkar and Özen (2005) and the building models presented. These findings should be verified by other studies for different ground-motion datasets and for different building models in order to investigate the disagreements between this study and other studies. Nevertheless, the good performance of *PGV* with respect to the other two IMs studied in this chapter stimulated this study to propose regression models for *PGV* to estimate inelastic oscillator displacement demands. This is described in detail in the next chapter.

CHAPTER 3

ESTIMATION OF INELASTIC SPECTRAL DISPLACEMENTS AS A FUNCTION OF PEAK GROUND VELOCITY

3.1 Introduction

The limited number of statistical results presented in Chapter 2 suggested that *PGV* can be considered as a candidate intensity measure for bridging the gaps between earthquake hazard and deformation demands on structural systems. This chapter presents a simple predictive model that can be used in estimating peak oscillator displacements as a function of *PGV*. The predictive model can be used for estimating constant ductility (μ) and normalized lateral strength (R) spectral displacements for a given initial oscillator periods. The constant ductility and normalized lateral strength displacement spectra can be used for design and seismic performance evaluation of structural systems (FEMA-356, ATC-40, FEMA- 44, Fajfar, 2000). The succeeding sections of this chapter first describe the regression model and then present a simple case study to show its implementation.

3.2 Regression Analysis

The general mathematical model for estimating the peak nonlinear oscillator displacement ($S_{d,ie}$) for a given μ or R value is given in Eq. (3.1).

$$S_{d,ie}\Big|_{R,\mu} = f(\theta) \cdot PGV \cdot T \tag{3.1}$$

The functional form f in Eq. (3.1) considers the influence of independent ground-motion parameters (θ) such as magnitude**,** distance, site class etc. for the estimation of $S_{d,ie}$. The regression analysis was conducted on the dimensionless dependent variable $S_{d,ie}/(PGV \times T)$ because this parameter resulted in a simpler predictive model as discussed in the next paragraphs. The influence of independent ground-motion parameters on the predicted parameter was investigated by studying the behavior of $S_{d,e}/(PGV \times T)$ that is the elastic response version of the predicted parameter. Some recent ground-motion prediction equations (GMPEs) that estimate both PGV and $S_{d,e}$ were used to achieve this objective.

The main assumption in this sensitivity analysis is that the general behavior of the predicted parameter will have a similar (but not the same) pattern both in the linear and nonlinear oscillator response. Figure 3.1 shows the comparative results from two recent GMPEs that are derived by Akkar and Bommer (2007a, 2007b) and Boore and Atkinson (2007). Functional forms and brief information about the prediction equations are given in Appendix C. These GMPEs are abbreviated as AB07 and BA07, respectively. The figures on the left display the results computed from AB07 whereas the pertaining results of BA07 are presented on the right hand side. The AB07 prediction equations were derived from a recently compiled European ground-motion database. The BA07 GMPE uses a worldwide ground-motion dataset that is compiled for Next Generation Attenuation (NGA) project. Both studies estimate the spectral and peak ground-motion quantities with certain differences in their functional forms. For example BA07 considers the nonlinear soil effects as a function of $V_{s,30}$ whereas AB07 does not account for soil nonlinearity in the predictive model. The first row in Figure 3.1 shows the influence of distance metric (R_{jb}) on $S_{d,e}/(PGV \times T)$ for the magnitude range of interest in this study. The

figures on the left and right panels display 3 set of curves for oscillator periods of T = 0.5, 1.0 and 2.0 s and each set compares 3 distinct R_{jb} distances (i.e. R_{jb} = 10, 20 and 30 km) for a given oscillator period.

The discrete T and R_{jb} values presented fairly cover the period and distance ranges in this study. All plots are produced for strike-slip events. The comparative plots show that for short-period oscillator response (T = 0.5 s) both GMPEs describe a slight departure for the R_{jb} = 10 km curve with respect to the R_{jb} = 20 and 30 km curves in the small magnitude range. As far as the long-period oscillator response (T = 2.0 s) is concerned, the AB07 curves follow a trend similar to the one described for T = 0.5 s whereas BA07 curves almost overlap each other for all R_{jb} distances. The differences between the GMPEs for T = 2.0 s may arise from their distinct magnitude scaling functional forms. The GMPEs considered do not show a distance-wise sensitivity for T = 1.0 s. Although it is crude, these observations may lead to an assumption that the discrepancies on $S_{d,e}/(PGV \times T)$ emerging from distance variation are secondary when compared to the magnitude influence. The second row in Figure 3.1 shows the significance of site class on $S_{d,e}/(PGV \times T)$. NEHRP site classes C and D are considered in the comparative plots as the ground-motion dataset consists of records from these site categories.

Akkar and Bommer (2007a, 2007b) classified NEHRP C and D site classes as stiff and soft soils, respectively. Boore and Atkinson (2007) does not use a specific site classification since their predictive model directly uses the $V_{s,30}$ values. For illustrative purposes $V_{s,30}$ = 450 m/s and 270 m/s are used in BA07 to represent stiff and soft soil sites, respectively. Each panel displays 3 sets of $S_{d,e}/(PGV \times T)$ vs. R_{jb} curves computed for T = 0.5, 1.0 and 2.0 s. Each set corresponds to a particular oscillator period and shows the variation in $S_{d,e}/(PGV \times T)$ for

stiff and soft sites, respectively. In order not to crowd the figures AB07 predictions were used for displaying the results for **M** = 7 whereas BA07 was used to illustrate the results from small magnitude events mimicked by **M** = 5. Similar to the first row plots, the style-of-faulting is strike-slip in these figures.

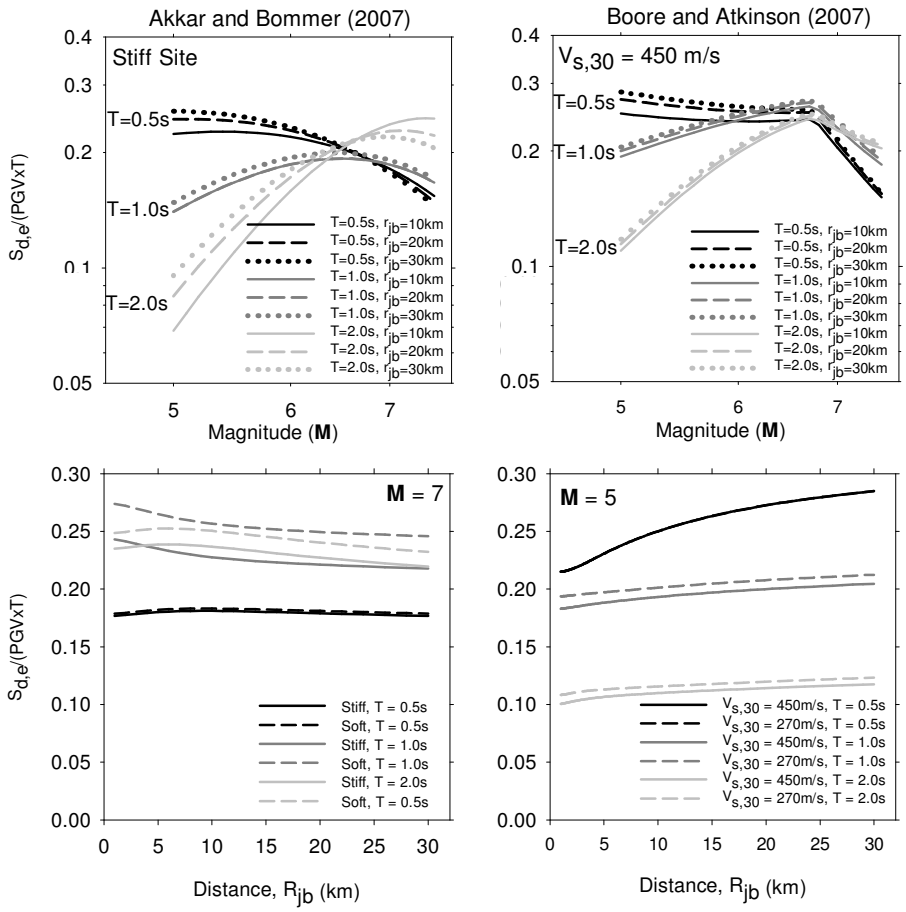

Figure 3.1. Influence of certain ground-motion parameters on $S_{d,e}/(PGV \times T)$.

Although there is a departure in $S_{d,e}/(PGV \times T)$ between soft and stiff soil sites for large magnitude and mid-period values (T = 1.0 s), the general picture from these plots may also advocate that magnitude is a more

prominent parameter than the site class in the variation of $S_{d,e}/(PGV \times T)$. Similar type of plots presented in Figure 3.1 was also computed for normal and reverse faulting. The observations are comparable to those presented for strike-slip faults based on these discussions, it is decided to consider the magnitude term as the only explanatory variable in the predictive model.

The quadratic variation of magnitude was selected for the proposed model that seems to adequately capture the variation of dimensionless dependent variable for the overall magnitude range when AB07 is considered. The quadratic magnitude variation is also reasonable for the trends revealed by BA07 for **M** ≤ 6.7. BA07 shows a sharp linear decay for **M** > 6.7 (called as "hinging effect" by the proponents) due to the magnitude scaling terms in the model that prevent oversaturation in the predicted ground-motion variable. It should be noted that the sole consideration of magnitude influence is rough and at the expense of sophistication a more complete model should contain the rest of the independent ground-motion parameters that are omitted in this study. In their predictive model Tothong and Cornell (2006) also considered magnitude as the only explanatory variable indicating that other seismological independent parameters are not as influential as magnitude in the estimation of $S_{d,ie}$. The final functional form used in the regression analyses is presented in Eq. (3.2).

$$\ln\left(\frac{S_{d,ie|R,\mu}}{PGV \times T}\right) = b_0 + b_1 M + b_2 M^2 + \varepsilon \cdot \sigma \qquad (3.2)$$

In the above expression b_0, b_1 and b_2 are the predictive variables to be determined from the regression analysis. The last term is the random

error term and it accounts for the variability in the dependent parameter due to the unconsidered predictor parameters in the model.

This term corresponds to the difference between the estimated and observed dependent variable that is called the residual in the regression analysis. If the fitted model correctly accounts for the variation of the observed data, the residual mean square is the unbiased estimator of the variance (σ^2) about the regression. However, if the model fails to explain the variation of observed data, the residuals contain both random and systematic errors due to model inadequacy resulting in biased σ^2 calculated from the residual mean square (Drapper and Smith, 1981). The ε in Eq. (3.2) denotes the number of standard deviations (σ) above or below the expected value of dependent variable.

There are number of regression techniques to estimate the predictive variables of a functional form. In this study the least squares regression was used that would estimate the same predictive variables as of maximum likelihood regression method given the random error terms are normally distributed with zero mean and σ^2 (Myers, 1986). This condition is satisfied here as discussed in the succeeding paragraphs. The regressions were done by period-by-period for 0.2s $\leq T \leq$ 2.0s with increments of 0.1 s. The inelastic oscillator displacements are estimated at 8 distinct μ and R values (i.e. μ or R = 1.5, 2, 3, 4, 5, 6, 7 and 8) for bilinear hysteretic model associated with 0% and 5% postyield stiffness ratio (α). The initial damping was taken as 5% of critical in all nonlinear oscillator responses. Tables 3.1-3.4 present four sets of regression coefficients in terms of μ and R as well as for the α values stated above.

Table 3.1 Regression coefficients for constant μ peak inelastic oscillator displacements when α = 0%

	μ = 1.5				μ = 2.0				μ = 3				μ = 4			
T (s)	b_0	b_1	b_2	σ	b_0	b_1	b_2	σ	b_0	b_1	b_2	σ	b_0	b_1	b_2	σ
0.2	-7.841	2.220	-0.204	0.451	-7.585	2.135	-0.195	0.431	-6.522	1.800	-0.166	0.368	-5.624	1.526	-0.142	0.358
0.3	-3.547	0.837	-0.085	0.371	-1.322	0.107	-0.025	0.361	-1.763	0.222	-0.029	0.330	-2.245	0.411	-0.045	0.315
0.4	-2.906	0.656	-0.069	0.368	-3.888	0.931	-0.087	0.330	-2.824	0.585	-0.057	0.297	-1.973	0.334	-0.037	0.279
0.5	-7.760	2.098	-0.172	0.327	-5.573	1.404	-0.117	0.300	-3.059	0.654	-0.060	0.306	-3.419	0.783	-0.070	0.292
0.6	-1.860	0.185	-0.018	0.348	-1.880	0.150	-0.012	0.318	-1.564	0.106	-0.011	0.311	-1.783	0.163	-0.013	0.298
0.7	-2.447	0.343	-0.028	0.342	-1.612	0.038	-0.001	0.331	-2.814	0.406	-0.028	0.353	-3.033	0.448	-0.027	0.334
0.8	-1.063	-0.121	0.010	0.343	-2.435	0.261	-0.016	0.323	-3.730	0.687	-0.049	0.337	-2.468	0.259	-0.013	0.343
0.9	-1.370	-0.113	0.016	0.351	-0.457	-0.397	0.037	0.337	-3.384	0.533	-0.035	0.337	-4.146	0.729	-0.046	0.345
1.0	-0.172	-0.490	0.045	0.340	1.668	-1.046	0.086	0.347	-3.184	0.376	-0.016	0.343	-6.418	1.362	-0.090	0.355
1.1	-0.979	-0.283	0.032	0.349	-3.590	0.509	-0.028	0.334	-7.184	1.588	-0.107	0.339	-9.271	2.241	-0.157	0.350
1.2	-3.702	0.482	-0.022	0.367	-7.283	1.619	-0.111	0.370	-10.673	2.656	-0.189	0.370	-10.053	2.443	-0.170	0.380
1.3	-5.969	1.190	-0.077	0.395	-6.517	1.358	-0.090	0.399	-9.690	2.333	-0.164	0.395	-8.921	2.052	-0.138	0.399
1.4	-6.199	1.195	-0.073	0.381	-6.225	1.222	-0.077	0.378	-9.002	2.052	-0.137	0.423	-8.391	1.891	-0.127	0.408
1.5	-4.936	0.712	-0.029	0.389	-5.305	0.847	-0.041	0.393	-10.073	2.352	-0.159	0.415	-7.012	1.360	-0.079	0.431
1.6	-6.997	1.356	-0.080	0.404	-7.248	1.391	-0.080	0.400	-7.326	1.425	-0.083	0.424	-5.470	0.843	-0.038	0.459
1.7	-7.233	1.414	-0.084	0.427	-7.325	1.445	-0.087	0.418	-7.608	1.558	-0.099	0.441	-5.228	0.749	-0.030	0.464
1.8	-8.038	1.653	-0.102	0.423	-6.752	1.248	-0.072	0.427	-6.545	1.184	-0.067	0.447	-4.348	0.408	0.001	0.466
1.9	-9.438	2.079	-0.135	0.437	-7.387	1.414	-0.082	0.446	-5.455	0.777	-0.031	0.451	-4.653	0.463	-0.001	0.476
2.0	-7.904	1.565	-0.093	0.444	-7.251	1.321	-0.072	0.470	-4.439	0.390	0.004	0.465	-4.183	0.324	0.008	0.489

	μ = 5.0				μ = 6.0				μ = 7.0				μ = 8.0			
T (s)	b_0	b_1	b_2	σ	b_0	b_1	b_2	σ	b_0	b_1	b_2	σ	b_0	b_1	b_2	σ
0.20	-5.564	1.520	-0.139	0.343	-5.276	1.446	-0.133	0.336	-5.069	1.387	-0.127	0.324	-4.757	1.297	-0.118	0.317
0.30	-2.306	0.453	-0.048	0.308	-2.120	0.415	-0.045	0.298	-2.323	0.491	-0.050	0.291	-3.808	0.942	-0.083	0.281
0.40	-1.845	0.280	-0.030	0.275	-1.397	0.146	-0.018	0.272	-0.691	-0.076	0.000	0.279	-0.813	-0.037	-0.002	0.282
0.50	-2.103	0.365	-0.036	0.290	-0.642	-0.106	0.003	0.294	-1.583	0.166	-0.016	0.304	-0.939	-0.036	0.001	0.317
0.60	-1.504	0.054	-0.002	0.314	-1.429	0.026	0.002	0.326	-2.930	0.485	-0.032	0.330	-3.377	0.636	-0.044	0.332
0.70	-2.082	0.156	-0.004	0.335	-2.117	0.160	-0.003	0.335	-2.006	0.108	0.003	0.332	-2.013	0.115	0.003	0.332
0.80	-1.693	-0.016	0.012	0.346	-3.299	0.508	-0.030	0.347	-4.618	0.913	-0.060	0.352	-4.754	0.955	-0.063	0.359
0.90	-4.724	0.926	-0.061	0.344	-6.363	1.418	-0.097	0.339	-8.393	2.023	-0.141	0.339	-9.169	2.251	-0.157	0.346
1.00	-7.568	1.719	-0.116	0.352	-9.540	2.317	-0.160	0.352	-9.462	2.273	-0.155	0.359	-10.330	2.541	-0.175	0.362
1.10	-10.401	2.552	-0.178	0.361	-11.002	2.730	-0.190	0.372	-10.290	2.497	-0.171	0.385	-9.687	2.301	-0.155	0.407
1.20	-10.235	2.466	-0.169	0.386	-9.871	2.321	-0.155	0.405	-8.620	1.912	-0.121	0.425	-8.046	1.734	-0.108	0.431
1.30	-7.793	1.660	-0.104	0.403	-8.139	1.745	-0.109	0.432	-7.299	1.476	-0.087	0.455	-6.607	1.256	-0.070	0.456
1.40	-7.282	1.473	-0.089	0.439	-6.111	1.081	-0.056	0.459	-5.730	0.946	-0.044	0.469	-5.305	0.796	-0.031	0.470
1.50	-4.805	0.638	-0.021	0.460	-5.097	0.735	-0.029	0.478	-4.757	0.610	-0.017	0.485	-4.236	0.428	-0.001	0.486
1.60	-4.245	0.454	-0.007	0.472	-3.788	0.291	0.008	0.475	-3.693	0.233	0.015	0.471	-3.444	0.140	0.023	0.456
1.70	-3.974	0.316	0.007	0.464	-3.443	0.126	0.024	0.463	-2.435	-0.195	0.050	0.446	-4.467	0.464	-0.004	0.452
1.80	-3.018	-0.028	0.037	0.468	-2.642	-0.145	0.046	0.459	-4.346	0.395	0.003	0.457	-4.032	0.299	0.011	0.462
1.90	-3.680	0.161	0.022	0.477	-3.114	0.006	0.033	0.473	-3.777	0.206	0.018	0.477	-2.932	-0.068	0.041	0.478
2.00	-3.232	0.012	0.034	0.491	-2.630	-0.177	0.049	0.485	-2.757	-0.143	0.047	0.489	-4.728	0.456	0.002	0.483

Table 3.2. Regression coefficients for constant μ peak inelastic oscillator displacements when $\alpha = 5\%$

	μ = 1.5				μ = 2.0				μ = 3				μ = 4			
T (s)	b_0	b_1	b_2	σ	b_0	b_1	b_2	σ	b_0	b_1	b_2	σ	b_0	b_1	b_2	σ
0.2	-8.054	2.281	-0.209	0.448	-7.669	2.153	-0.197	0.427	-7.044	1.938	-0.176	0.361	-6.586	1.797	-0.162	0.342
0.3	-3.580	0.847	-0.086	0.372	-2.082	0.340	-0.044	0.358	-3.075	0.664	-0.068	0.317	-3.580	0.835	-0.080	0.297
0.4	-3.031	0.690	-0.071	0.367	-4.262	1.039	-0.096	0.320	-3.315	0.729	-0.069	0.296	-3.212	0.701	-0.066	0.273
0.5	-8.143	2.210	-0.180	0.328	-5.764	1.467	-0.123	0.301	-4.657	1.145	-0.099	0.290	-3.621	0.808	-0.071	0.262
0.6	-1.878	0.186	-0.018	0.345	-1.504	0.034	-0.004	0.311	-1.560	0.073	-0.008	0.294	-2.670	0.414	-0.033	0.281
0.7	-2.416	0.336	-0.028	0.338	-0.861	-0.192	0.016	0.317	-4.599	0.946	-0.070	0.318	-3.020	0.460	-0.032	0.314
0.8	-1.603	0.031	-0.001	0.341	-2.027	0.122	-0.005	0.316	-3.197	0.484	-0.033	0.314	-2.398	0.219	-0.010	0.318
0.9	-1.123	-0.197	0.022	0.351	-1.198	-0.164	0.018	0.336	-2.981	0.396	-0.025	0.317	-3.856	0.624	-0.039	0.328
1.0	-0.119	-0.508	0.046	0.336	0.875	-0.809	0.068	0.334	-5.011	0.938	-0.061	0.323	-8.216	1.947	-0.139	0.319
1.1	-2.179	0.103	0.001	0.344	-3.731	0.539	-0.030	0.327	-8.425	1.982	-0.141	0.332	-9.209	2.224	-0.159	0.340
1.2	-3.716	0.489	-0.023	0.365	-7.698	1.750	-0.122	0.355	-10.012	2.453	-0.176	0.354	-9.703	2.320	-0.163	0.364
1.3	-6.557	1.369	-0.091	0.380	-6.005	1.196	-0.078	0.385	-10.417	2.536	-0.180	0.369	-10.525	2.524	-0.175	0.379
1.4	-5.850	1.089	-0.065	0.374	-6.563	1.320	-0.085	0.368	-9.043	2.051	-0.138	0.384	-9.690	2.224	-0.150	0.386
1.5	-5.859	1.020	-0.055	0.384	-5.662	0.954	-0.050	0.382	-9.201	2.062	-0.137	0.394	-8.281	1.743	-0.110	0.405
1.6	-7.067	1.377	-0.082	0.404	-6.912	1.273	-0.070	0.393	-8.042	1.664	-0.105	0.417	-6.170	1.054	-0.056	0.421
1.7	-7.661	1.538	-0.093	0.427	-6.941	1.315	-0.077	0.415	-7.534	1.507	-0.094	0.424	-6.483	1.117	-0.059	0.425
1.8	-8.071	1.661	-0.103	0.419	-7.395	1.460	-0.090	0.424	-7.529	1.468	-0.088	0.419	-6.744	1.166	-0.061	0.425
1.9	-9.422	2.084	-0.137	0.434	-7.358	1.412	-0.084	0.442	-7.840	1.515	-0.089	0.432	-6.729	1.133	-0.057	0.430
2.0	-8.101	1.630	-0.099	0.444	-7.557	1.428	-0.082	0.460	-7.489	1.389	-0.079	0.437	-5.570	0.745	-0.026	0.446
	μ = 5.0				μ = 6.0				μ = 7.0				μ = 8.0			
T (s)	b_0	b_1	b_2	σ	b_0	b_1	b_2	σ	b_0	b_1	b_2	σ	b_0	b_1	b_2	σ
0.2	-6.216	1.685	-0.151	0.323	-5.582	1.497	-0.136	0.309	-5.222	1.393	-0.127	0.285	-5.088	1.352	-0.122	0.275
0.3	-4.541	1.148	-0.104	0.280	-4.906	1.275	-0.113	0.269	-4.769	1.235	-0.109	0.258	-4.389	1.108	-0.098	0.250
0.4	-2.612	0.505	-0.049	0.264	-2.937	0.597	-0.054	0.254	-3.328	0.713	-0.062	0.242	-3.828	0.856	-0.071	0.238
0.5	-2.961	0.590	-0.053	0.254	-3.549	0.749	-0.062	0.254	-5.355	1.279	-0.100	0.252	-5.339	1.262	-0.097	0.248
0.6	-4.494	0.971	-0.075	0.281	-4.573	0.993	-0.075	0.272	-4.907	1.092	-0.082	0.263	-5.344	1.212	-0.090	0.264
0.7	-3.886	0.734	-0.053	0.307	-3.147	0.503	-0.035	0.291	-3.754	0.661	-0.044	0.294	-4.305	0.838	-0.058	0.279
0.8	-2.470	0.240	-0.012	0.313	-4.513	0.897	-0.064	0.301	-5.985	1.349	-0.098	0.294	-7.594	1.816	-0.131	0.295
0.9	-6.066	1.326	-0.094	0.302	-7.747	1.851	-0.134	0.312	-8.450	2.056	-0.149	0.308	-9.107	2.237	-0.161	0.314
1.0	-8.866	2.151	-0.155	0.317	-9.487	2.320	-0.166	0.319	-10.491	2.617	-0.187	0.331	-10.423	2.574	-0.182	0.338
1.1	-9.862	2.399	-0.170	0.341	-9.417	2.245	-0.157	0.343	-9.560	2.273	-0.158	0.353	-10.369	2.501	-0.174	0.361
1.2	-9.992	2.386	-0.166	0.360	-9.296	2.141	-0.145	0.367	-9.065	2.054	-0.137	0.376	-9.440	2.145	-0.142	0.381
1.3	-10.172	2.374	-0.160	0.381	-9.827	2.248	-0.149	0.396	-8.291	1.748	-0.110	0.392	-8.063	1.657	-0.101	0.387
1.4	-9.815	2.214	-0.145	0.397	-7.788	1.558	-0.093	0.400	-7.233	1.375	-0.078	0.394	-7.715	1.513	-0.088	0.388
1.5	-6.821	1.248	-0.069	0.413	-6.630	1.167	-0.062	0.405	-7.084	1.299	-0.071	0.397	-7.265	1.343	-0.074	0.397
1.6	-6.482	1.115	-0.058	0.422	-6.361	1.056	-0.052	0.413	-6.106	0.957	-0.043	0.407	-6.692	1.122	-0.054	0.404
1.7	-6.316	1.032	-0.050	0.419	-5.932	0.888	-0.037	0.411	-5.874	0.848	-0.032	0.410	-6.080	0.899	-0.036	0.410
1.8	-6.046	0.912	-0.039	0.411	-5.761	0.807	-0.030	0.412	-5.951	0.846	-0.031	0.414	-6.545	1.025	-0.045	0.415
1.9	-5.149	0.608	-0.014	0.424	-5.785	0.795	-0.028	0.419	-6.011	0.847	-0.031	0.415	-7.686	1.380	-0.073	0.416
2.0	-4.814	0.480	-0.003	0.433	-5.510	0.681	-0.018	0.416	-7.144	1.192	-0.057	0.416	-8.008	1.462	-0.079	0.414

Table 3.3. Regression coefficients for constant *R* peak inelastic oscillator displacements when $\alpha = 0\%$

	R = 1.5				R = 2.0				R = 3				R = 4			
T (s)	b_0	b_1	b_2	σ	b_0	b_1	b_2	σ	b_0	b_1	b_2	σ	b_0	b_1	B_2	σ
0.2	-8.420	2.431	-0.221	0.441	-7.523	2.191	-0.201	0.417	1.684	-0.863	0.059	0.414	3.620	-1.554	0.125	0.448
0.3	-4.203	1.047	-0.101	0.382	-2.061	0.333	-0.040	0.346	-0.845	-0.092	0.001	0.398	-0.025	-0.371	0.028	0.407
0.4	-2.733	0.572	-0.059	0.359	-1.820	0.238	-0.028	0.333	1.412	-0.810	0.060	0.333	1.929	-1.014	0.082	0.329
0.5	-7.767	2.095	-0.170	0.329	-6.837	1.799	-0.147	0.305	-1.888	0.337	-0.037	0.289	1.375	-0.794	0.061	0.335
0.6	-1.921	0.204	-0.019	0.357	-1.808	0.143	-0.011	0.325	-1.240	-0.012	0.001	0.317	-1.877	0.180	-0.011	0.359
0.7	-3.032	0.549	-0.045	0.351	-3.056	0.514	-0.039	0.340	-2.417	0.238	-0.009	0.369	-3.356	0.546	-0.033	0.375
0.8	-1.178	-0.080	0.007	0.342	-2.510	0.278	-0.016	0.335	-2.485	0.287	-0.016	0.354	-4.599	0.948	-0.065	0.401
0.9	-1.979	0.136	-0.007	0.346	-1.402	-0.100	0.016	0.352	-1.052	-0.210	0.025	0.362	-2.841	0.338	-0.015	0.376
1.0	1.322	-0.968	0.084	0.346	1.129	-0.913	0.079	0.357	-1.646	-0.093	0.021	0.361	-5.209	1.036	-0.067	0.392
1.1	-1.284	-0.175	0.024	0.363	-1.058	-0.298	0.037	0.354	-6.989	1.548	-0.105	0.359	-8.479	1.977	-0.134	0.388
1.2	-3.614	0.482	-0.023	0.372	-4.411	0.709	-0.039	0.389	-7.305	1.580	-0.103	0.397	-10.580	2.574	-0.177	0.402
1.3	-6.228	1.286	-0.085	0.395	-5.051	0.862	-0.048	0.400	-9.103	2.113	-0.143	0.424	-9.221	2.129	-0.142	0.414
1.4	-6.242	1.223	-0.075	0.392	-6.540	1.300	-0.080	0.387	-8.509	1.885	-0.122	0.424	-7.498	1.563	-0.097	0.437
1.5	-6.260	1.142	-0.063	0.384	-5.360	0.856	-0.040	0.384	-7.342	1.460	-0.085	0.439	-7.763	1.580	-0.094	0.450
1.6	-6.600	1.220	-0.067	0.399	-4.809	0.613	-0.017	0.393	-7.817	1.556	-0.090	0.435	-7.757	1.567	-0.094	0.478
1.7	-7.499	1.508	-0.091	0.409	-6.327	1.102	-0.057	0.415	-6.118	1.058	-0.056	0.460	-7.700	1.555	-0.095	0.486
1.8	-7.862	1.617	-0.100	0.413	-6.052	1.032	-0.054	0.434	-5.555	0.868	-0.041	0.468	-5.973	0.966	-0.046	0.479
1.9	-9.732	2.183	-0.143	0.445	-7.073	1.321	-0.075	0.453	-4.965	0.633	-0.020	0.466	-5.366	0.735	-0.025	0.473
2.0	-10.069	2.242	-0.145	0.467	-6.297	1.022	-0.048	0.471	-5.749	0.832	-0.032	0.471	-4.943	0.577	-0.012	0.480
	R = 5.0				R = 6.0				R = 7.0				R = 8.0			
T (s)	b_0	b_1	b_2	σ	b_0	b_1	b_2	σ	b_0	b_1	b_2	σ	b_0	b_1	b_2	σ
0.2	4.021	-1.687	0.141	0.461	3.982	-1.688	0.145	0.437	3.791	-1.638	0.144	0.419	3.541	-1.550	0.139	0.403
0.3	1.987	-1.029	0.085	0.396	2.259	-1.114	0.095	0.380	2.478	-1.203	0.105	0.386	1.731	-1.002	0.093	0.395
0.4	1.925	-1.018	0.085	0.368	1.144	-0.787	0.070	0.391	1.212	-0.820	0.075	0.409	1.827	-1.020	0.092	0.416
0.5	0.728	-0.649	0.056	0.383	1.695	-0.966	0.083	0.411	0.990	-0.758	0.069	0.409	0.494	-0.603	0.058	0.405
0.6	-3.261	0.572	-0.037	0.373	-4.092	0.802	-0.051	0.377	-4.440	0.902	-0.057	0.388	-4.417	0.886	-0.054	0.400
0.7	-2.408	0.286	-0.014	0.402	-2.827	0.386	-0.018	0.398	-4.465	0.875	-0.054	0.400	-4.609	0.893	-0.052	0.398
0.8	-4.716	0.954	-0.063	0.413	-4.385	0.820	-0.050	0.429	-4.940	0.975	-0.059	0.413	-5.716	1.194	-0.074	0.412
0.9	-6.285	1.368	-0.090	0.394	-8.635	2.060	-0.140	0.397	-8.191	1.915	-0.128	0.405	-8.324	1.958	-0.131	0.413
1.0	-7.825	1.814	-0.123	0.397	-7.355	1.614	-0.103	0.413	-8.984	2.106	-0.139	0.413	-9.985	2.413	-0.162	0.412
1.1	-9.408	2.235	-0.151	0.396	-9.621	2.296	-0.155	0.407	-9.481	2.242	-0.149	0.416	-10.494	2.556	-0.173	0.425
1.2	-9.872	2.325	-0.155	0.418	-9.329	2.158	-0.142	0.427	-9.432	2.197	-0.145	0.440	-9.824	2.322	-0.155	0.449
1.3	-7.883	1.704	-0.108	0.427	-7.036	1.418	-0.083	0.442	-6.945	1.382	-0.080	0.452	-7.281	1.492	-0.089	0.461
1.4	-7.059	1.419	-0.085	0.438	-5.851	1.022	-0.052	0.449	-4.619	0.606	-0.018	0.468	-3.758	0.322	0.006	0.489
1.5	-6.482	1.197	-0.065	0.469	-4.704	0.635	-0.021	0.485	-4.087	0.428	-0.004	0.491	-2.608	-0.042	0.033	0.511
1.6	-5.107	0.756	-0.032	0.489	-3.232	0.158	0.015	0.499	-3.960	0.378	-0.001	0.499	-3.367	0.178	0.016	0.499
1.7	-5.497	0.844	-0.038	0.481	-4.081	0.386	-0.001	0.478	-3.303	0.129	0.021	0.487	-2.590	-0.117	0.042	0.495
1.8	-4.977	0.627	-0.017	0.489	-3.830	0.250	0.014	0.486	-2.590	-0.146	0.046	0.494	-2.879	-0.067	0.041	0.496
1.9	-4.317	0.399	0.002	0.490	-5.136	0.618	-0.012	0.488	-3.921	0.232	0.018	0.488	-3.810	0.191	0.022	0.492
2.0	-4.433	0.413	0.001	0.493	-5.098	0.610	-0.013	0.489	-5.944	0.845	-0.029	0.484	-5.265	0.634	-0.012	0.494

Table 3.4. Regression coefficients for constant *R* peak inelastic oscillator displacements when $\alpha = 5\%$

	R = 1.5				R = 2.0				R = 3				R = 4			
T (s)	b_0	b_1	b_2	σ	b_0	b_1	b_2	σ	b_0	b_1	b_2	σ	b_0	b_1	b_2	σ
0.2	-8.383	2.408	-0.219	0.442	-8.064	2.351	-0.215	0.403	-2.069	0.344	-0.042	0.366	-2.279	0.322	-0.029	0.382
0.3	-4.008	0.990	-0.098	0.381	-3.170	0.705	-0.072	0.345	-4.668	1.162	-0.104	0.364	-3.011	0.621	-0.057	0.348
0.4	-3.164	0.713	-0.071	0.361	-3.058	0.641	-0.062	0.325	-1.762	0.204	-0.023	0.308	-2.177	0.313	-0.028	0.286
0.5	-7.728	2.086	-0.170	0.335	-7.314	1.956	-0.160	0.310	-4.474	1.113	-0.097	0.254	-3.009	0.595	-0.051	0.278
0.6	-2.036	0.243	-0.022	0.353	-1.771	0.132	-0.011	0.315	-2.073	0.245	-0.021	0.285	-1.766	0.122	-0.008	0.299
0.7	-3.015	0.542	-0.045	0.347	-2.516	0.352	-0.028	0.324	-3.969	0.733	-0.051	0.320	-4.165	0.813	-0.058	0.327
0.8	-1.116	-0.102	0.009	0.340	-2.908	0.400	-0.026	0.323	-3.368	0.557	-0.039	0.321	-5.600	1.260	-0.093	0.337
0.9	-1.912	0.110	-0.005	0.345	-1.583	-0.045	0.010	0.342	-1.852	0.052	0.002	0.338	-4.379	0.841	-0.059	0.335
1	0.945	-0.850	0.074	0.342	0.246	-0.643	0.058	0.346	-2.173	0.095	0.003	0.333	-6.286	1.390	-0.099	0.342
1.1	-1.863	0.013	0.008	0.365	-1.294	-0.211	0.028	0.347	-6.606	1.441	-0.100	0.332	-8.455	1.981	-0.139	0.347
1.2	-3.678	0.506	-0.025	0.372	-4.608	0.778	-0.046	0.374	-8.206	1.884	-0.130	0.368	-9.988	2.397	-0.167	0.350
1.3	-6.532	1.374	-0.091	0.389	-5.936	1.145	-0.071	0.386	-9.586	2.273	-0.158	0.377	-10.968	2.667	-0.186	0.356
1.4	-6.317	1.249	-0.077	0.390	-6.594	1.318	-0.083	0.372	-10.121	2.390	-0.164	0.380	-9.631	2.207	-0.147	0.377
1.5	-6.569	1.241	-0.071	0.382	-5.493	0.899	-0.045	0.373	-8.405	1.787	-0.112	0.398	-9.250	2.030	-0.130	0.399
1.6	-7.398	1.478	-0.088	0.401	-5.828	0.942	-0.044	0.390	-8.113	1.656	-0.100	0.411	-8.472	1.790	-0.113	0.429
1.7	-7.914	1.642	-0.102	0.409	-6.363	1.114	-0.059	0.412	-7.376	1.453	-0.088	0.431	-8.779	1.875	-0.120	0.439
1.8	-8.196	1.724	-0.109	0.413	-6.971	1.323	-0.078	0.428	-7.493	1.467	-0.088	0.439	-8.269	1.664	-0.100	0.435
1.9	-9.660	2.161	-0.142	0.446	-7.867	1.580	-0.096	0.446	-7.281	1.365	-0.079	0.441	-7.920	1.529	-0.089	0.441
2	-10.297	2.318	-0.151	0.465	-7.185	1.308	-0.071	0.460	-7.231	1.302	-0.071	0.444	-7.278	1.301	-0.069	0.440
	R = 5.0				R = 6.0				R = 7.0				R = 8.0			
T (s)	b_0	b_1	b_2	σ	b_0	b_1	b_2	σ	b_0	b_1	b_2	σ	b_0	b_1	b_2	σ
0.2	-1.257	0.009	-0.001	0.364	-0.815	-0.118	0.011	0.347	0.038	-0.372	0.031	0.336	0.515	-0.515	0.043	0.403
0.3	-2.338	0.401	-0.037	0.322	-0.905	-0.065	0.003	0.311	-0.168	-0.313	0.025	0.311	-0.419	-0.256	0.024	0.395
0.4	-1.673	0.135	-0.011	0.296	-1.743	0.131	-0.007	0.312	-1.279	-0.033	0.008	0.322	-1.327	-0.031	0.010	0.416
0.5	-3.224	0.618	-0.049	0.305	-2.634	0.410	-0.030	0.310	-3.209	0.560	-0.038	0.308	-3.742	0.705	-0.047	0.405
0.6	-3.786	0.734	-0.053	0.298	-5.603	1.295	-0.096	0.307	-6.398	1.540	-0.114	0.302	-6.802	1.660	-0.122	0.400
0.7	-4.326	0.876	-0.063	0.329	-4.691	0.990	-0.072	0.319	-5.901	1.370	-0.101	0.314	-6.928	1.683	-0.124	0.398
0.8	-5.457	1.194	-0.086	0.348	-5.407	1.160	-0.082	0.337	-5.937	1.303	-0.091	0.334	-6.603	1.500	-0.105	0.412
0.9	-6.883	1.591	-0.114	0.329	-8.056	1.923	-0.137	0.331	-8.611	2.073	-0.146	0.339	-8.812	2.118	-0.148	0.413
1	-9.611	2.406	-0.175	0.339	-9.235	2.240	-0.158	0.344	-9.191	2.200	-0.153	0.344	-9.513	2.287	-0.159	0.412
1.1	-9.100	2.156	-0.150	0.355	-9.299	2.197	-0.151	0.352	-9.549	2.267	-0.156	0.362	-10.005	2.396	-0.165	0.425
1.2	-10.429	2.515	-0.174	0.357	-10.247	2.442	-0.168	0.368	-9.641	2.239	-0.151	0.374	-9.136	2.067	-0.136	0.449
1.3	-10.542	2.519	-0.173	0.368	-9.976	2.312	-0.155	0.374	-9.574	2.166	-0.142	0.377	-9.067	1.986	-0.126	0.461
1.4	-10.309	2.400	-0.161	0.375	-9.010	1.977	-0.127	0.382	-7.587	1.496	-0.087	0.388	-7.474	1.435	-0.081	0.489
1.5	-8.652	1.860	-0.119	0.403	-8.068	1.653	-0.101	0.404	-7.376	1.405	-0.080	0.408	-7.036	1.280	-0.069	0.511
1.6	-7.573	1.502	-0.091	0.423	-6.757	1.205	-0.065	0.421	-7.012	1.262	-0.067	0.414	-7.315	1.337	-0.072	0.499
1.7	-7.526	1.444	-0.084	0.429	-6.627	1.133	-0.057	0.415	-6.833	1.171	-0.059	0.406	-7.037	1.214	-0.060	0.495
1.8	-7.762	1.489	-0.086	0.429	-7.189	1.289	-0.069	0.414	-6.679	1.096	-0.051	0.400	-6.429	0.989	-0.041	0.496
1.9	-8.429	1.676	-0.099	0.432	-8.178	1.574	-0.090	0.416	-7.397	1.308	-0.068	0.408	-7.099	1.192	-0.057	0.492
2	-7.394	1.338	-0.073	0.434	-8.155	1.548	-0.087	0.423	-8.337	1.584	-0.088	0.412	-8.316	1.569	-0.087	0.494

The associated σ values are also listed in these tables. Note that the random error term (σ) is independent of magnitude that can be considered as a deficiency of the predictive model since some of the recent prediction equations do consider the magnitude influence on σ. The magnitude-dependent standard deviations might have been incorporated into the predictive model by implementing pure error

analysis as outlined in Douglas and Smit (2001). This was not done for the current study as the data resolution is limited to partition the database into different magnitude-distance bins to observe the magnitude influence on the aleatory variability. Bommer et al. (2007) showed that the magnitude dependence on the random variability in ground motion prediction models require further work because different magnitude-distance binning schemes may significantly influence the variation of σ as a function of magnitude.

Figures 3.2 and 3.3 display the variation of regression coefficients (b_0, b_1 and b_2) as a function of period. Figure 3.2 presents these coefficients for constant ductility for α = 0% (first column) and α = 5% (second column). Figure 3.3 shows the same information for normalized lateral strength estimations. In general, the regression coefficients vary eratically with significant fluctuations as a function of period. Neverthless, the overall variation in these coefficients derived for constant ductility or constant strength with different postyield stiffness ratios suggest a similar behavior. Regression coefficients derived for α=5% constitute the lower bound with respect to those derived for α=0%. One can state that the largest differences between constant ductility and constant strength regression coefficients occur in the short period range, which may be due to the significant differences in the behavior of short-period osillator response under constant ductility and constant strength (Miranda, 2001). The investigation of intricate variations in these coefficients is out of scope of this study.

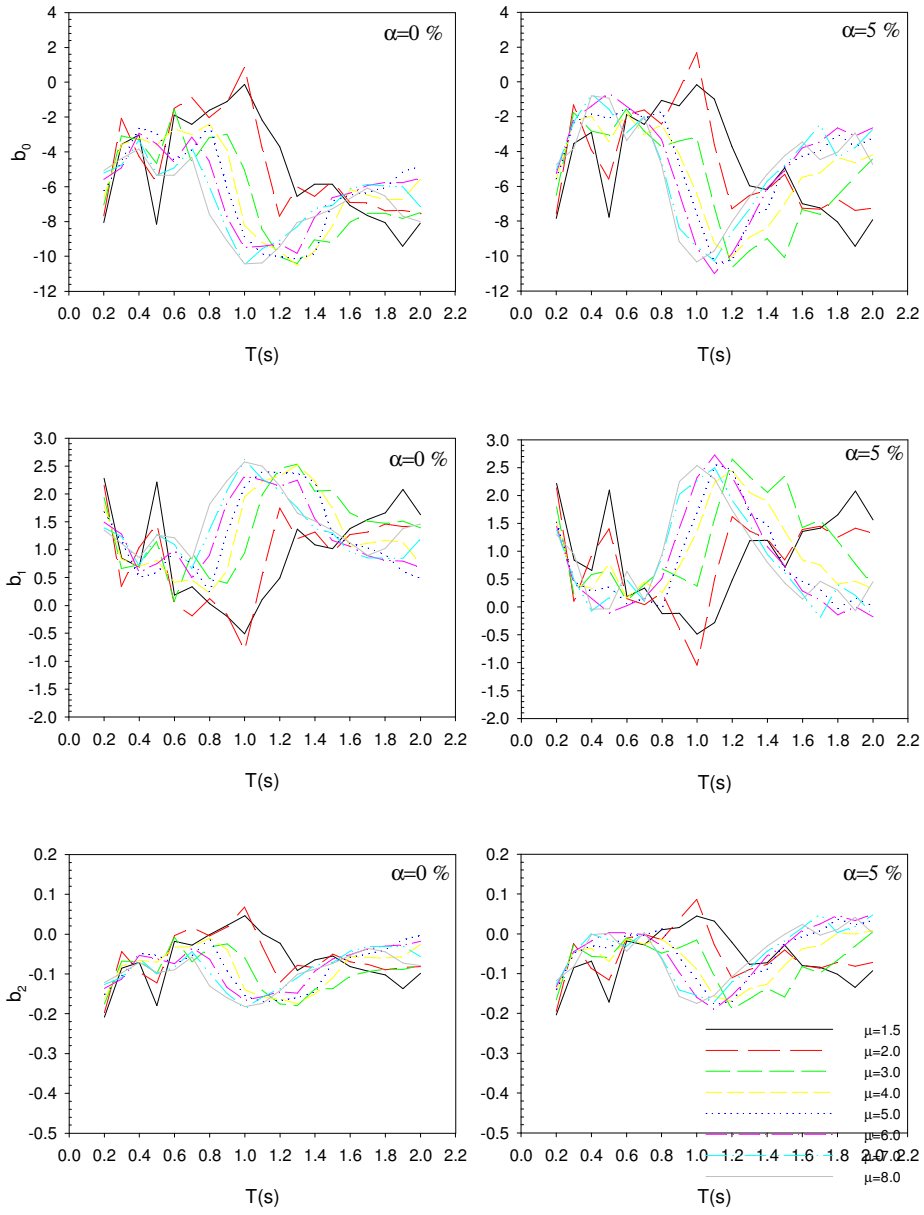

Figure 3.2. The variation of regression coefficients (b_0,b_1 and b_2) as a function of period for constant ductility

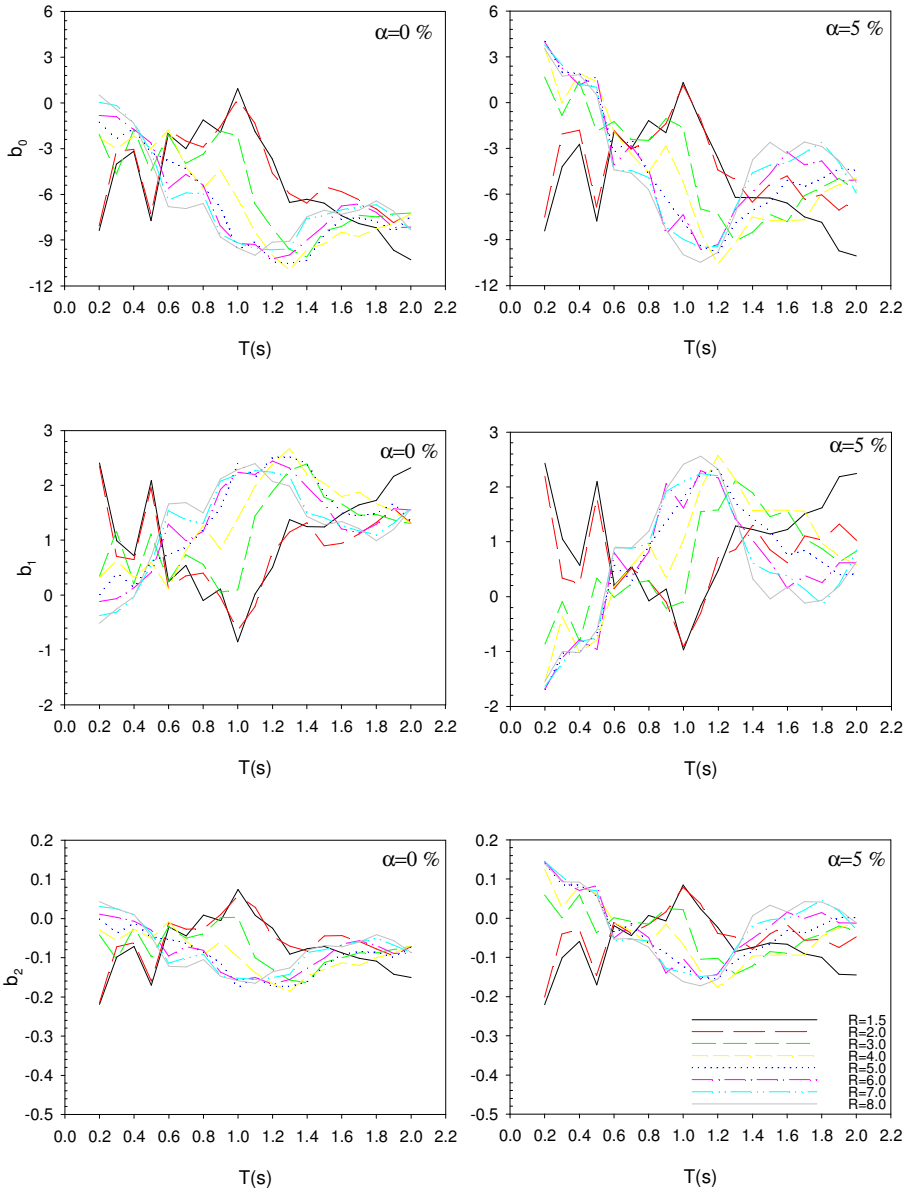

Figure 3.3. The variation of regression coefficients (b_0,b_1 and b_2) as a function of period for normalized lateral strength

Detailed analysis of variance (ANOVA) was carried out in order to judge the adequacy of the predictive model for each set of T-μ-α (or T-R-α). The ANOVA calculations accounted for the random variation of repeated observations in the predicted variable for distinct T-**M** pairs (Drapper and Smith, 1981). F-test was applied at the 5% significance level to examine the lack of model fit. Except for short periods, there was no lack of model fit at the 5% significance levelin the T-μ-α (or T-R-α) pairs indicating that the predictive model can fairly represent the variation of the observed data.

The corresponding R^2 statistics also showed that the model can generally explain more than 50% of the data variation that can be accepted as quite satisfactory for datasets containing repeated observations (Drapper and Smith, 1981). Therefore the residual mean squares were accepted as the unbiased estimators of σ^2 about the regression line. As noted previously the above calculations are only valid under the assumption that residuals are normally distributed with mean zero and variance σ^2. Figure 3.4 shows the sample normal probability plots of residuals at μ and R equal to 4 for T = 0.5, 1.0, 1.5 and 2.0 s when α = 0%.

Figure 3.5 repeats the same exercise for α = 5%. Both figures indicate that the normal distribution with mean zero assumption for residuals is reasonable since the residuals fall near the solid line that connects different percentiles for normal distribution. Thus, the variances computed from the residual mean squares can fairly account for the aleatory uncertainty associated with the predictive model.

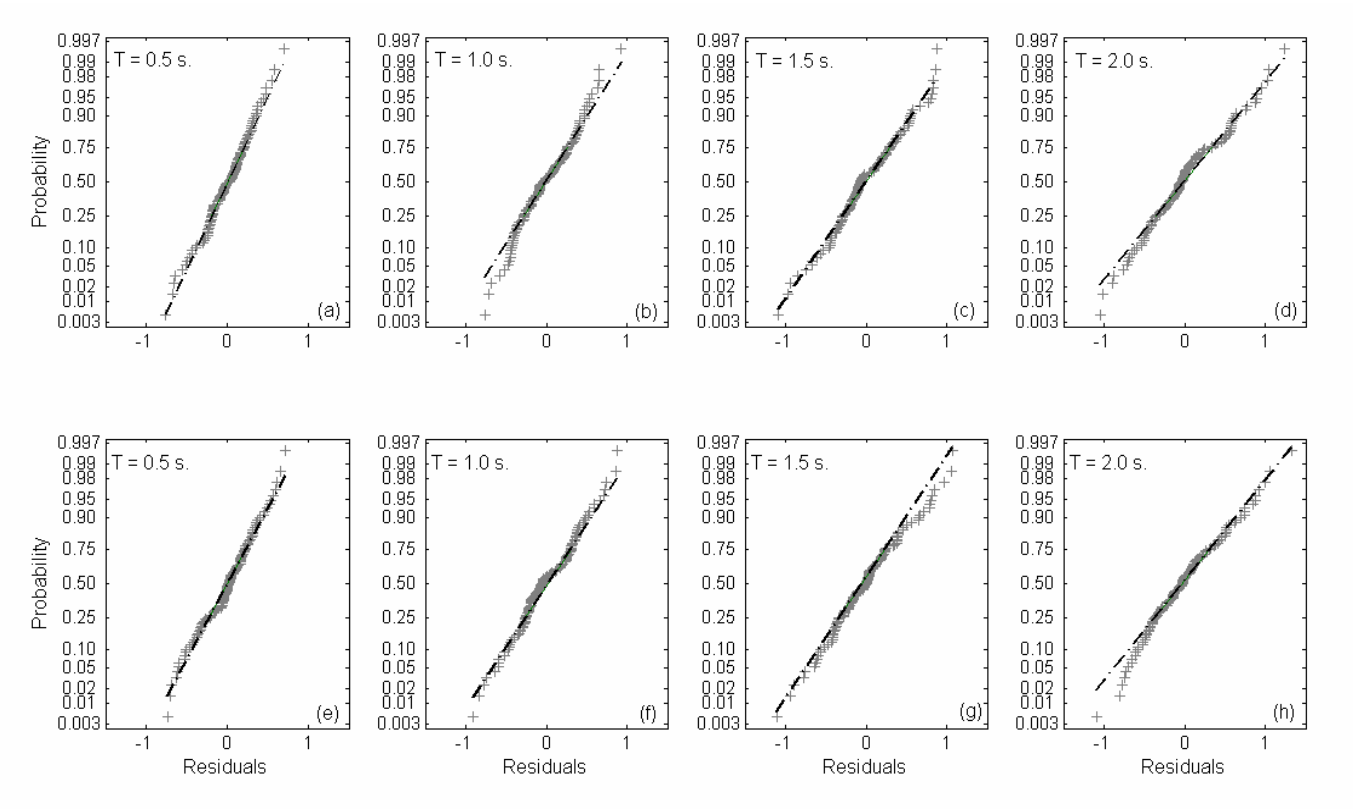

Figure 3.4. Normal probability plots of the residuals at μ and R equal to 4 (upper and lower rows, respectively) for T = 0.5, 1.0, 1.5 and 2.0 s with 0%.

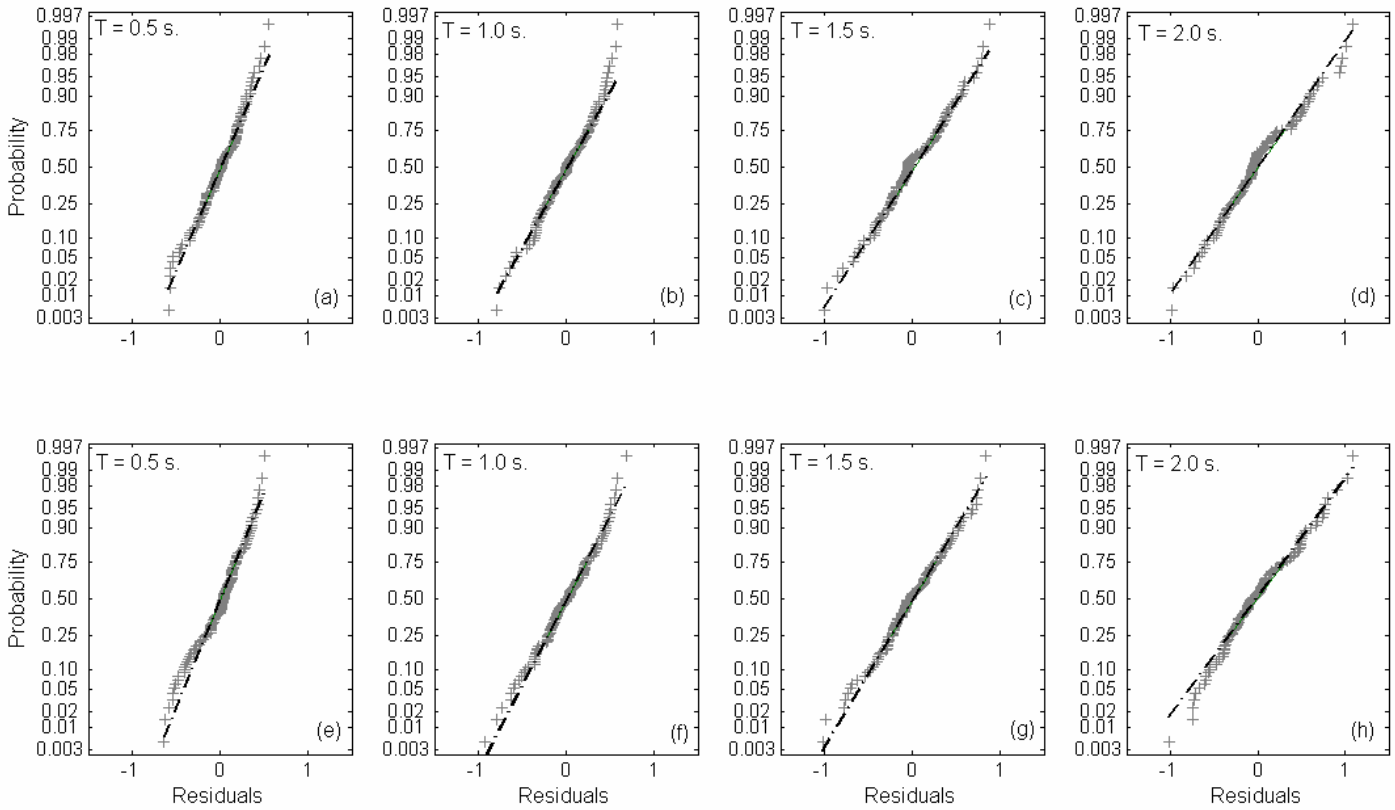

Figure 3.5. Normal probability plots of the residuals at μ and R equal to 4 (upper and lower rows, respectively) for T = 0.5, 1.0, 1.5 and 2.0 s with 5%.

Residuals were also examined to confirm that the predictions are unbiased due to the omission of other explanatory parameters in the predictive model that are discussed in the previous paragraphs. Figure 3.6 presents the residual plots against magnitude at T = 0.5, 1.0, 1.5 and 2.0 s for μ = 6 (first row) and for R = 6 (second row). Figure 3.6 shows the residuals vs. estimated dependent parameter plots of the entire database for μ and R equal to 1.5, 3.0, 5.0 and 7.0. Similar to Figure 3.6 the upper and lower rows display the relevant plots for constant ductility and strength, respectively. Both figures present residual scatters for α = 0% because the associated dispersion is relatively higher when compared to the residuals of α = 5% case. The solid straight lines in each plot show the trends in the residuals; a significant slope in these linear trends would suggest the biased estimations of the predictive model.

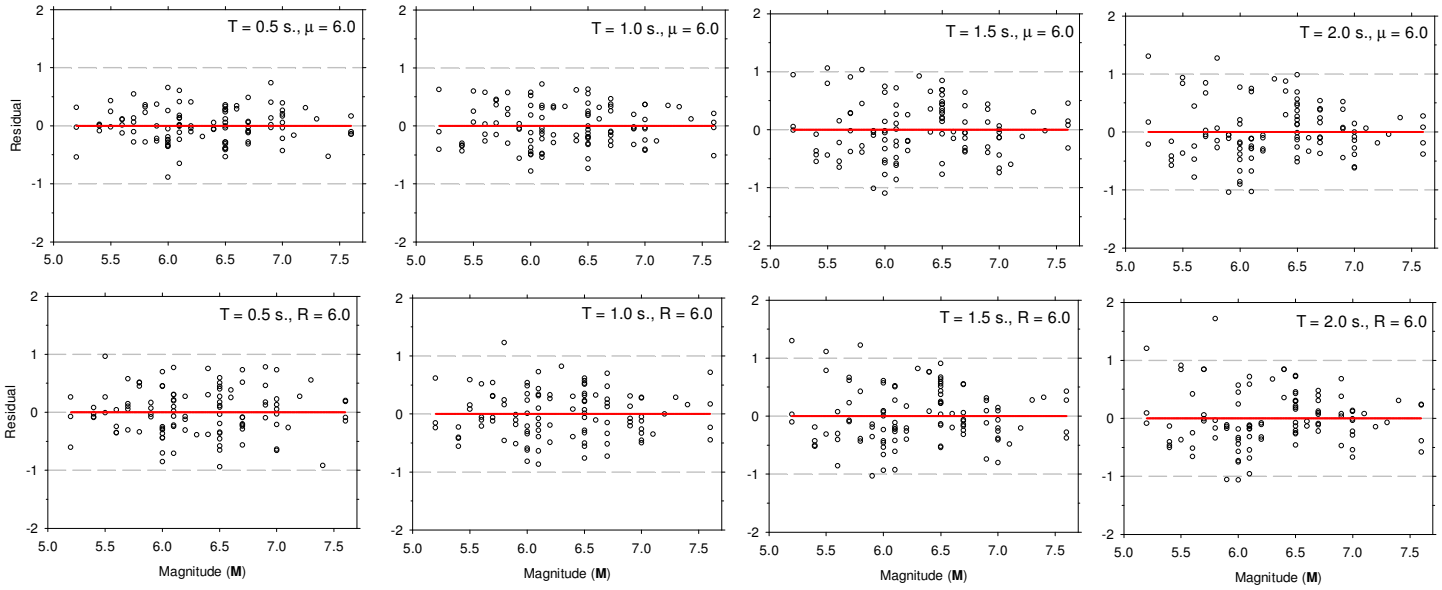

Figure 3.6. Residual plots as a function of **M** for $\mu = 6$ (upper row) and $R = 6$ (lower row) at $T = 0.5$, 1.0, 1.5 and 2 s when $\alpha = 0\%$.

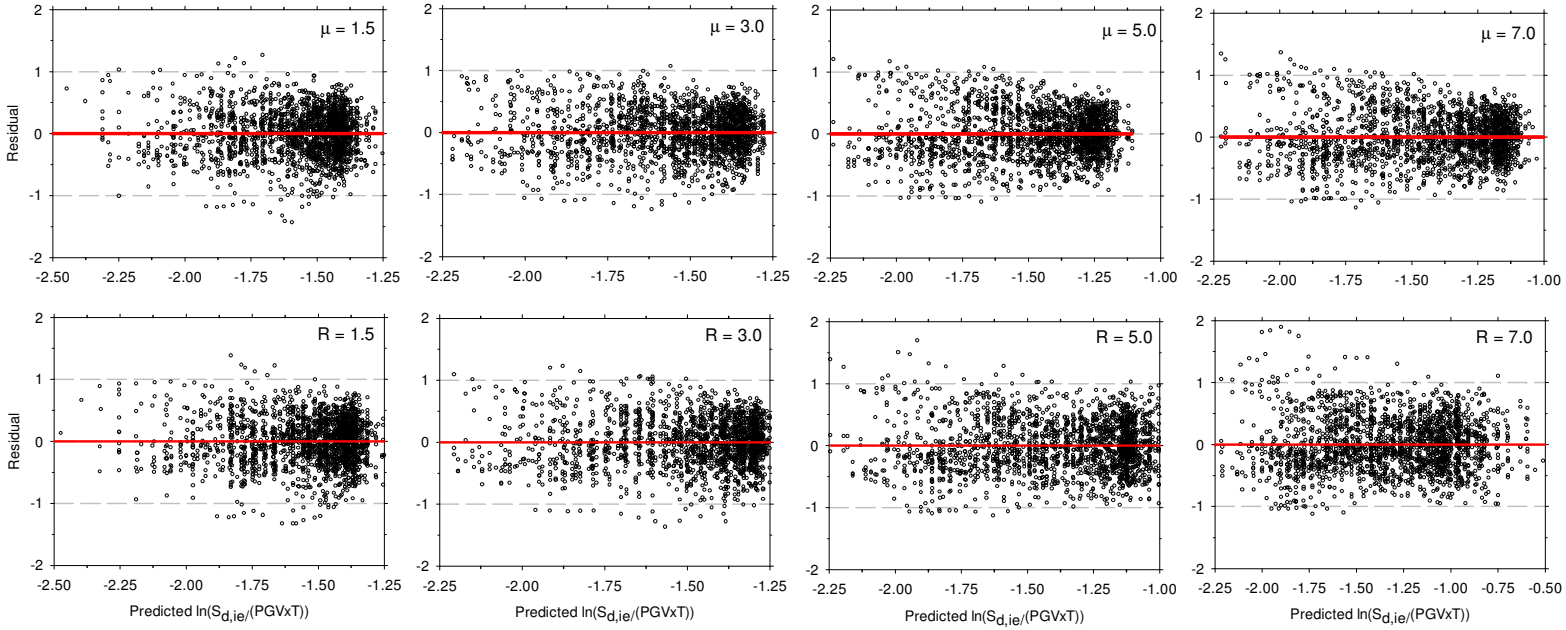

Figure 3.7. Residual plots in terms of the dependent parameter for distinct μ and R values considering the entire database.

The plots in Figures 3.6 and 3.7 do not exhibit a biased trend in the residuals. This confirms the fact that the model used in this study accounts for the variation of the dependent parameter in a satisfactory manner despite disregarding the other predictor parameters in this study. Note that the residuals reported for normalized lateral strength are greater than those of constant displacement ductility. This is an expected phenomenon since the peak oscillator displacements computed for constant R values are not limited to a predefined value which is the case for constant μ peak oscillator displacements.

The efficiency of the model in capturing the central tendency of the predicted variable, $\ln(S_{d,ie}/PGV \times T)$, as a function of **M** is presented in Figures 3.8-3.15. The plots in Figures 3.8-3.11 display the scatters of constant-strength $\ln(S_{d,ie}/PGV \times T)$ for elastoplastic and bilinear hysteretic behavior computed at oscillator periods of T=0.5s and T=2.0s. These figures contain the average $\ln(S_{d,ie}/PGV \times T)$ values (black squares) computed for the magnitude bins of 5.0-5.5, 5.5-6.0, 6.0-6.5, 6.6-7.0 and 7+. Second-order polynomial fits (black lines) to the average $\ln(S_{d,ie}/PGV \times T)$ values and the estimations obtained from the proposed model (red curves) are superimposed to these plots. The relatively high R^2 values of the polynomial fits that are listed in Table 3.5 suggest that the quadratic behavior addresses the general trend of the data fairly well. The red curves almost overlap the general variation in the observed data (i.e. black squares and the black curves). This advocates the adeuqacy of the proposed model in estimating $S_{d,ie}$ as a function of **M** and T. Neverthless, in some of the large R and short-period cases (e.g. R=5–T=0.5s and R=6–T=0.5s) the average $\ln(S_{d,ie}/PGV \times T)$ values vary in a constant manner. This suggests the lack of model fit at relatively short periods as reported in the previous paragraphs via the information revealed in F-statistics. Figures 3.12-3.15 present similar information for constant ductility oscillator response. These figures yield relatively similar results to those discussed for constant strength.

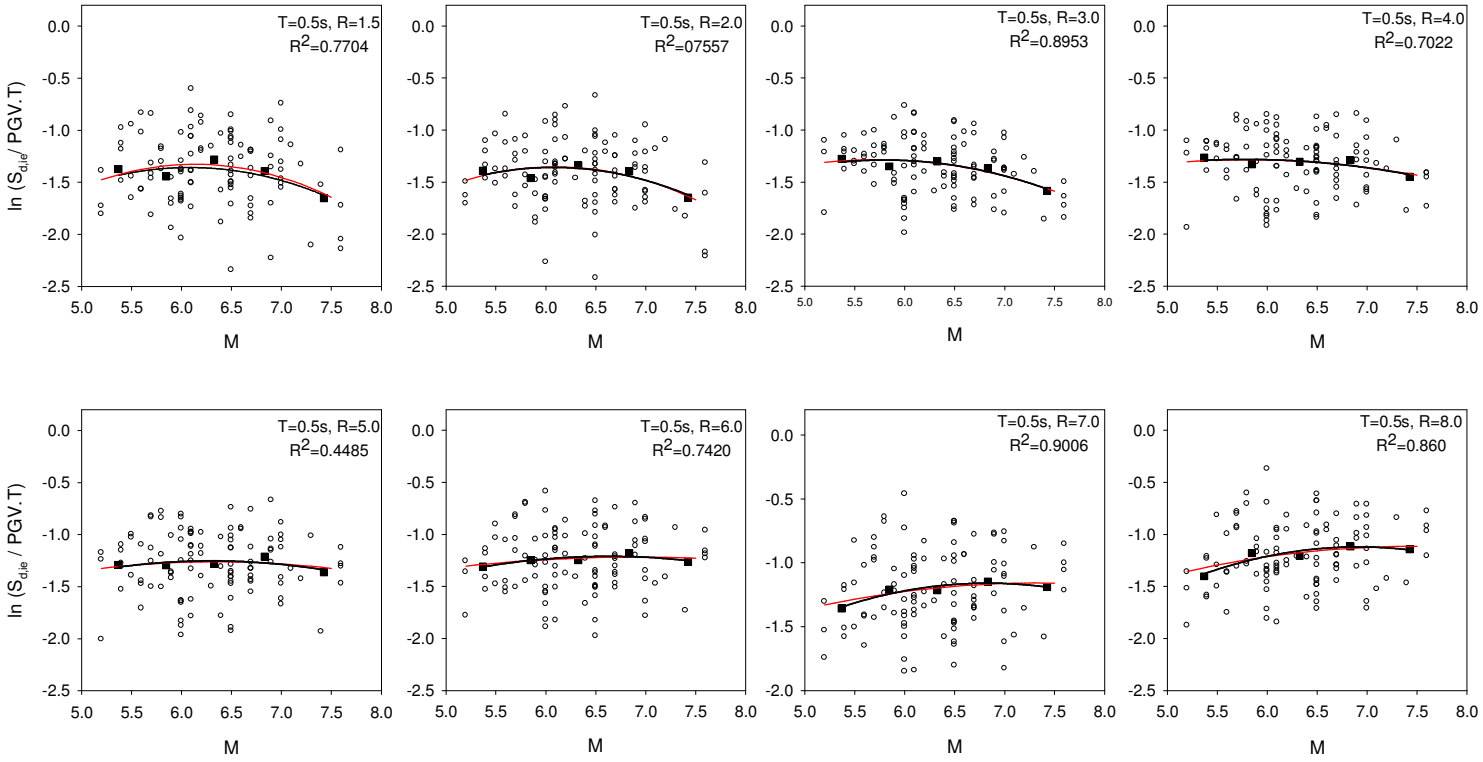

Figure 3.8. The dependent parameter vs magnitude plots with the estimation of the predictive model for different R values when α=0 % (T=0.5 s)

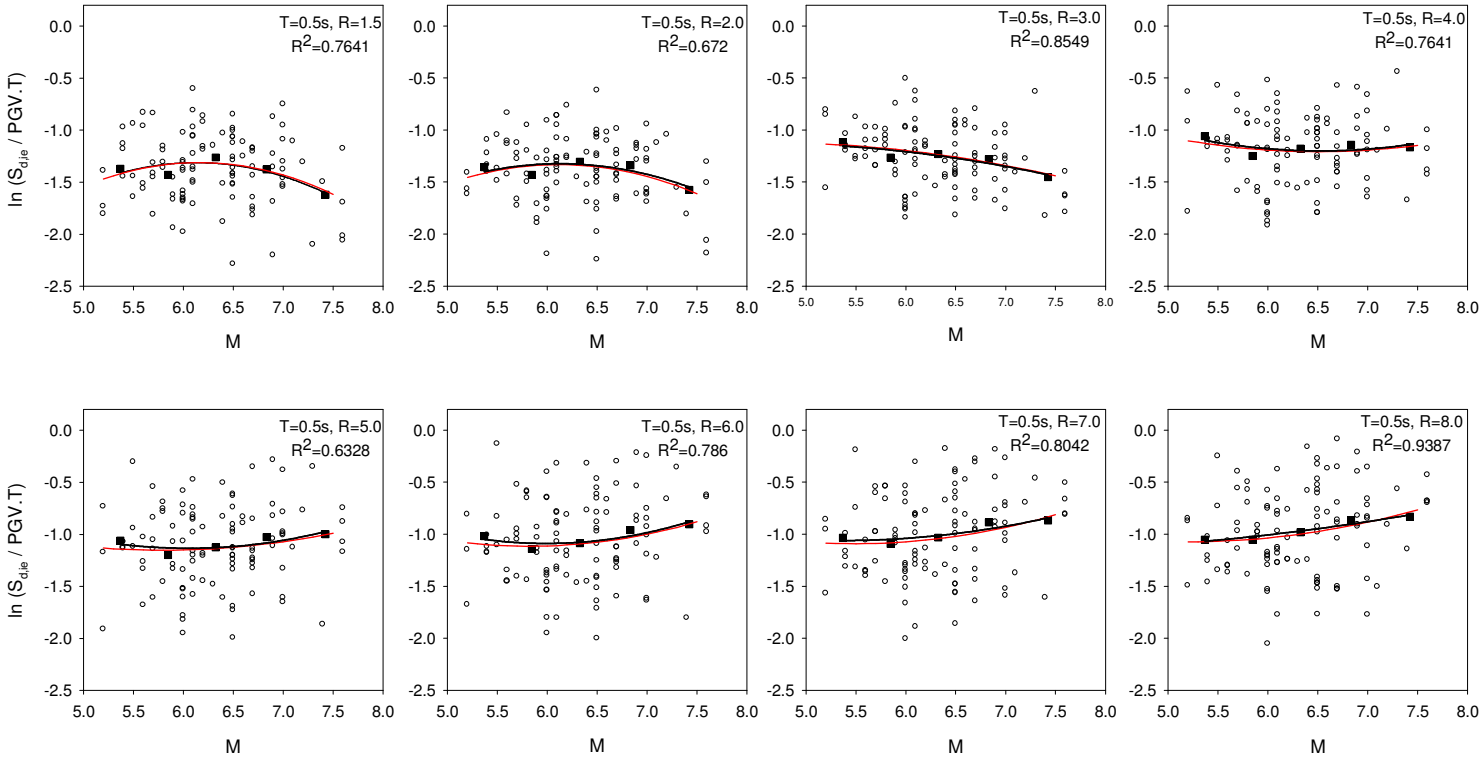

Figure 3.9. The dependent parameter vs magnitude plots with the estimation of predictive model for different *R* values when α=5 % (*T*=0.5 s)

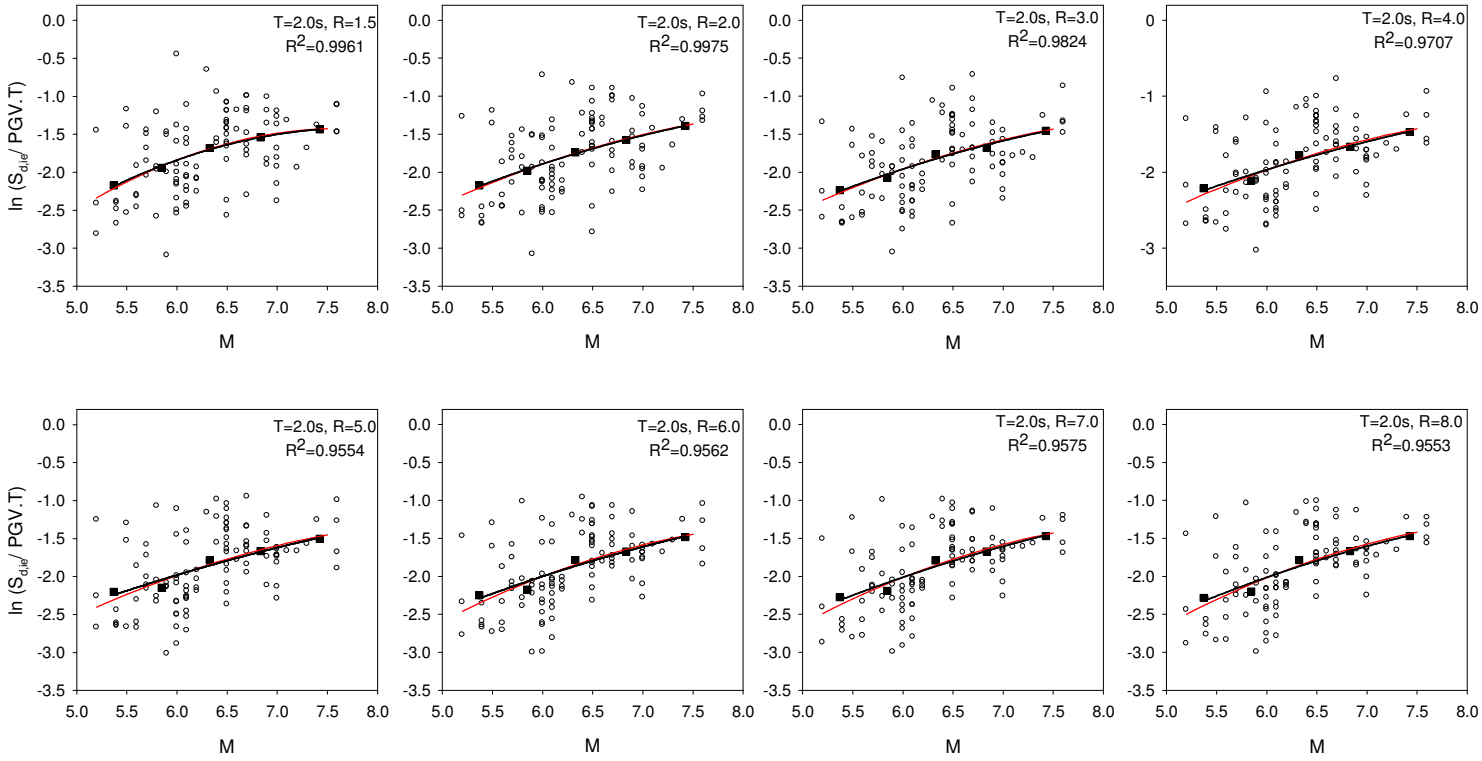

Figure 3.10. The dependent parameter vs magnitude plots with the estimation of predictive model for different *R* values when α=0 % (*T*=2.0 s)

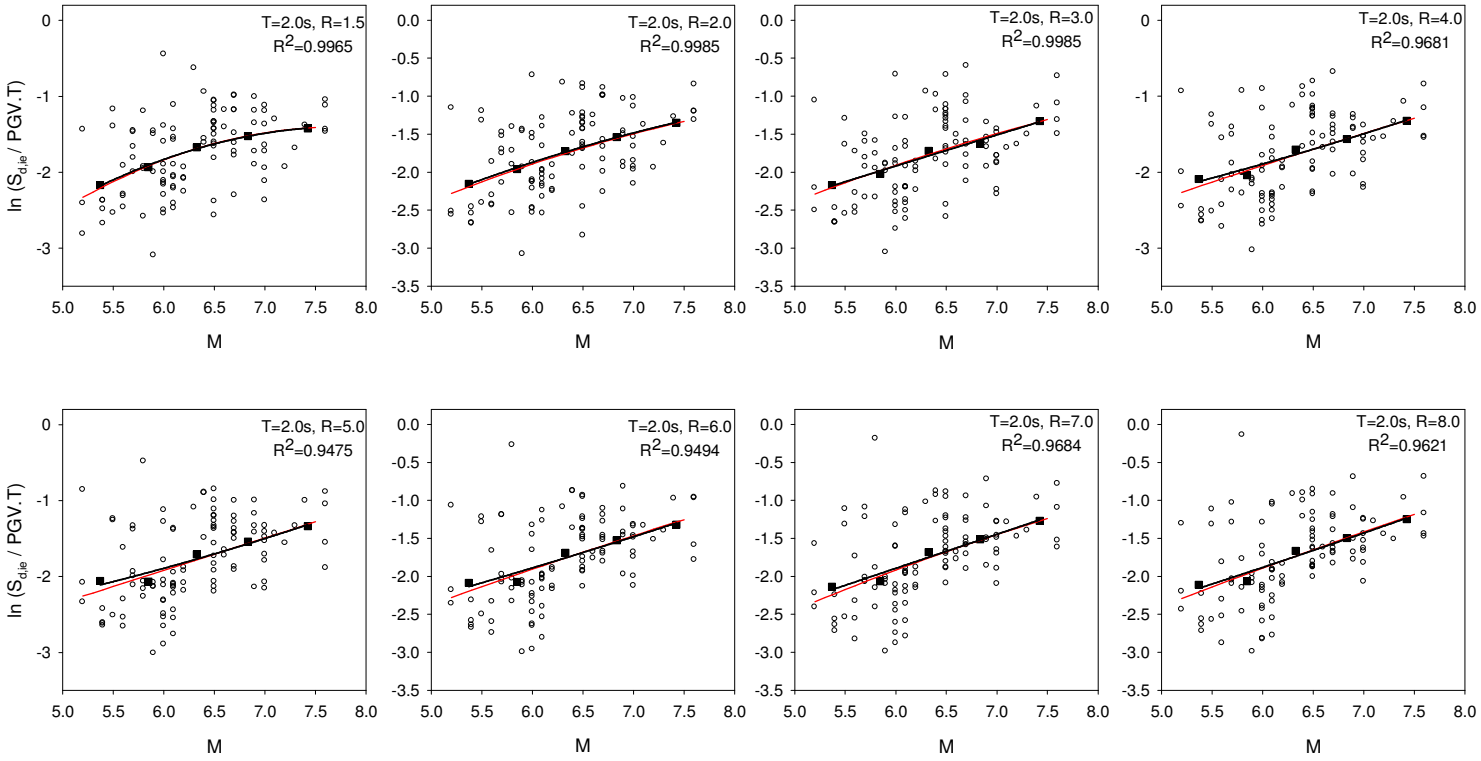

Figure 3.11. The dependent parameter vs magnitude plots with the estimation of the predictive model for different *R* values when α = 5 % (*T*=2.0 s)

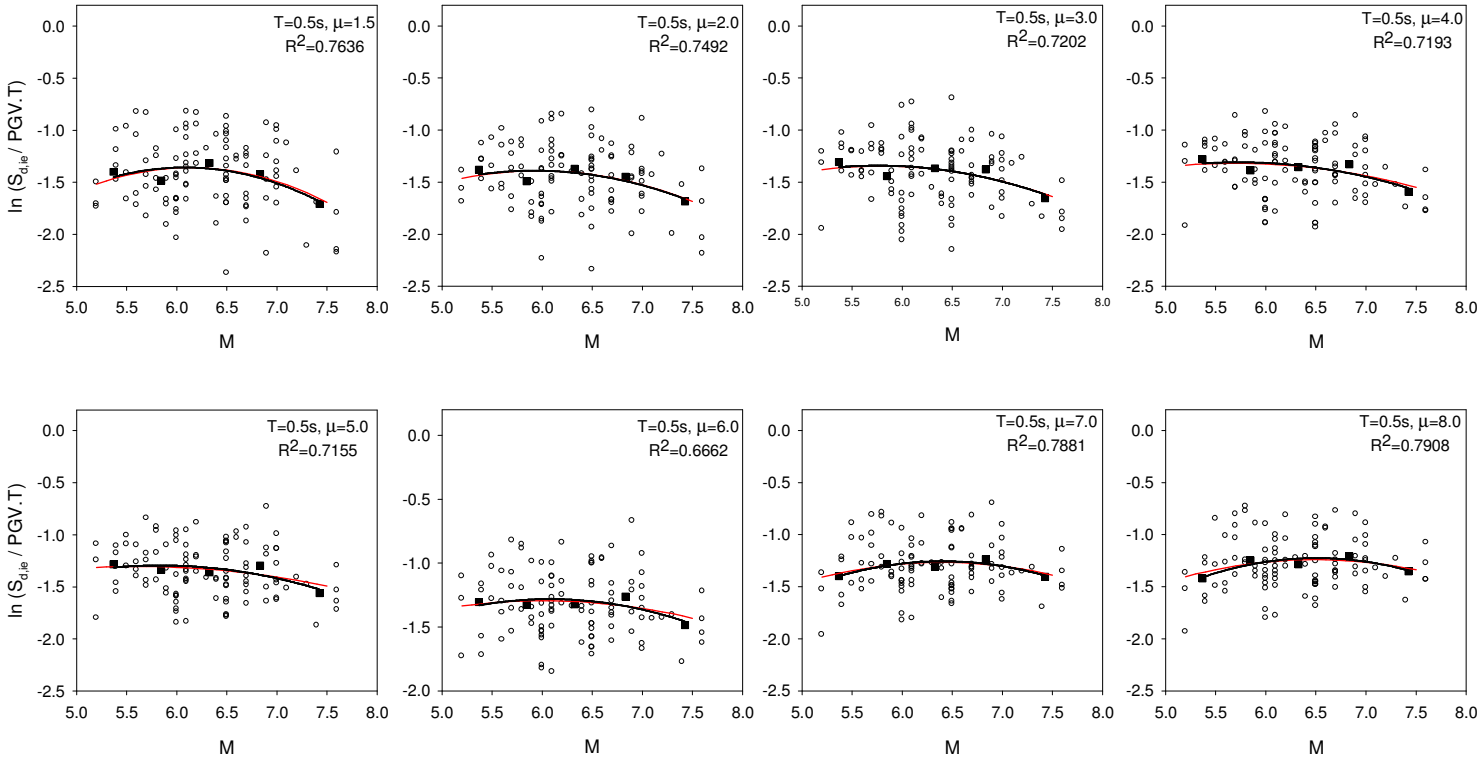

Figure 3.12. The dependent parameter vs magnitude plots with the estimation of predictive model for different μ values when α = 0 % (T=0.5 s)

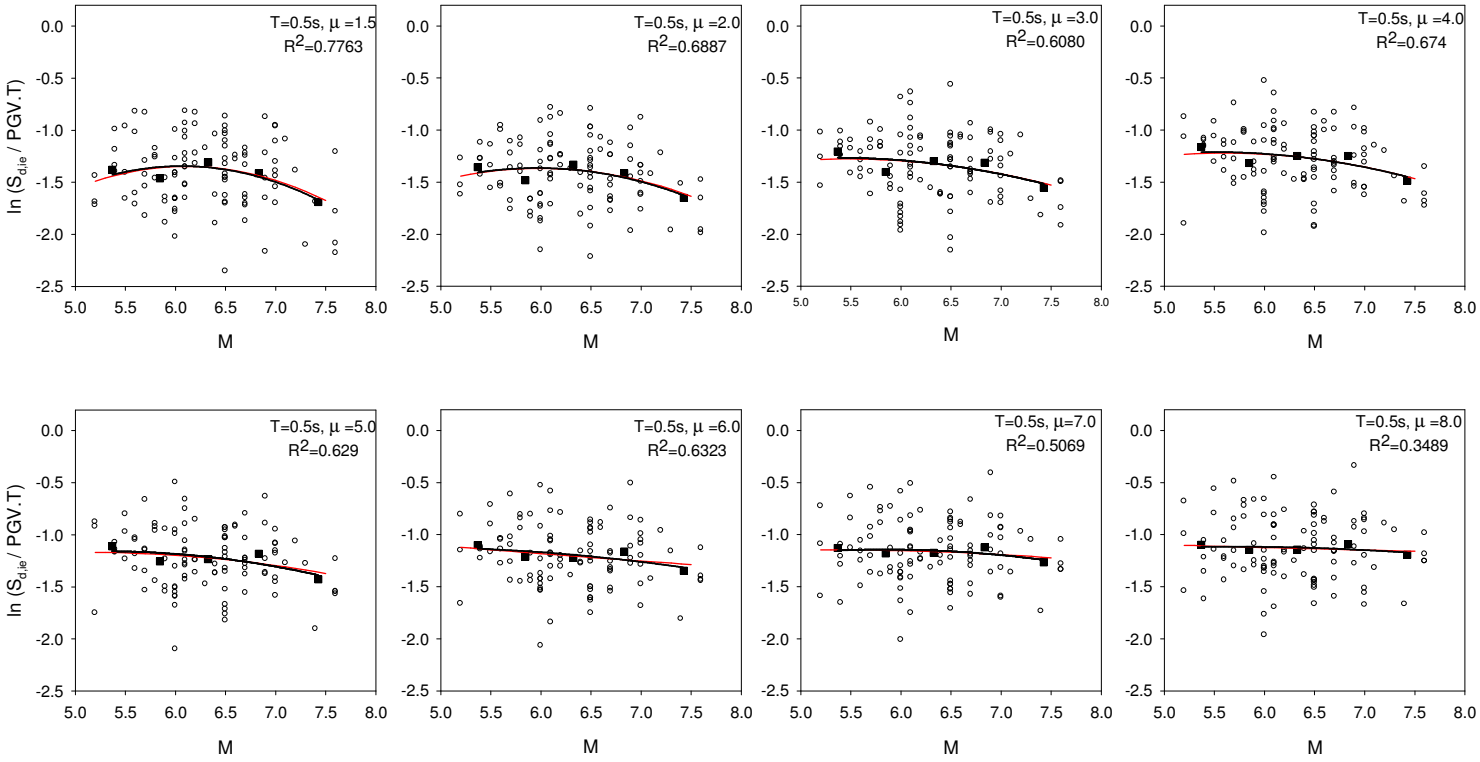

Figure 3.13. The dependent parameter vs magnitude plots with the estimation of predictive model for different μ values when α = 5 % (T=0.5 s)

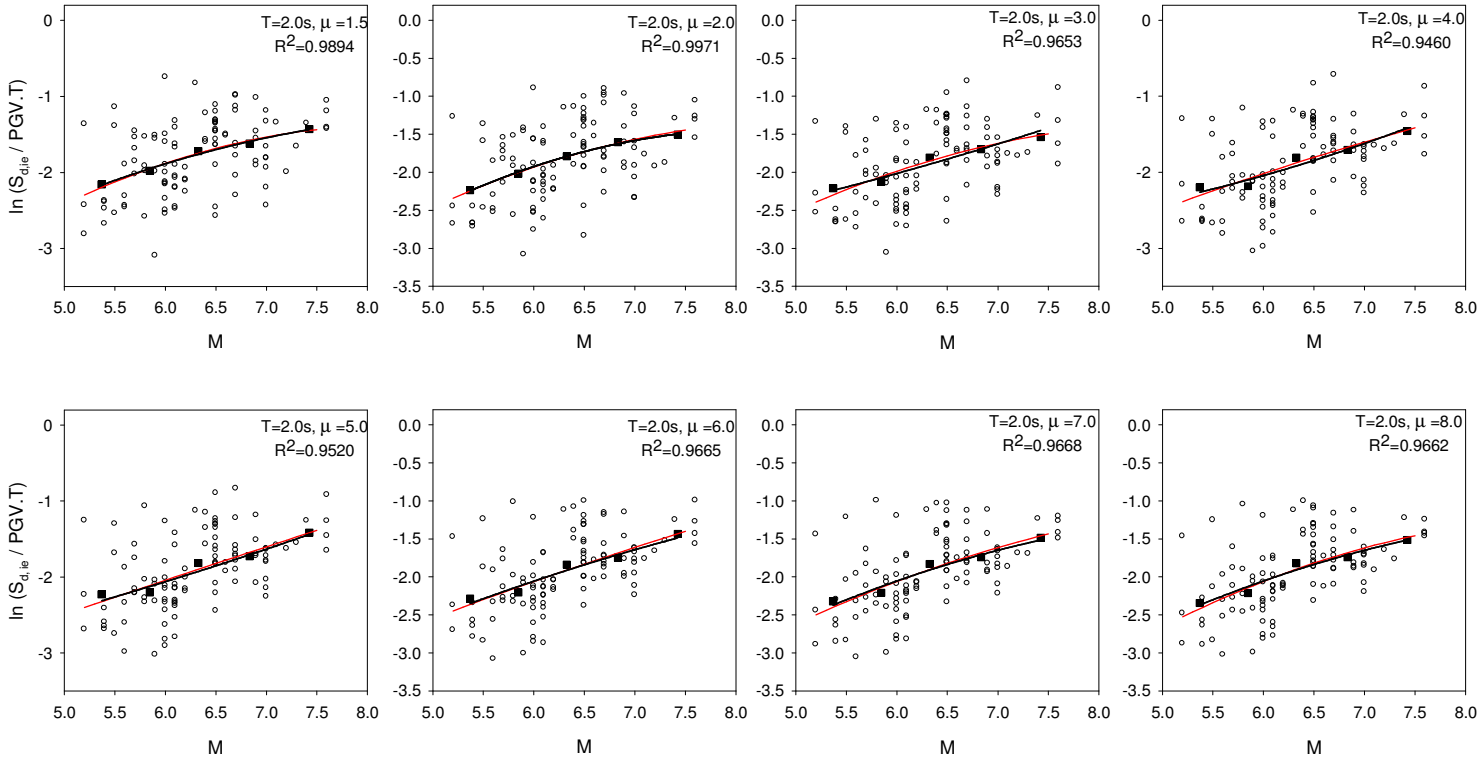

Figure 3.14. The dependent parameter vs magnitude plots with the estimation of predictive model for different μ values when α =0 % (T=2.0 s)

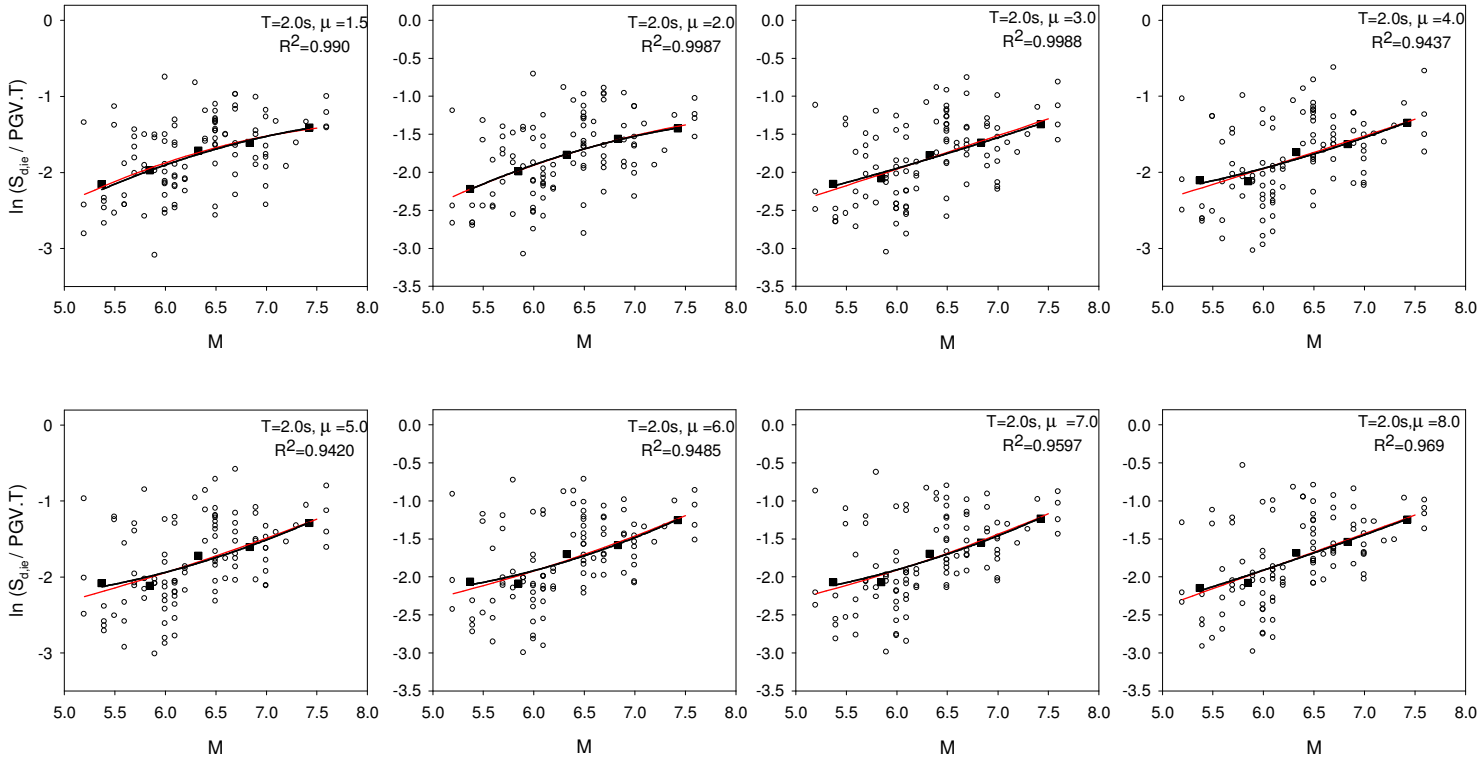

Figure 3.15. The dependent parameter vs magnitude plots with the estimation of predictive model for different μ values when α =5 % (T=2.0 s)

Table 3.5 R^2 values of the quadratic fits presented in Figures 3.8 – 3.15

	T=0.5 s		T=2.0 s			T=0.5 s		T=2.0 s	
R	**α = 0%**	**α = 5%**	**α = 0%**	**α = 5%**	**μ**	**α = 0%**	**α = 5%**	**α = 0%**	**α = 5%**
1.5	0.7704	0.7641	0.9961	0.9965	1.5	0.7636	0.7763	0.9894	0.9900
2	0.7557	0.6720	0.9975	0.9985	2	0.7492	0.6887	0.9971	0.9987
3	0.8953	0.8459	0.9824	0.9985	3	0.7202	0.6080	0.9653	0.9988
4	0.7022	0.3456	0.9707	0.9681	4	0.7193	0.6741	0.9460	0.9437
5	0.4485	0.6328	0.9554	0.9475	5	0.7155	0.6290	0.9520	0.9420
6	0.7420	0.7860	0.9562	0.9494	6	0.6662	0.6323	0.9665	0.9485
7	0.9006	0.8042	0.9575	0.9684	7	0.7881	0.5059	0.9668	0.9597
8	0.8600	0.9287	0.9553	0.9621	8	0.7968	0.3489	0.9662	0.9690

3.3 Simplified expressions for standard deviations

The smooth variation of σ listed in Tables 3.1 – 3.4 encouraged this study to derive empirical equations that can be directly used for the calculation of random error in the predictive model. Equations (3.3) and (3.4) show these expressions for constant μ when α = 0% and 5%, respectively. Equations (3.5) and (3.6) describe the same relationships for constant *R*. Figure 3.16 shows surface plots for the variation of σ computed from these generic expressions as a function of oscillator period for a given μ (or *R*) and α value. The plots also include the 3D scatters of actual variation of σ to examine the match described by the empirical functions in Eqs. (3.3)-(3.6). The visual inspection between the surface plots and the actual 3D scatters suggests that some compromises were made at the expense of developing these generic expressions for σ. Nevertheless the smooth σ surfaces can fairly address the variation of random error in the predictive model along with the structural parameters considered in this study. In general, the standard deviations tend to decrease with decreasing level of inelasticity (i.e., μ or *R* value) and oscillator period except for very short periods where σ displays an increasing trend. When compared to the

constant ductility plots, the constant strength standard deviations are relatively higher due to the reasoning explained in the previous paragraph. The standard deviations decrease significantly when α attains values larger than 0%. The last two observations are consistent with the previous studies on nonlinear oscillator response (e.g. Ruiz-García and Miranda, 2003; Chopra and Chintanapakdee, 2004). Note that the generic expressions derived for σ can be of practical use if the predictive model is implemented to PSHA together with the GMPEs as presented in the next section.

$$\sigma = 0.27\left(1.15^{\mu}\right)\left(\mu^{-0.57}\right) + 0.08T\left(0.83^{\mu}\right)\left(\mu^{0.94}\right) + \frac{0.01}{T^2}\left(0.71^{\mu}\right)\left(\mu^{0.4}\right) \tag{3.3}$$

$$\sigma = 0.27\left(1.09^{\mu}\right)\left(\mu^{-0.45}\right) + 0.085T\left(0.89^{\mu}\right)\left(\mu^{0.61}\right) + \frac{0.01}{T^2}\left(0.74^{\mu}\right)\left(\mu^{0.31}\right) \tag{3.4}$$

$$\sigma = 0.075\left(4.48^{R^{-1}}\right)\left(R^{0.67}\right) + 1.24T\left(0.035^{R^{-1}}\right)\left(R^{-1.4}\right) + \frac{0.007}{T^2}\left(0.6^{R}\right)\left(R^{1.28}\right) \tag{3.5}$$

$$\sigma = 0.05\left(8.35^{R^{-1}}\right)\left(R^{0.7}\right) + 1.92T\left(0.02^{R^{-1}}\right)\left(R^{-1.32}\right) + \frac{0.008}{T^2}\left(0.66^{R}\right)\left(R^{0.87}\right) \tag{3.6}$$

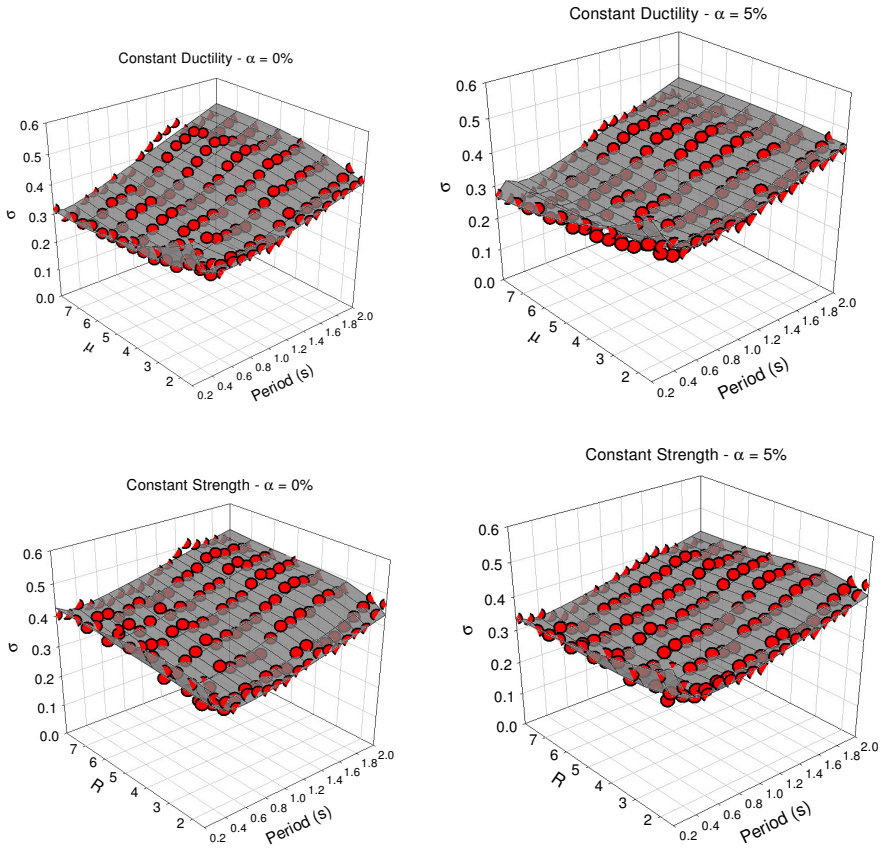

Figure 3.16. Smooth variation of standard deviations (σ) derived from Eqs. (3.3) – (3.6) for the predictive model. The scatters are the actual σ presented in Tables 3.1 – 3.4.

3.4 Application of the Proposed Model

The proposed predictive model can estimate the peak inelastic oscillator displacements for a *PGV* value that is computed from a GMPE. Recalling the general functional form of the model in Eq. (3.1) and applying random variables theory under the assumption that both *PGV* and $S_{d,ie/R,\mu}$ are log normal independent variables, one can incorporate the random error associated with the predicted *PGV* to the overall $S_{d,ie}$ estimation. This is given in Eq. (3.7).

$$Var\left[\ln\left(S_{d,ie}\big|_{R,\mu}\right)\right] = Var\left[\ln\left(f(\theta)\right)\right] + Var\left[\ln(PGV)\right] \quad (3.7)$$

The term on the left hand side of Eq. (3.7) is the total variance of the peak inelastic oscillator displacement estimation that contains random error terms due to the predictive model presented and the *PGV* estimated from a GMPE (first and second terms on the left hand side, respectively). Note that the predictive model presented in this study is derived for random horizontal component definition and this requires a careful consideration of the GMPE employed for *PGV* estimation. If the chosen GMPE is not revised for the random components effect, one must use a consistent scaling to bring the horizontal component definition of the chosen GMPE in agreement with the random component definition used here. Beyer and Bommer (2006) established empirical relationships between different horizontal component definitions of *PGV* for their median estimations and for the associated random error terms. These relationships can be used efficiently to obtain compatible and consistent results from the proposed predictive model when the GMPE considered yields *PGV* estimations other than the random horizontal component definition.

Figures 3.17 and 3.18 show the variation in the expected $S_{d,ie}$ for a set of constant μ and R values and for reverse style faulting events of increasing magnitude (**M** = 5.5, 6.0 and 7.0) at a soft site (NEHRP D) located 5 km from the surface projection of the fault rupture. Figure 3.17 presents the $S_{d,ie}$ estimations for α = 0% that can mimic the inelastic displacement demands on steel frames. Figure 3.18 displays the expected $S_{d,ie}$ for α = 5% that fairly represents inelastic concrete frames. The first column in each figure displays the constant ductility spectral displacement plots for **M** = 5.5, 6.0 and 7.0, respectively. The second column presents the same information for normalized lateral

strength spectral displacements. The *PGV* values of the scenario events were computed from Akkar and Bommer (2007a) that uses geometric mean component definition for the estimation of *PGV*. The empirical relationships proposed by Beyer and Bommer (2006) were used to adjust the differences between the random component and geometric mean definitions. Both figures clearly display the magnitude influence on the variation of $S_{d,ie}$. For small magnitude events (**M** = 5.5), the inelastic peak oscillator displacements start oscillating about a constant plateau after $T \approx 1.5 - 2.0$ s. For other magnitude values the inelastic spectral displacements follow a continuously increasing pattern with increasing oscillator periods. This observation is consistent with the previous studies that highlight the strong relationship between magnitude and spectral corner periods that define the commencement of constant spectral displacement plateau (e.g. Faccioli et al., 2004; Bommer and Elnashai, 1999, FEMA, 2003). The *PGV* dependent predictive model seems to capture this effect adequately underlining once again the strong correlation between *PGV* and magnitude that has already been addressed by many studies (e.g. Wu et al., 2003; Akkar and Bommer 2007a). Another common observation from these figures is that the spectral periods for the commencement of "equal displacement rule" (i.e. inelastic spectral displacements practically attaining equal peak displacements of the corresponding elastic oscillators regardless of the level of inelasticity) are sensitive to the level of *PGV* that is essentially related with the magnitude. The increase in *PGV* (that is dictated by the increase in magnitude) shifts the spectral regions towards longer periods where "equal displacement rule" holds. Tothong and Cornell (2006) while deriving their inelastic spectral displacement prediction equation also noted this observation.

The influence of postyield stiffness ratio as well as the distinct oscillator responses imposed by constant μ and R on the peak inelastic oscillator

displacements were also observed by comparing the relevant plots in Figures 3.17 and 3.18. The postyield stiffness is particularly influential in reducing the peak inelastic oscillator displacements in the short period spectral region. The differences in $S_{d,ie}$ at the short periods for displacement ductility and normalized lateral strength spectra are notable since the latter spectral type does not impose any limit on the computed peak inelastic oscillator displacements that in turn affects the short-period displacement demands on structural systems. These observations have already been noted by various studies (e.g. Ruiz-García and Miranda, 2003, Chopra and Chintanapakdee, 2004) and the proposed model can capture these prominent features of nonlinear oscillator response. Figure 3.17 presents the changes in the expected $S_{d,ie}$ as a function of *PGV* varying at distances 1 km $\leq R_{jb} \leq$ 30 km. The GMPE proposed by Boore and Atkinson (2007) was used to simulate the distance dependent variation of *PGV* for a scenario event of **M** = 7 and for a site class having $V_{s,30}$ = 270 m/s. The first column plots in Figure 3.9 show corresponding changes in $S_{d,ie}$ at various levels of μ for α = 5% rendering useful information for the preliminary design of concrete frame buildings. The second column in Figure 3.19 exhibits same type of plots for normalized lateral strength peak oscillator displacements that can be used for the seismic performance assessment of the same type structural systems. Each column contains 3 panels to represent peak inelastic oscillator displacements at T = 0.5, 1.0 and 1.5 s (top, middle and bottom panel, respectively). Similar to the plots in Figures 3.17 and 3.18 the geometric mean *PGV* estimation by Boore and Atkinson (2007) was adjusted for random horizontal component definition via the relationships proposed by Beyer and Bommer (2006). This way coherent $S_{d,ie}$ estimations were obtained from the proposed predictive model.

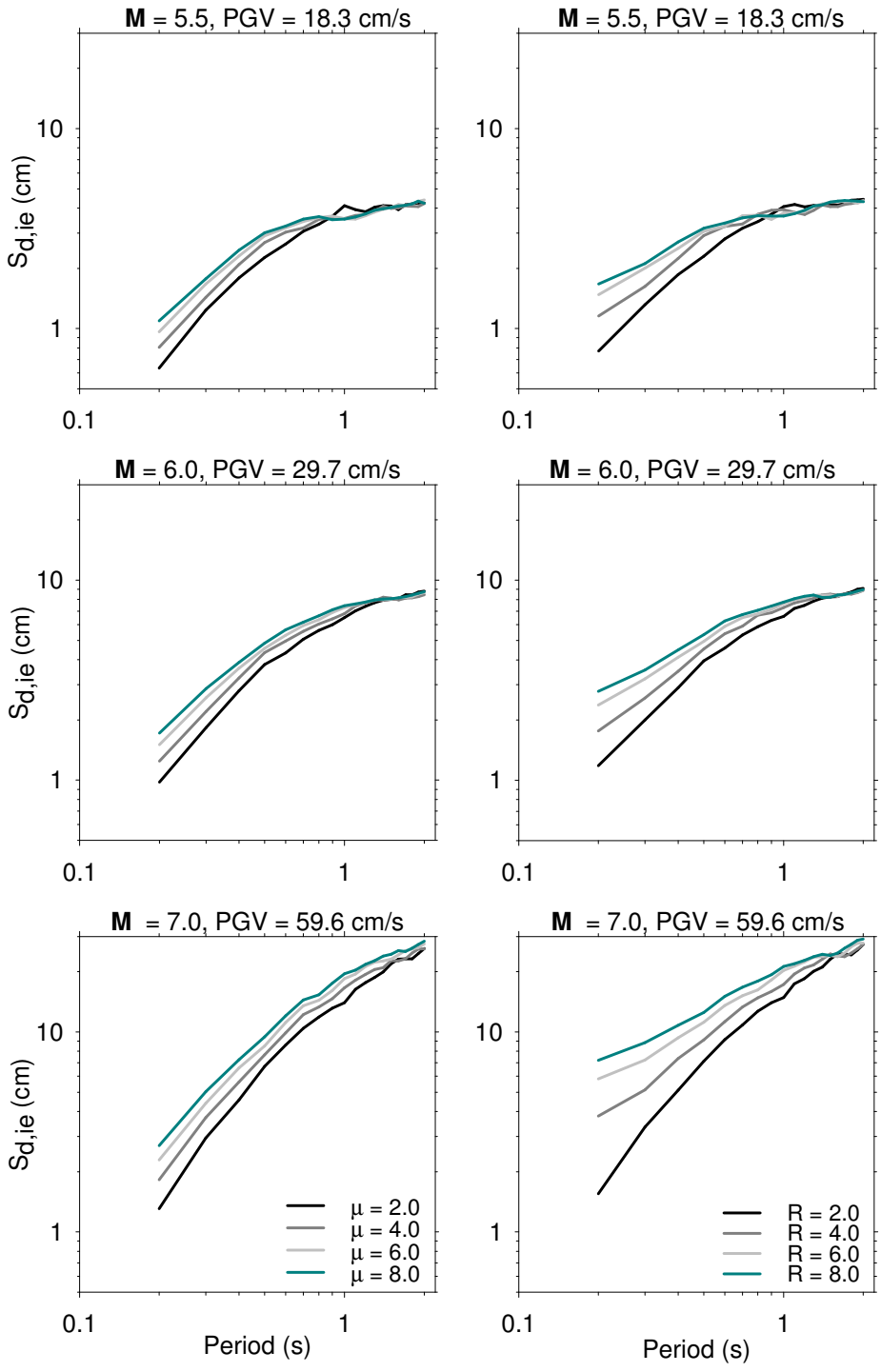

Figure 3.17. Inelastic spectral displacement estimations of the proposed predictive model for constant μ (first column) and constant R (second column) as a function of magnitude when $\alpha = 0\%$.

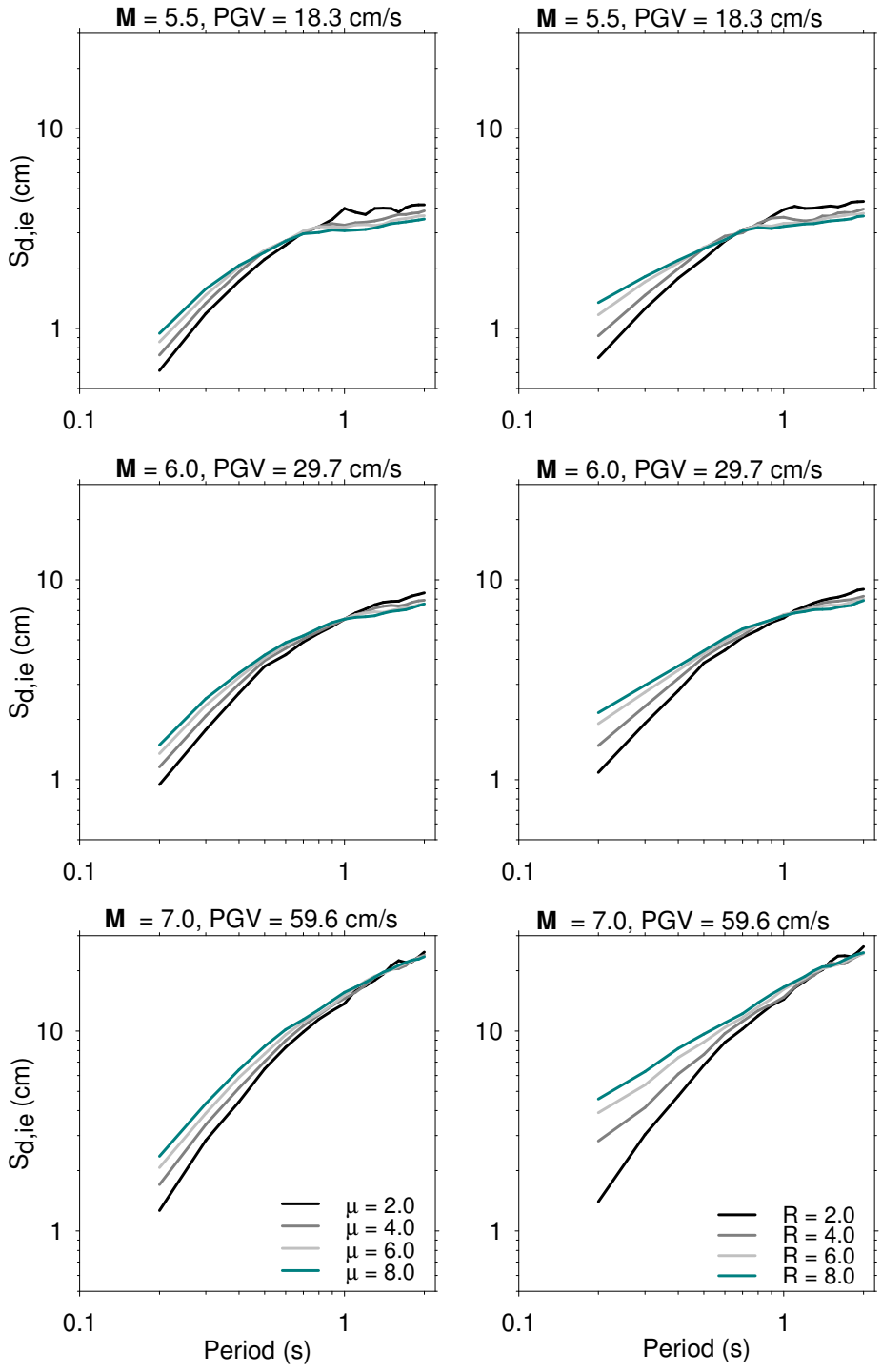

Figure 3.18. Inelastic spectral displacement estimations of the proposed predictive model for constant μ (upper row) and constant R (lower row) as a function of magnitude when $\alpha = 5\%$.

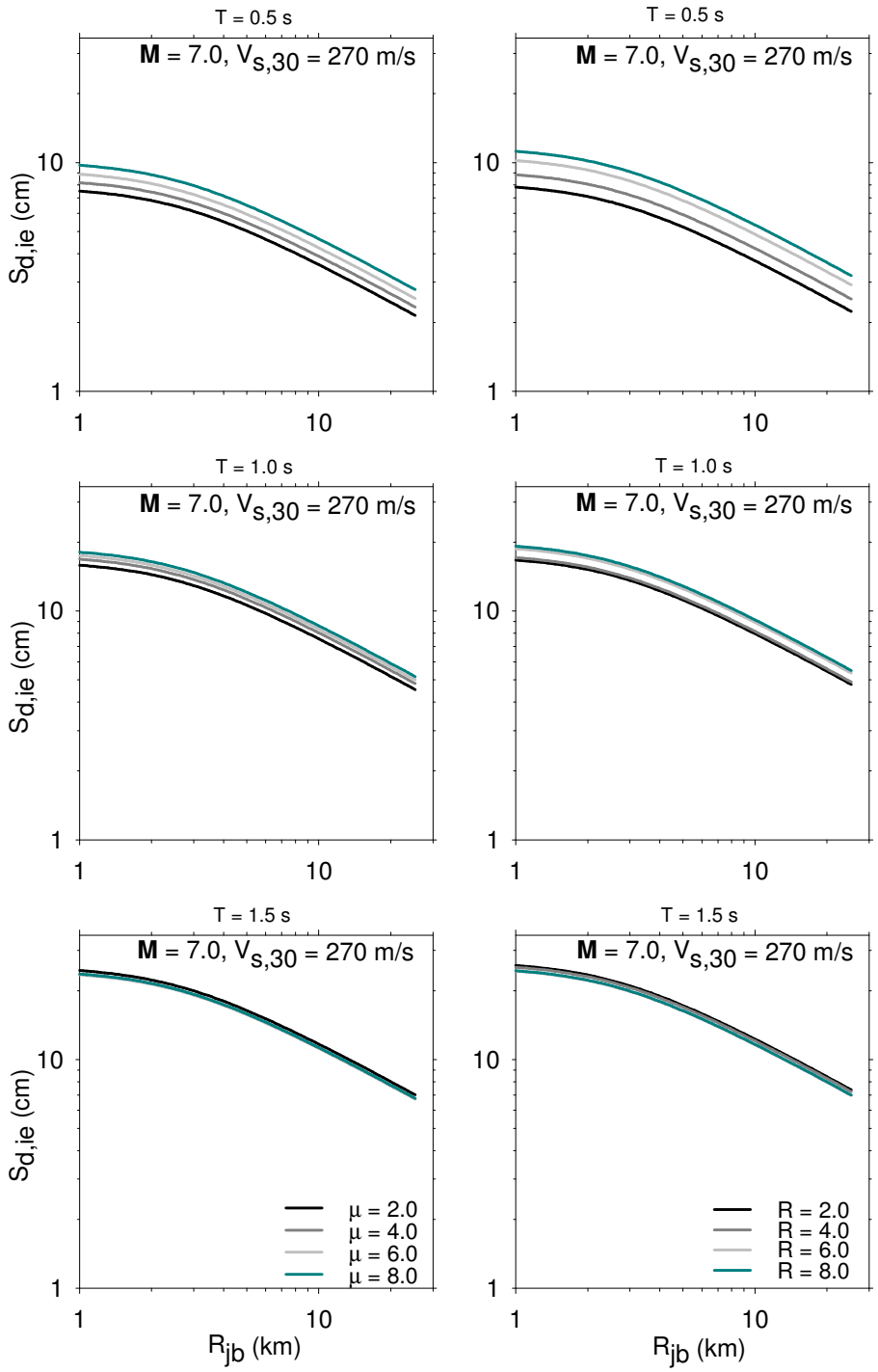

Figure 3.19. Influence of *PGV* variation as a function of distance on inelastic spectral displacement estimations for constant ductility (first column) and for constant strength (second column).

The plots consistently show that the distance dependent decay in *PGV* results in a decrease in $S_{d,ie}$ estimations. For short-period systems the change in *PGV* as a function of distance has more prominent influence at different levels of inelasticity that are described by various values of μ and *R*. This influence diminishes gradually as the structural period shifts to longer periods and it is almost invisible after T = 1.5 s for the particular α value used. The reason behind this observation can be related to the postyield stiffness ratio, the rate of change in distance-dependent *PGV* variation and the magnitude-dependent corner periods that define either the equal displacement spectral ranges or the constant displacement spectral plateau. The proposed model can fairly account for these seismological parameters that play important role on the peak inelastic oscillator displacements.

CHAPTER 4

CONCLUDING REMARKS

4.1 General

The main objective of this study is to propose a model to estimate the nonlinear peak oscillator deformation demands as a function of peak ground velocity (*PGV*) which is a promising ground-motion intensity measure having a strong relationship with earthquake magnitude. The predictive model considers the random error term that is a function of period (T) and displacement ductility (μ) or normalized lateral strength ratio (R).

The secondary objective of this study is to observe the relationships between some of the ground-motion intensity measures (*PGA*, *PGV* and $PS_a(T_1)$) and the global deformation demands of multi-degree-of freedom systems (i.e. maximum interstory drift ratio, *MIDR* and maximum roof drift ratio, *MRDR*). This way the study compares and verifies the observations of Akkar and Özen (2005) that are validated only for single-degree-of-freedom systems.

As a part of this thesis, recently developed ground-motion prediction equations (GMPE) for *PGV* by Akkar and Bommer (2007a) and Boore and Atkinson (2007) are used for displaying the practicality and applicability of the proposed model via GMPEs.

4.2 Summary and Conclusions of Chapter 2

Chapter 2 includes information about the ground-motion records and modeling and design of buildings used in this study. The important seismological features of the records and the detailed dimensioning of the structural members in the building models are also presented. The results of response history analyses (RHA) for building models as well as the specific conditions and assumptions taken into account in the RHA are provided within the context of this chapter.

The study has made use of two sets of ground-motion records of moderate-to large-events recorded on site classes NEHRP C and NEHRP D. None of the sets contains dominant pulse signals. The first set is composed of 60 ground-motion records and it is used to investigate the relationship between some of the ground-moton intensity indices and the global deformation demands of MDOF models with 3, 5, 7 and 9 stories. This set is divided into 3 bins each having 20 records according to the *PGV* values. The *PGV* range of first bin records is 1 cm/s < *PGV* < 20 cm/s wheras the *PGV* ranges of second and third bins are 20 cm/s < *PGV* < 40 cm/s and 40 cm/s < *PGV* < 60 cm/s, respectively. The second set is comprised of 109 records in total; 54 of which is from the European ground-motion dataset compiled by Akkar and Bommer (2007) and the rest is from the first set. The second data set describes the random component effect.

Five different building models (e1, e2, e3, e1' and e2') of different number of stories (i.e. 3, 5, 7 and 9 story) are designed from three different median design spectra assembled according to the above sub-bins of first ground-motion dataset. e1, e2 and e3 models are designed according to median spectra of the first, second and third bin, respectively. The e1' and e2' models preserve the size and dimensions

of e1 and e2 models, respectively. Their reinforcement are calculated according to the design spectrum of the third bin. The nonlinear time history and pushover analyses of the models are conducted by using the IDARC-2D structural analysis software under three different structural behaviors: non degrading, stiffness degrading and stiffness and strength degrading, respectively. *MRDR* and *MIDR* values are taken as the global deformation demand measures for MDOF systems and the relationships between these demand measures and intensity measures (*PGA*, *PGV* and $PS_a(T_1)$) are investigated and evaluated through Spearman's correlation coefficient (ρ) .

The most important observations obtained from this chapter are listed below:

- Pushover curves idealized according to ATC-40 reveal good agreement with the absolute maximum roof displacement versus base shear plots that are obtained from RHA. The pushover curves are computed using the inverted triangular loading pattern and the above match between the pushover curves and RHA results verify the first-mode dominant behavior of the models.

- The ρ values tend to increase for *PGV* vs. *MRDR* and *PGV* vs. *MIDR* scatters with increasing story number in all three hysteretic behaviors. This observation advocates that *PGV* corelates well with the global deformation demands with increasing story number. There is no clear relationship between the increase in story number and the associated ρ values for *PGA* vs. *MRDR* and *PGA* vs. *MIDR*. In the case of $PS_a(T_1)$ vs. *MRDR* and $PS_a(T_1)$ vs. *MIDR* a trend that is similar to the one observed in *PGV* is identified. However, the associated ρ values of $PS_a(T_1)$ are smaller than those of *PGV*.

- The comparisons between the ρ values of all ground-motion intensity measures reveal that regardless of the hysteretic behaviors investigated the highest ρ values are the ones associated with *PGV*.

- An observation valid for all hysteretic behaviors and for all ground-motion intensity measures is that the associated ρ values of *MRDR* are higher than those of *MIDR* for 3 and 9 story models while for 5 and 7 stories ρ values of *MIDR* is higher with few exceptions.

4.3 Summary and Conclusions of Chapter 3

This chapter presents a predictive model for estimating the constant ductility (μ) and normalized lateral strength (R) spectral displacements for a given initial period, magnitude and *PGV* value. Sensitivity analysis that considered the influence of ground-motion parameters such as magnitude, distance, site class etc. on the dimensionless predictive parameter $S_{d,e}$ / *(PGVxT)* is conducted to use it in the predictive model. The proposed model also accounts for the random error by the empirical equations that are function of R (or μ) and T. In order to demonstrate the use of the predictive model with ground-motion prediction equations, case studies are provided in the last section of this chapter under different scenarios. Major observations obtained from this chapter are listed below:

- Sensitivity analyses conducted using the ground-motion prediction equations of Akkar and Bommer (2007a, 2007b) and Boore and Atkinson (2007) showed that magnitude influence on the predicted parameter is considerably high when compared to

the influence of distance. The investigation on the effect of faulting style on the predicted parameter revealed that style of faulting is not as influential as magnitude.

- As for the effect of site class on the predicted parameter $S_{d,e}$ / *(PGVxT)* a departure between soft and stiff site is observed for large magnitude and mid-period values while there is no clear difference for low-period values in the curves of stiff and soft sites.

- The assumption of the regression method used (Least Squares Regression) that dictates normal distribution for random error terms with zero mean and σ^2 is satisfied by the normal probability plots of the residuals. As a matter of fact, it can be concluded that aleatory uncertainty associated with the predictive model can be fairly explained well by the variances computed from the residual mean squares.

- When the residual plots of the model as a function magnitude are considered, the associated dispersion is relatively higher in α=0% than in α=5%. However, in both cases the plots do not exhibit a biased trend in the residuals.

- The variation of standard deviations shows that the σ values decrease with increasing α value and with decreasing level of inelasticity.

- The $S_{d,ie}$ vs. period plots obtained from the application of the proposed model revealed that the increase in *PGV* shifts spectral regions towards longer periods.

- At short period ranges, the difference between $S_{d,ie}$ values of ductility and normalized lateral strength are notable.

- $S_{d,ie}$ vs. R_{jb} plots showed that distance dependent decrease in PGV values resulted in a decrease in $S_{d,ie}$ estimations especially for short periods.

It is concluded that the predictive model is adequate in differentiating the difference in nonlinear oscillator response imposed by the constant ductility and normalized lateral strength ratio. These features make the predictive model versatile for preliminary design and seismic performance of a broad class of building systems.

4.4 Recommendations for Further Studies

The following issues can be addressed in a broader sense in further studies:

- The proposed model is developed from a limited number of ground-motion records. The model can be improved by adding more records in the regression analyses stage to account for a wide range of ground motion features inherited in the records.

- More complex predictive models can be developed by considering the influence of independent ground-motion parameter (style of faulting, site class, distance etc.) other than magnitude. Similar models can be obtained for a specific style of faulting or site classes using the specifically selected ground motion records.

- Expressions that calculate the random error can be investigated further by considering the magnitude influence.

- The compatibility of the proposed model with ground motion prediction equations for *PGV* other than Akkar and Bommer (2007a) and Boore and Atkinson (2007) can be investigated.

REFERENCES

Akkar S, Bommer J.J., *Empirical prediction equations for peak ground velocity derived from strongmotion records from Europe and the Middle East*, Bulletin of the Seismological Society of America 2007a; 97(2): 511-530.

Akkar S, Bommer J.J., *Prediction of elastic displacement response spectra in Europe and the Middle East,* Earthquake Engineering and Structural Dynamics 2007b; 36: 1275-1301.

Akkar S, Bommer JJ., *Influence of long-period filter cut-off on elastic spectral displacements,* Earthquake Engineering and Structural Dynamics 2006; 35(9): 1145-1165.

Akkar S, Özen, Ö., *Effect of peak ground velocity on deformation demands for SDOF systems*, Earthquake Engineering and Structural Dynamics 2005; 34(13): 1551-1571.

Akkar S., Sucuoğlu H and Yakut A., *Displacement-based fragility functions for low- and mid-rise ordinary concrete buildings*, Earthquake Spectra, 2005; 21(4): 901-927.

Arroyo D, Terán A., *Strength reduction factors for ductile structures with passive energy dissipating devices*, Journal of Earthquake Engineering; 2003 7(2): 297-325.

ASCE., *Prestandard and commentary for the seismic rehabilitation of buildings,* Report No. FEMA 356, American Society of Civil Engineers, Washington DC, 2000.

ATC, *Improvement of nonlinear static seismic analysis procedures*. Report No. FEMA 440, Applied Technology Council, Washington DC, 2005.

Atkinson, G. M. and Boore, D. M., *Ground-motion relations for eastern North America*, Bulletin of the Seismological Society of America 85(1), 17–30,1995

Baéz J.I, Miranda E., *Amplification factors to estimate inelastic displacement demands for the design of structures in the near field,* Proceedings of 12th World Conference on Earthquake Engineering, CDRom Auckland, New Zealand, 2000.

Beyer K, Bommer J.J., *Relationships between median values and between aleatory variabilities for different definitions of the horizontal component of motion*, Bulletin of the Seismological Society of America 2006; 96(4A):1512-1522.

Bommer J.J, Stafford P.J, Alarcón J.E. and Akkar S., *Ground-motion predictions over extended magnitude range*, Bulletin of the Seismological Society of America 2007, in press.

Bommer J.J, Elnashai A.S., *Displacement spectra for seismic design,*. Journal of Earthquake Engineering 1999; 3(1):1-32.

Boore D.M, Atkinson G., *Ground-Motion Predictions Equations for the Average Horizontal Component of PGA, PGV, and 5%-Damped SA at Spectral Periods between 0.01 s and 10.0*, Submitted for publication in Earthquake Spectra, 2007.

Bray J.D, Rodriguez-Marek A., *Characterization of forward-directivity ground motions in the near-fault region,* Soil Dynamics and Earthquake Engineering 2004; 24(11): 815-828.

Campbell, K. W., *Empirical near-source attenuation relationships for horizontal and vertical components of peak ground acceleration, peak ground velocity, and pseudo-absolute acceleration response spectra*, Seismological Research Letters 68(1), 154–179, 1997

Chakraborati A, Gupta V.K., *Scaling of strength reduction factors for degrading elasto-plastic oscillators*, Earthquake Engineering and Structural Dynamics 2005; 34:189–206.

Chopra A.K, Chintanapakdee C., *Comparing response of SDF systems to near-fault and far-fault earthquake motions in the context of spectral regions*, Earthquake Engineering and Structural Dynamics 2001; 30:1769–1789.

Chopra A.K, Chintanapakdee C., *Inelastic Deformation Ratios for Design and Evaluation of Structures: Single-Degree-of-Freedom Bilinear Systems*, Journal of Structural Engineering 2004; 130:1309-1319.

Cuesta I, Aschheim M.A, Fajfar P., *Simplified R-Factor Relationships for Strong Ground Motions*, Earthquake Spectra 2003; 19(1):25-45.

Douglas J, Smit P.M., *How Accurate Can Strong Ground Motion Attenuation Relations Be?,* Bulletin of the Seismological Society of America 2001; 91(6): 1917-1923.

Draper N.R, Smith H., *Applied Regression Analysis*, Second edition, John Wiley & Sons Inc., New York, 709 pp, 1981.

Douglas, J., *Earthquake ground motion estimation using strong-motion records:A review of equations for the estimation of peak ground accelerations and response spectral ordinates*, Earth-Science Reviews 61, 43-104, 2003

Elghadamsi F, Mohraz B., *Inelastic earthquake spectra*, Earthquake Engineering and Structural Dynamics 1987; 15:91–104.

Faccioli E, Paolucci R, Rey J., *Displacement spectra for long periods*, Earthquake Spectra 2004; 20(2):347-376.

Fajfar, P., Vidic, T., and Fischinger., M., *A measure of earthquake motion capacity to damage medium-period structures*, Soil Dynamics and Earthquake Engineering,1990, 9(5), 236–242.

Farrow K.T, Kurama A., *SDOF demand index relationships for performance-based seismic design*, Earthquake Spectra,1998; 19:799-838

FEMA, N*EHRP guidelines for the seismic rehabilitation of buildings. Guidelines (FEMA 273) and Commentary (FEMA-274)*, Federal Emergency Management Agency, Washington DC, 1997.

FEMA, *The 2003 NEHRP recommended provisions for new buildings and other structures. Part 1: Provisions (FEMA 450)*, Federal Emergency Management Agency, Washington DC, 2003.

Frisenda, M., Massa, M., Spallarossa, D., Ferretti, G. and Eva, C., *Attenuation relationships for low magnitude earthquakes using standard seismometric records*, Journal of Earthquake Engineering 9(1), 23–40, 2005

Gregor, N., Silva, W. and Darragh, B., *Development of attenuation relations forpeak particle velocity and displacement*, Pearl Report to PG&E/CEC/Caltrans/Pacific Engineering and Analysis, Retrieved from http://www. pacificengineering.org/rpts page1.html on February 12, 2002

Joyner W.B, Boore D.M., *Peak horizontal acceleration and velocity from strong-motion records including records from the 1979 Imperial Valley, California, earthquake*, Bulletin of the Seismological Society of America 1981; 71(6): 2011-2038.

Karmakar D, Gupta V.K., *Estimation of strength reduction factors via normalized pseudo-acceleration response spectrum*, Earthquake Engineering and Structural Dynamics 2007; 36:751–763.

Kramer, S.L, *Geotechnical Earthquake Engineering*, Prentice Hall, New Jersey, 1996

Krawinkler, *Challenges and Progress in Performance-based Earthquake Engineering*, International Seminar on Seismic Engineering for Tomorrow – In Honor of Professor Hiroshi Akiyama Tokyo, Japan, November 26, 1999

Kurama Y.C, Farrow K.T, *Ground motion scaling methods for different site conditions and structure characteristics*, Earthquake Engineering and Structural Dynamics, 2003; 32 (15): 2423–2450.

MacRae G.A, Tagava H., *Methods to estimate displacements of PG&E structures*, Final Report PG&E/PEER Task No. 505, Seattle Washington, 2002.

MacRae G.A, Morrow D.V, Roeder C.W, *Near-fault ground motion effects on simple structures,* Journal of Structural Engineering, 2001; 127(9): 996-1004.

MacRae G.A, Roeder C.W, *Near-field ground motion effects on short structures*, Final Report to PG&E/PEER, Pacific Earthquake Engineering Research Center, Richmond, CA, 1999.

Mahin S.A., Bertero V.V, *An evaluation of inelastic seismic design spectra*, Journal of Structural Division, 1981; 107: 1777-1795.

Metin,A., *Inelastic deformation demands on moment-resisting frame structures*, M.S Dissertation, METU,Ankara, 2006

Miranda E., *Inelastic displacement ratios for structures on firm sites*, Journal of Structural Engineering, 2000; 126:1150-1159.

Miranda E., Bertero V.V., *Evaluation of strength reduction factors for earthquake-resistant design*, Earthquake Spectra, 1994; 10(2), 357–397.

Miranda E., *Site dependent strength reduction factors*, Journal of Structural Engineering 1993; 119: 3503-3519.

Miranda E, *Estimation of inelastic deformation demands of SDOF systems*, Journal of Structural Engineering (ASCE) 2001;127 (9):105-112

Molas, G. L. and Yamazaki, F., *Attenuation of response spectra in Japan using new JMA records*, Bulletin of Earthquake Resistant Structures ,1996, 29, 115–128.

Myers R.H., *Classical and modern regression with applications*, PWS Publishers, Boston Massachusetts, 359 pp, 1986.

Nassar A.A, Krawinkler H., *Seismic Demands for SDOF and MDOF Systems*. Report No. 95, The John A. Blume Earthquake Engineering Center, Stanford University, CA, 1991.

Newmark N.M, Hall W.J., *Seismic Design Criteria for Nuclear Reactor Facilities*, Report No. 46, Building Practices for Disaster Mitigation, National Bureau of Standards, U.S. Department of Commerce, 209-236, 1973.

Newmark N.M, Hall W.J., *Earthquake Spectra and Design*. EERI Monograph Series, Earthquake Engineering Research Institute, Oakland, CA, 1982.

Ordaz M, Pérez-Rocha L.E., *Estimation of strength-reduction factors for elasto-plastic systems: A new approach*, Earthquake Engineering and Structural Dynamics 1998; 27:889–901.

Pankow, K. L. and Pechmann, J. C., *The SEA99 ground-motion predictive relations and new peak ground velocity relation*, Bulletin of the Seismological Society of America, 2004, 94(1), 341–348.

Press W.H, Flannery B.P, Teukolsky S.A and Vetterling W.T., *Numerical recipes: the art of scientific computation (FORTRAN version)*, Cambridge University Press, Cambridge, 702 pp, 1989.

Riddell R., On *ground motion intensity indices*, Earthquake Spectra, 2007; 23(1): 147-173.

Riddell R, Garcia J.E, Garces E., *Inelastic deformation response of SDOF systems subjected to earthquakes*, Earthquake Engineering and Structural Dynamics, 2002; 31:515-538.

Ruiz García J, Miranda E., *Inelastic ratios for design of structures on soft soils sites*, Journal of Structural Engineering, 2004; 130(12): 2051-2061.

Ruiz-García J, Miranda E., *Inelastic displacement ratios for evaluation of existing structures*, Earthquake Engineering and Structural Dynamics 2003; 32:1237-1258.

Sadigh, R. K. and Egan, J. A., *Updated relationships for horizontal peak ground velocity and peak ground displacements for shallow crustal earthquakes,* Proceedings of the Sixth US National Conference on Earthquake Engineering, Seattle, Paper No. 317, 1998

Sewel R.T., *Damage effectiveness of earthquake ground motion: characterizations based on the performance of structures and equipment,* PhD Thesis, Department of Civil and Environmental Engineering, Stanford University, Stanford CA., 619 pp., 1989.

Singh, S.K., Gansl, B.K., Bhattacharya, S.N., Pacheco, J.F., Dattatrayam, R.S., Ordaz, M., Kamal, G.S. and Hough, S.E., *Estimation of ground motion for Bhuj (26 January 2001; Mw 7.6) and for future earthquakes in India*, Bulletin of Seismological Society of America, 2003, 93(1), 353–370.

Sucuoğlu H., Yazgan U., and Yakut A., *A Screening Procedure for Seismic Risk Assessment in Urban Building Stocks*, Earthquake Spectra, 2007; 23(2): 441-458.

Tothong P., Cornell A.C., *An empirical ground-motion attenuation relation for inelastic spectral displacement*, Bulletin of the Seismological Society of America 2006; 96(6): 2146-2164.

Tromans, I. J. and Bommer, J. J., *The attenuation of strong-motion peaks in Europe*, Proceedings of the Twelfth European Conference on Earthquake Engineering, London, Paper 394, 2002

Valles, R.E., Reinhorn, A.M., Kunnath, S.K., Li, C., and Madan, A., *IDARC-2D: A program for the inelastic damage analysis of buildings,*, National Center for Earthquake Engineering Research, State University of New York at Buffalo, 1996

Veletsos A.S., Newmark N.M., *Effect of inelastic behavior on the response of simple systems to earthquake motions*, Proceedings of 2nd World Conf. on Earthquake Engineering, Vol. II, Tokyo, 895–912., 1960.

Vidic T., Fajfar P., Fischinger M., *Consistent inelastic design spectra: strength and displacement*, Earthquake Engineering and Structural Dynamics 1994; 23:507–521.

Yılmaz, H., *Correlation of deformation demands with ground motion intensity*, M.S Dissertation, METU, Ankara, 2007

Wu Y.M, Teng TI, Shin T.C, Hsiao N.C., Relationship between peak ground acceleration, peak ground velocity and intensity in Taiwan. Bulletin of the Seismological Society of America 2003; 93:386-396.

APPENDIX A

MDOF MODELS

A.1. General

Four different story reinforced concrete models are employed in this study depicting the low to mid rise building stock of general construction practice in Turkey as 3, 5, 7 and 9 stories respectively. Each model further divided into 5 subgroups. The subgroups are based on the design spectra used. Five subgroups can be listed as follows:

- e1 - Models are designed using the design spectrum obtained from the Bin 1 (0 cm/s < *PGV*<20 cm/s)
- e2 - Models are designed using the design spectrum obtained from the Bin 2 (20 cm/s < *PGV*<40 cm/s)
- e3 - Models are designed using the design spectrum obtained from the Bin 3 (40 cm/s < *PGV*<60 cm/s)
- e1' – The reinforcement detailing of e1 models are redesigned using the response spectrum of Bin 3
- e2' – The reinforcement detailing of e2 models are redesigned using the response spectrum of Bin 3

The reinforcement designs of the models are conducted by SAP 2000 v.8.2.3. The values on the stress-strain curves of steel and concrete are calculated as suggested by IDARC-2D after the decision of the compressive strength of the materials (Figure A.1 and A.2), (Valles et al, 1996).

Concrete

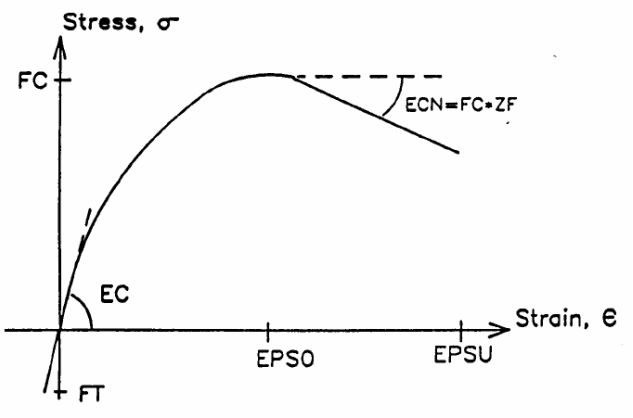

Figure A.1 Stress- strain curve of concrete

FC : *Unconfined compressive strength* - 20 MPa

EC *: Initial young's modulus* - 26800

EPSO *:Strength at max. Strength of concrete* - 0.2%

FT : *Stress at tension cracking* - 2.4 MPa

EPSU : *Ultimate strain in compression (%)* - 0 %

ZF : *Parameter defining slop of falling branch* - 0

Reinforcement

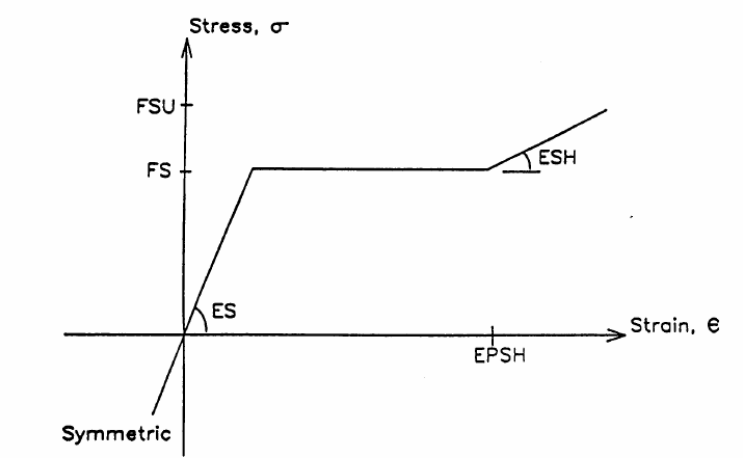

Figure A.2 Stress- strain curve of steel

FS:Yield strength - 420 MPa

FSU : Ultimate strength - 588 MPa

ES : Modulus of elasticity - 200000

ESH : Modulus of strain hardening - 3333

EPSH : Strain at start of hardening (%) - 3.0 %

FSU =1.4*FS ESH = (ES/60) ksi EPSH=3 %

During the column and beam design the following values are taken for the members. Well confinement is selected for the members, which reflects the effectiveness of the confinement (Figure A.3). The corresponding values are taken for rigid zone length, hoop bar diameter and spacing, diameter and spacing of stirrups, distance from centroid to cover as shown in Table A.1.

Figure A.3. Confinement effectiveness (Valles et al, 1996)

Table A.1 Some specific distances used in the design of members

Distances used in design of members	Beam	Column	Distances used in design of members	Beam	Column
Rigid zone length (cm)	22.5	25	Cover to centroid of the steel (cm)	5	-
Distance from centroid			Effective slab width (cm)	30	-
of reinf. to face of column (cm)	-	6.5	Slab Thickness (cm)	0	-
Hoop bar diameter (cm)	-	1.2	Diameter of stirrups (cm)	1	-
Hoop bar spacing (cm)	-	7.5	Spacing of stirrups (cm)	13.5	-

A.2 Model 3e1

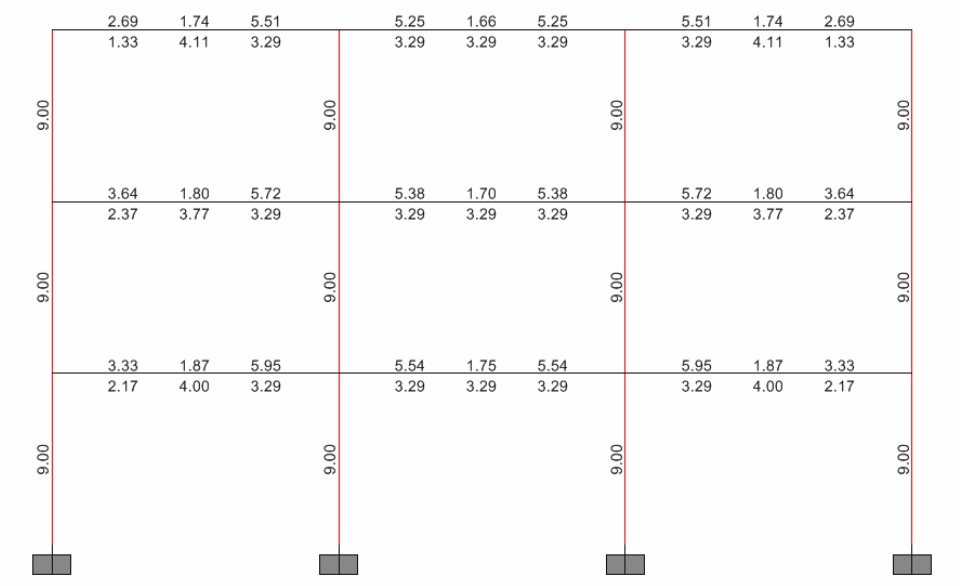

Figure A.4 Reinforcement areas in cm^2 for 3e1

A.3 Model 3e2

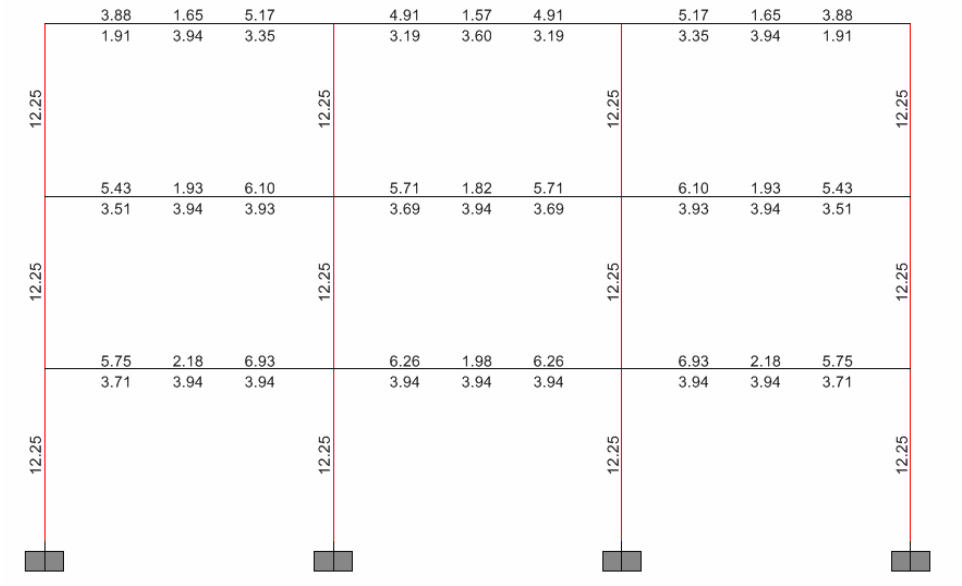

Figure A.5 Reinforcement areas in cm^2 for 3e2

A.4 Model 3e3

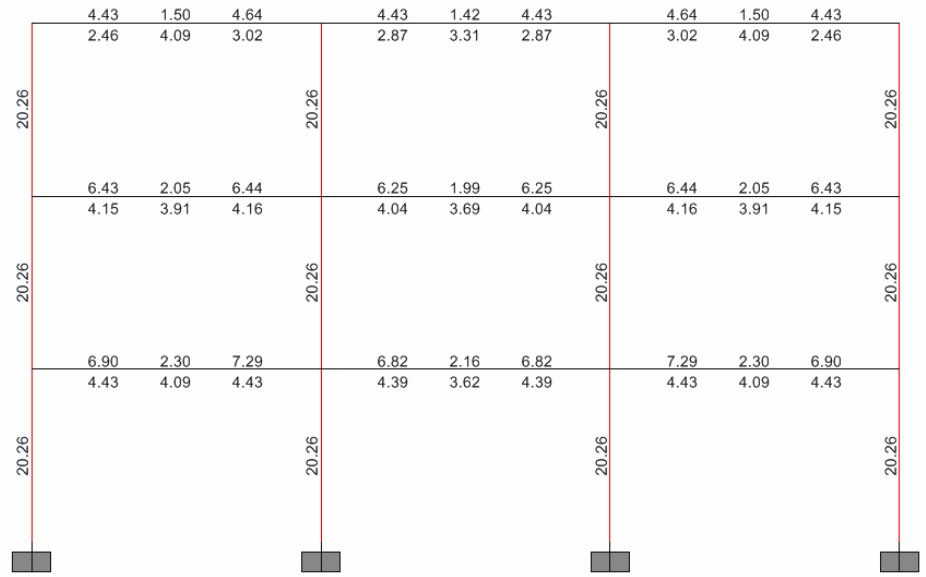

Figure A.6 Reinforcement areas in cm^2 for 3e3

A.5 Model 3e1'

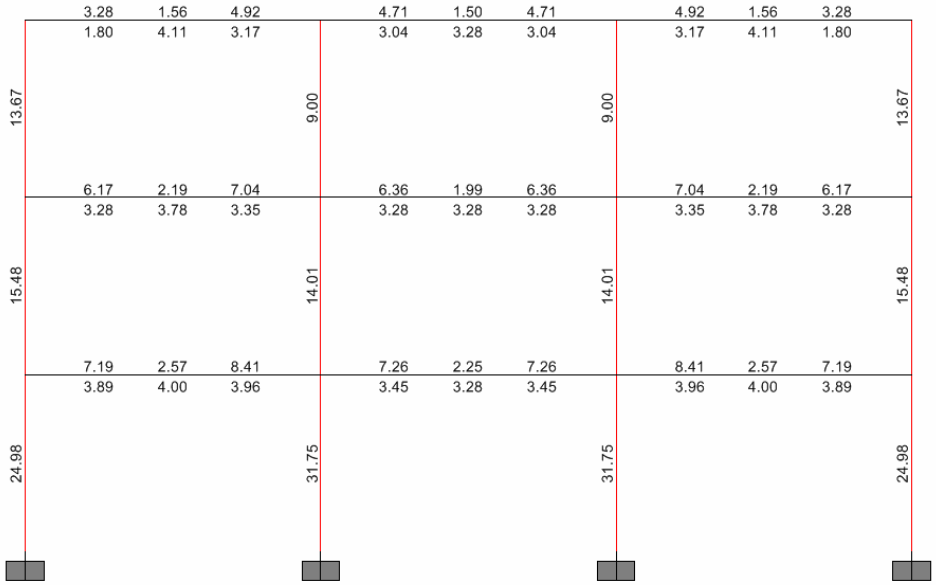

Figure A.7 Reinforcement areas in cm^2 for 3e1'

A.6 Model 3e2'

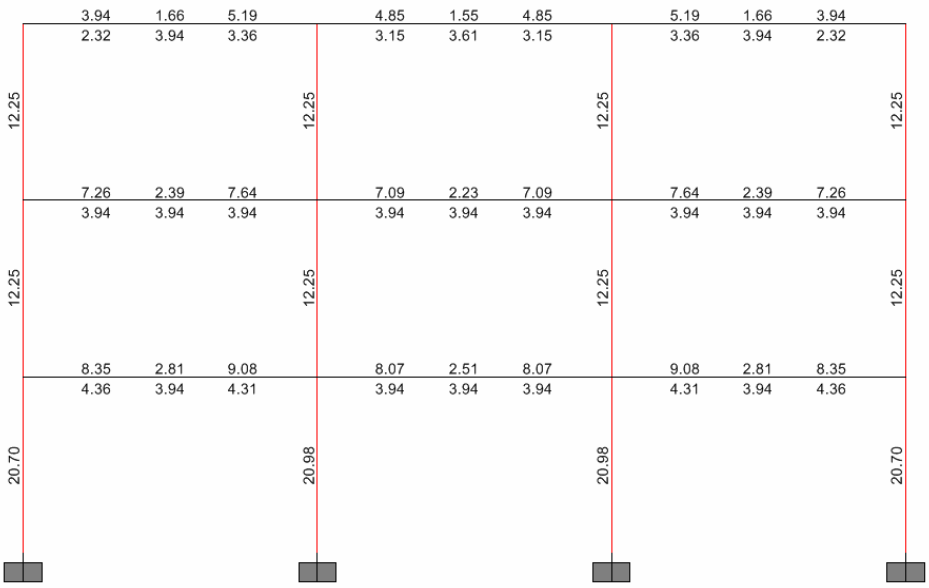

Figure A.8 Reinforcement areas in cm^2 for 3e2'

A.7 Model 5e1

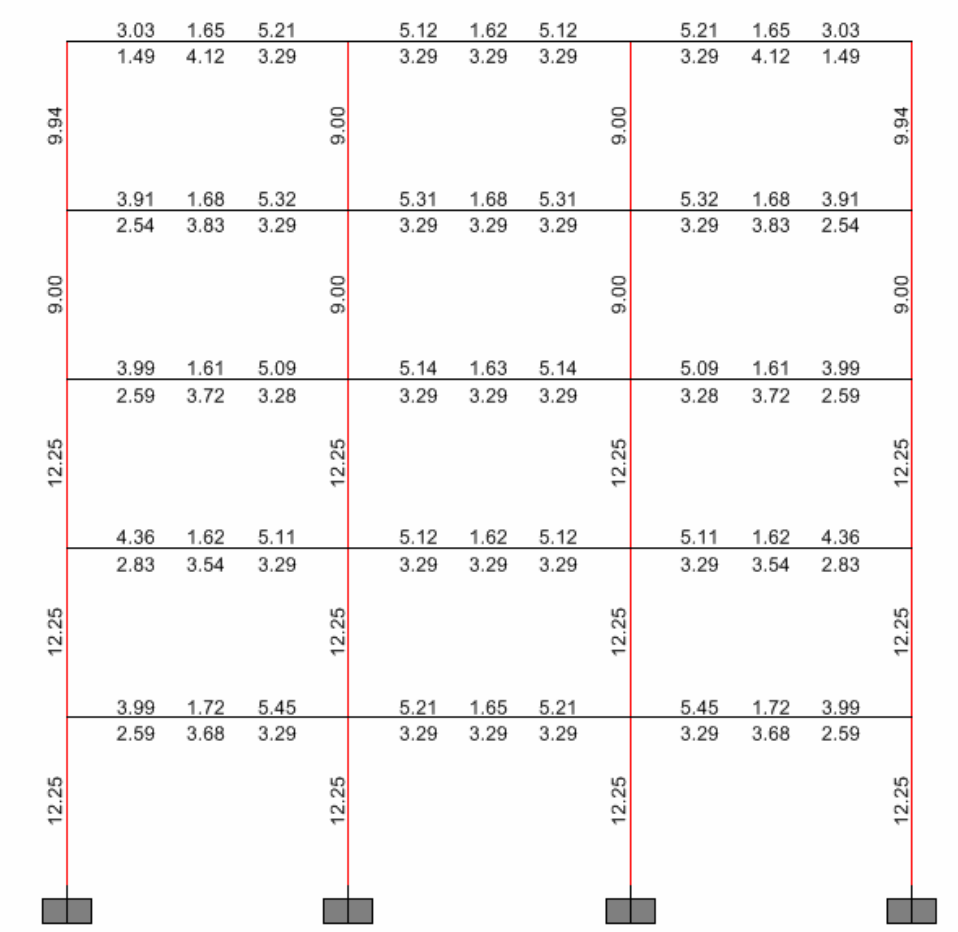

Figure A.9 Reinforcement areas in cm^2 for 5e1

A.8 Model 5e2

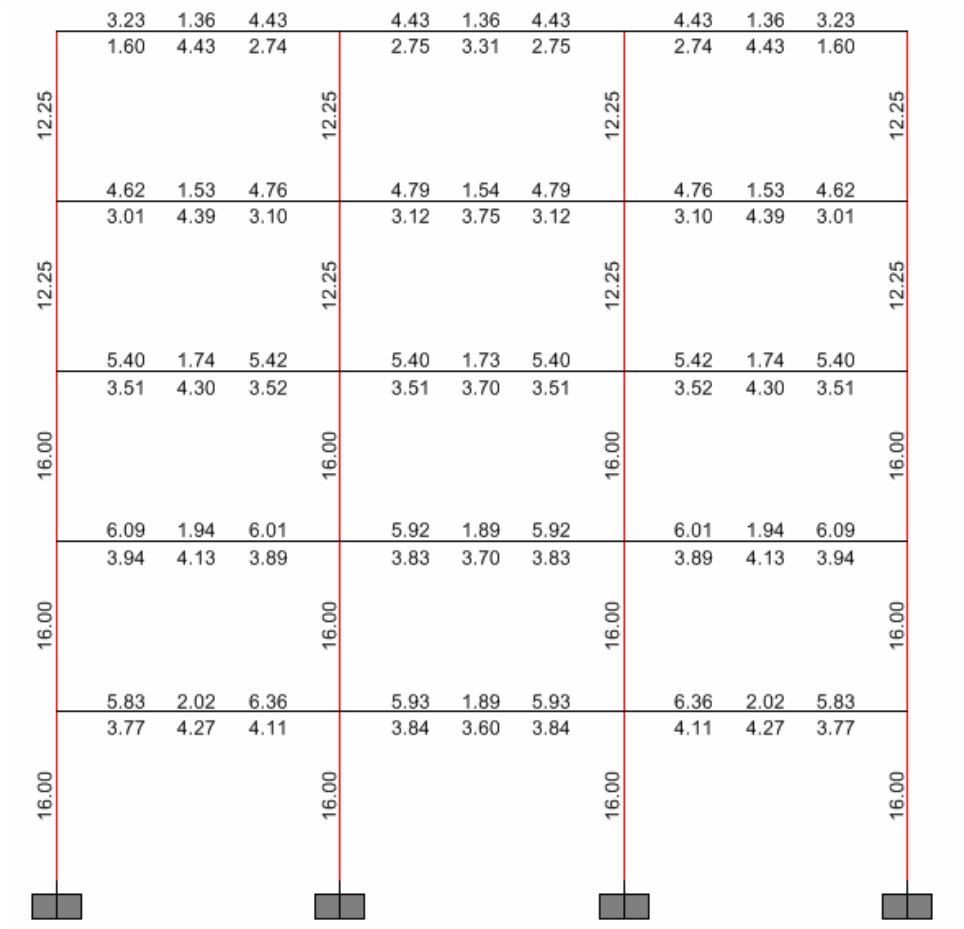

Figure A.10 Reinforcement areas in cm^2 for 5e2

A.9 Model 5e3

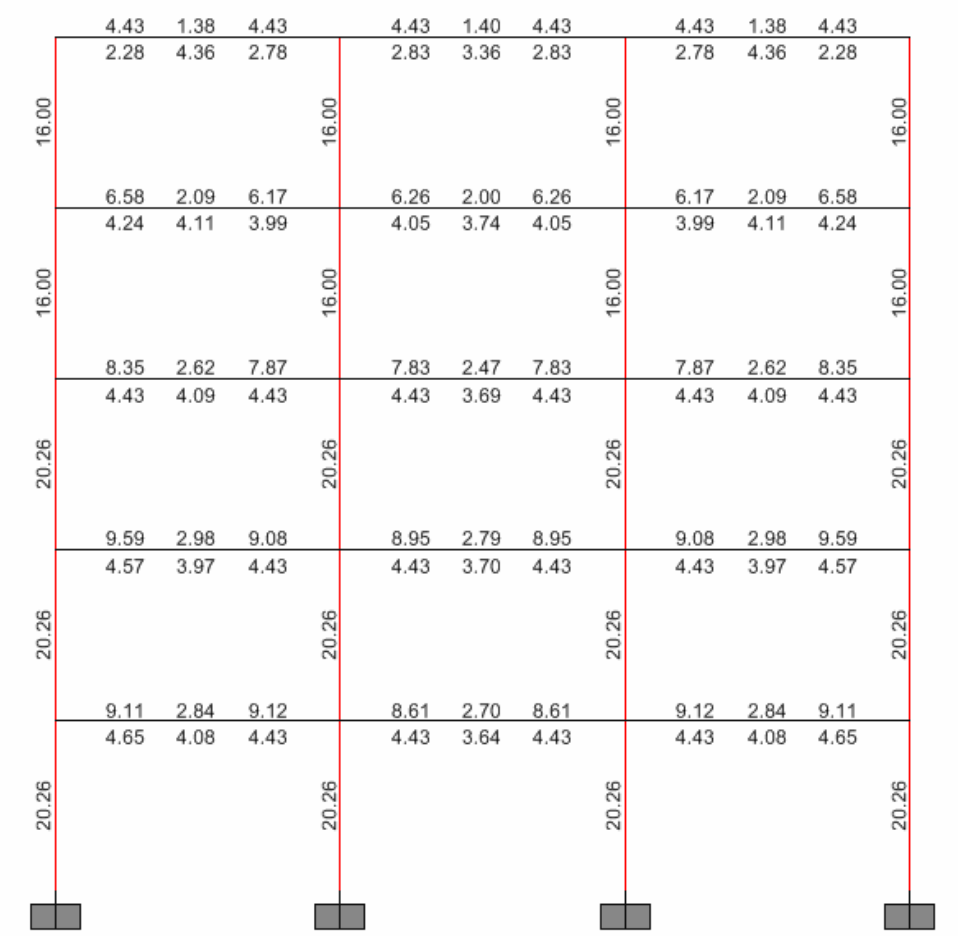

Figure A.11 Reinforcement areas in cm^2 for 5e3

A.10 Model 5e1'

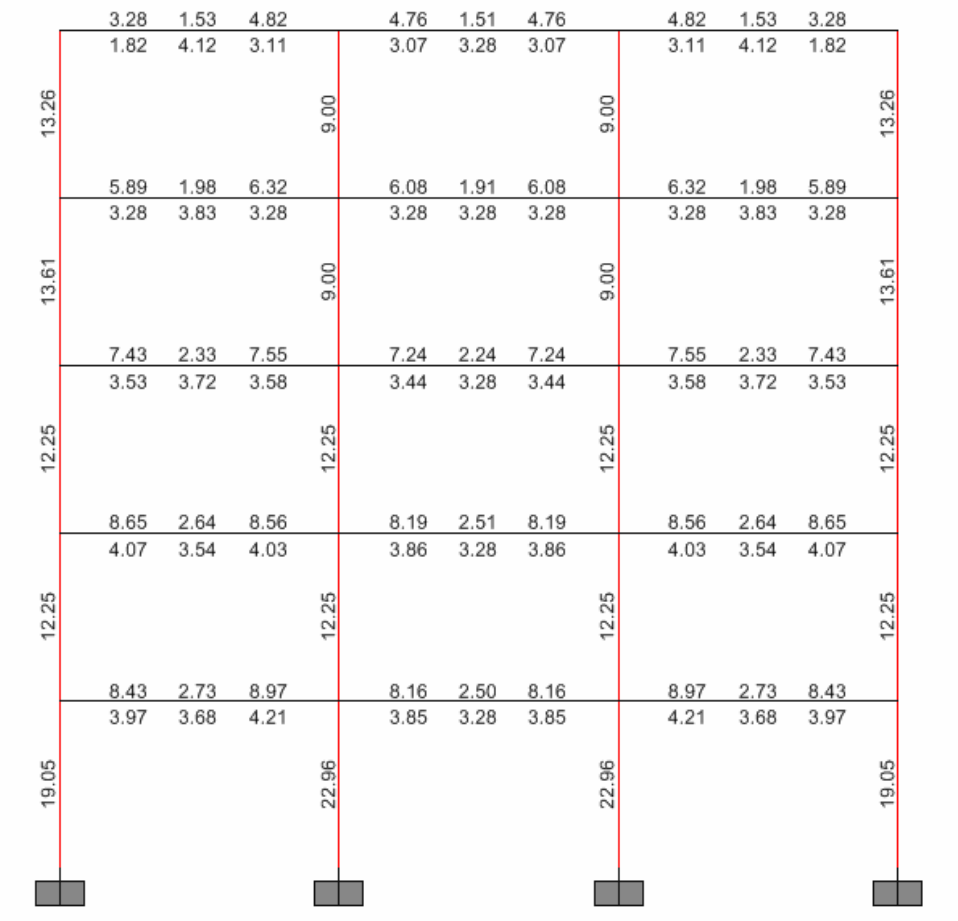

Figure A.12 Reinforcement areas in cm^2 for 5e1'

A.11 Model 5e2'

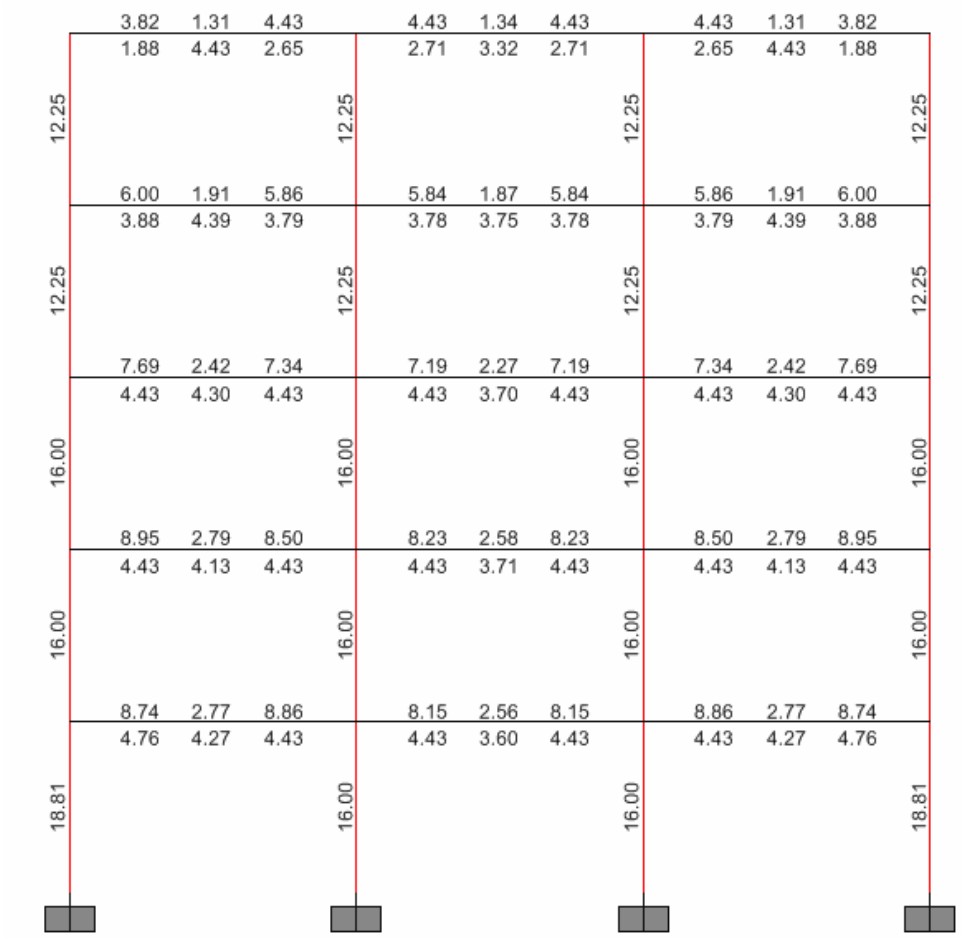

Figure A.13 Reinforcement areas in cm^2 for 5e2'

A.12 Model 7e1

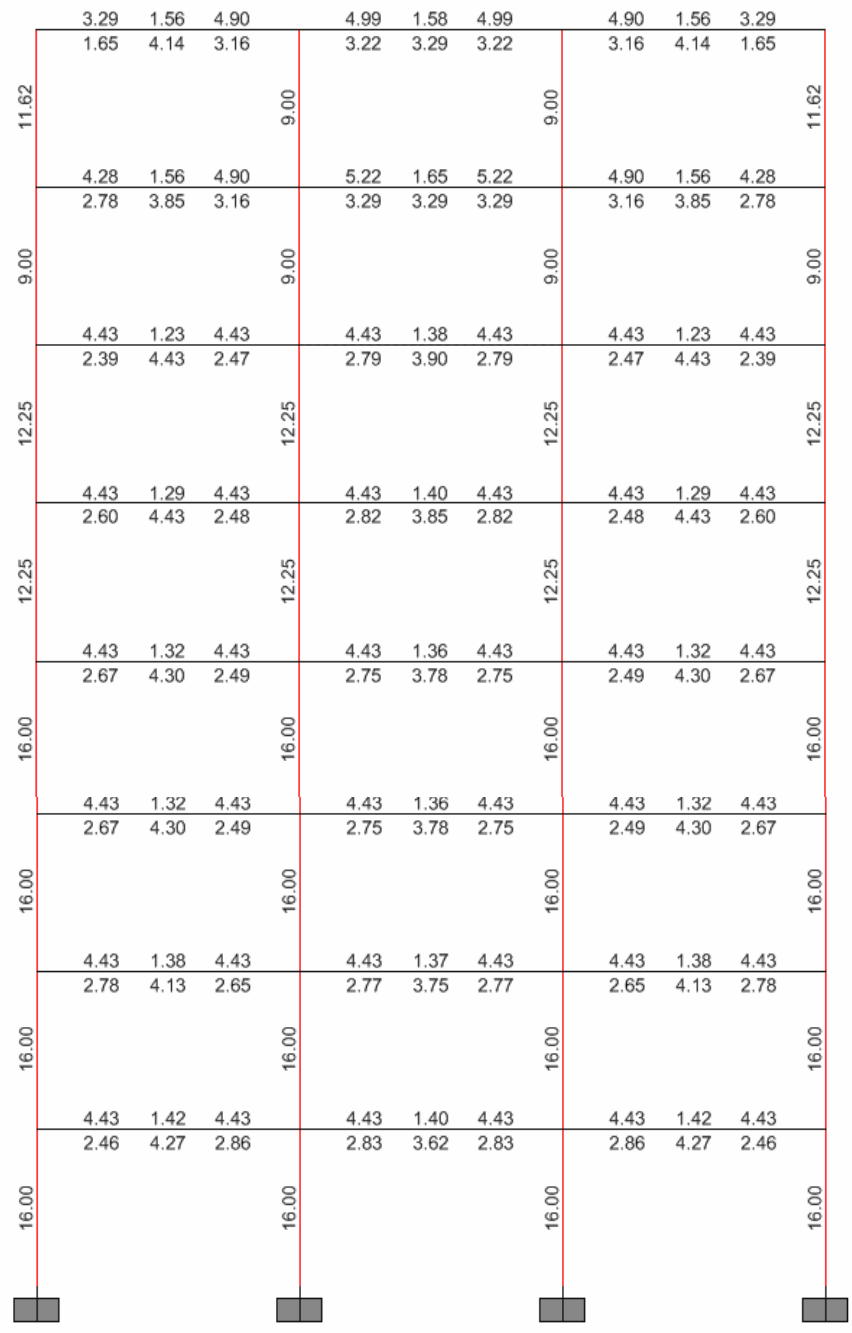

Figure A.14 Reinforcement areas in cm^2 for 7e1

A.13 Model 7e2

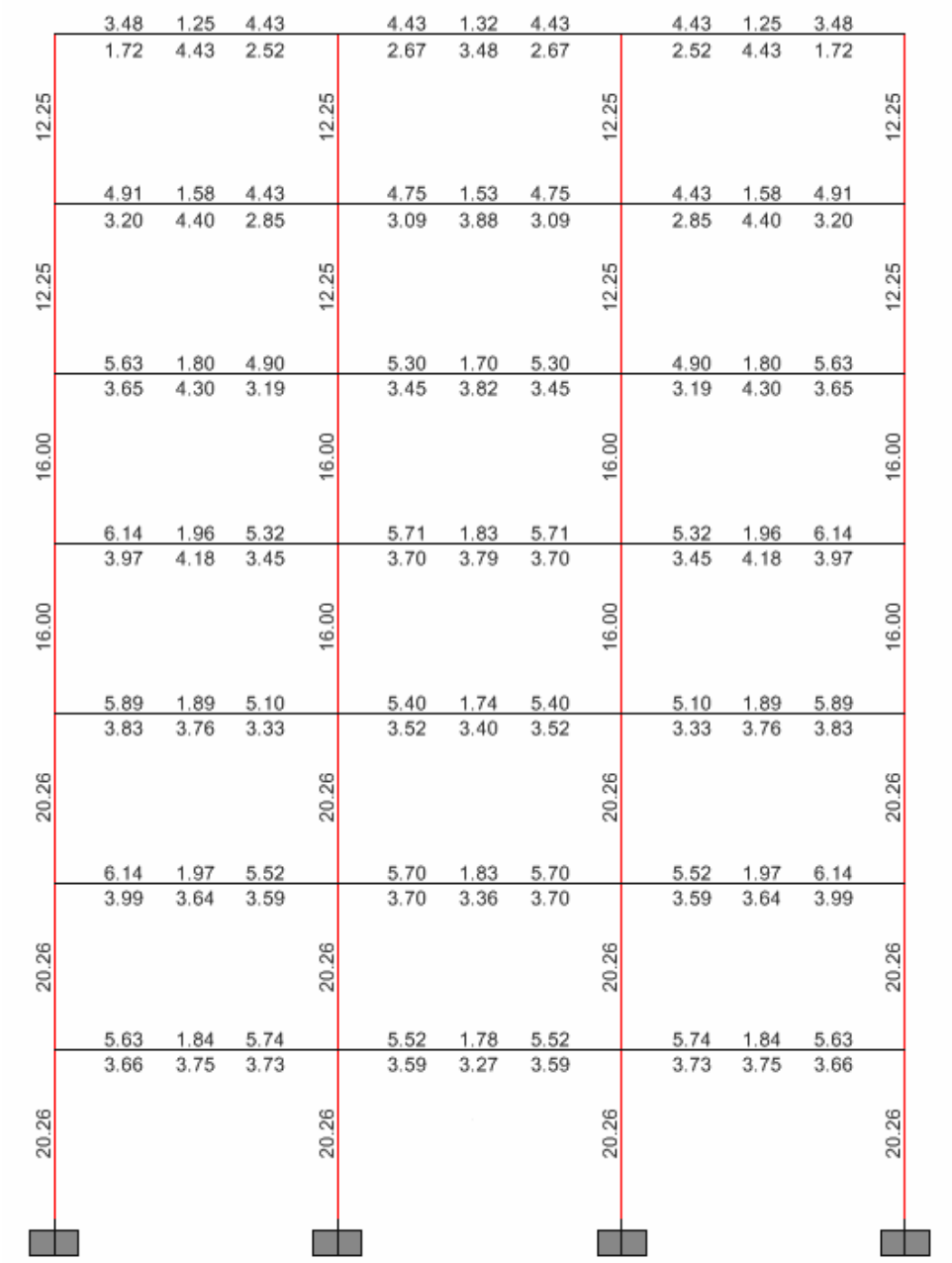

Figure A.15 Reinforcement areas in cm^2 for 7e2

A.14 Model 7e3

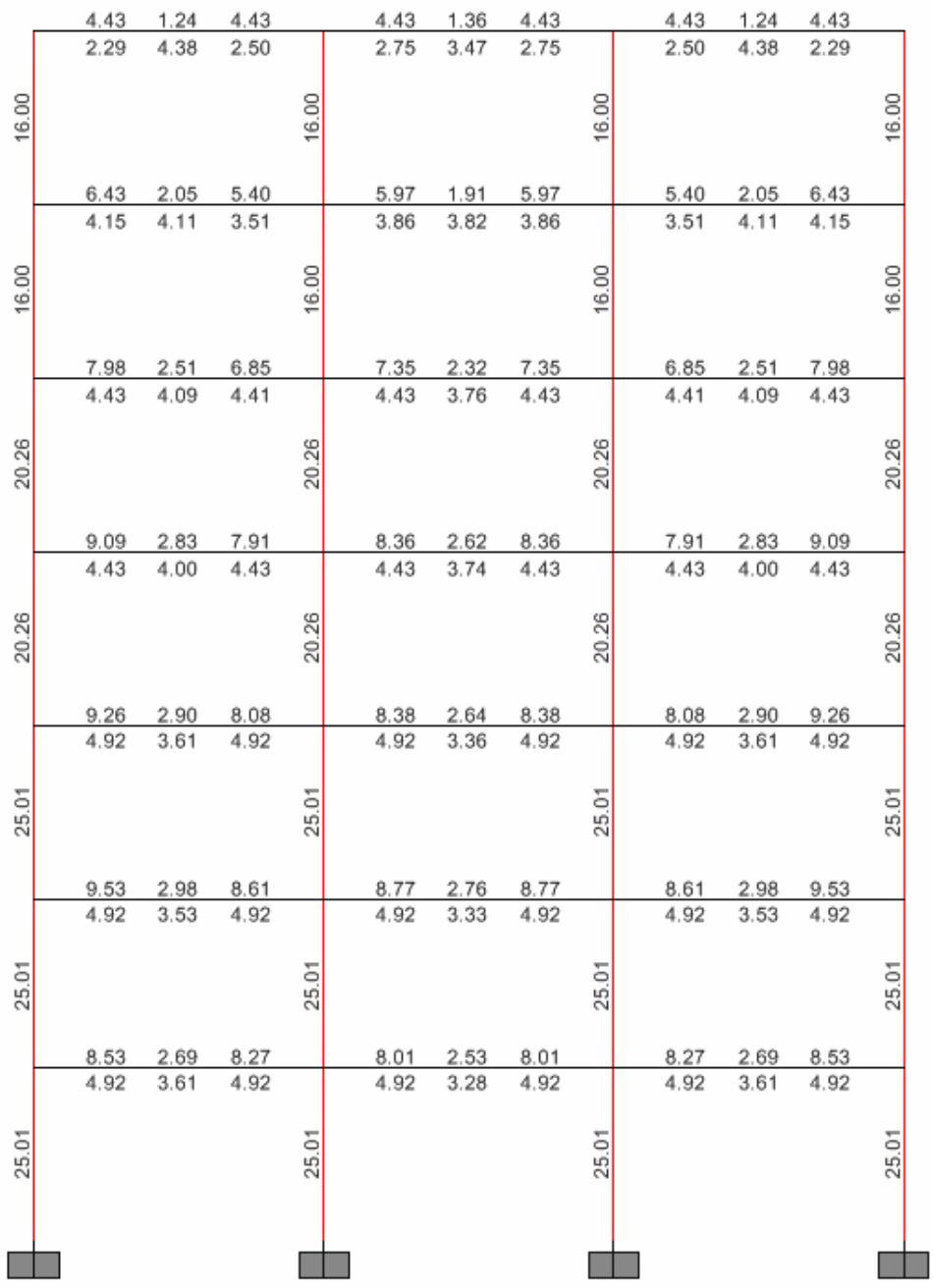

Figure A.16 Reinforcement areas in cm^2 for 7e3

A.15 Model 7e1'

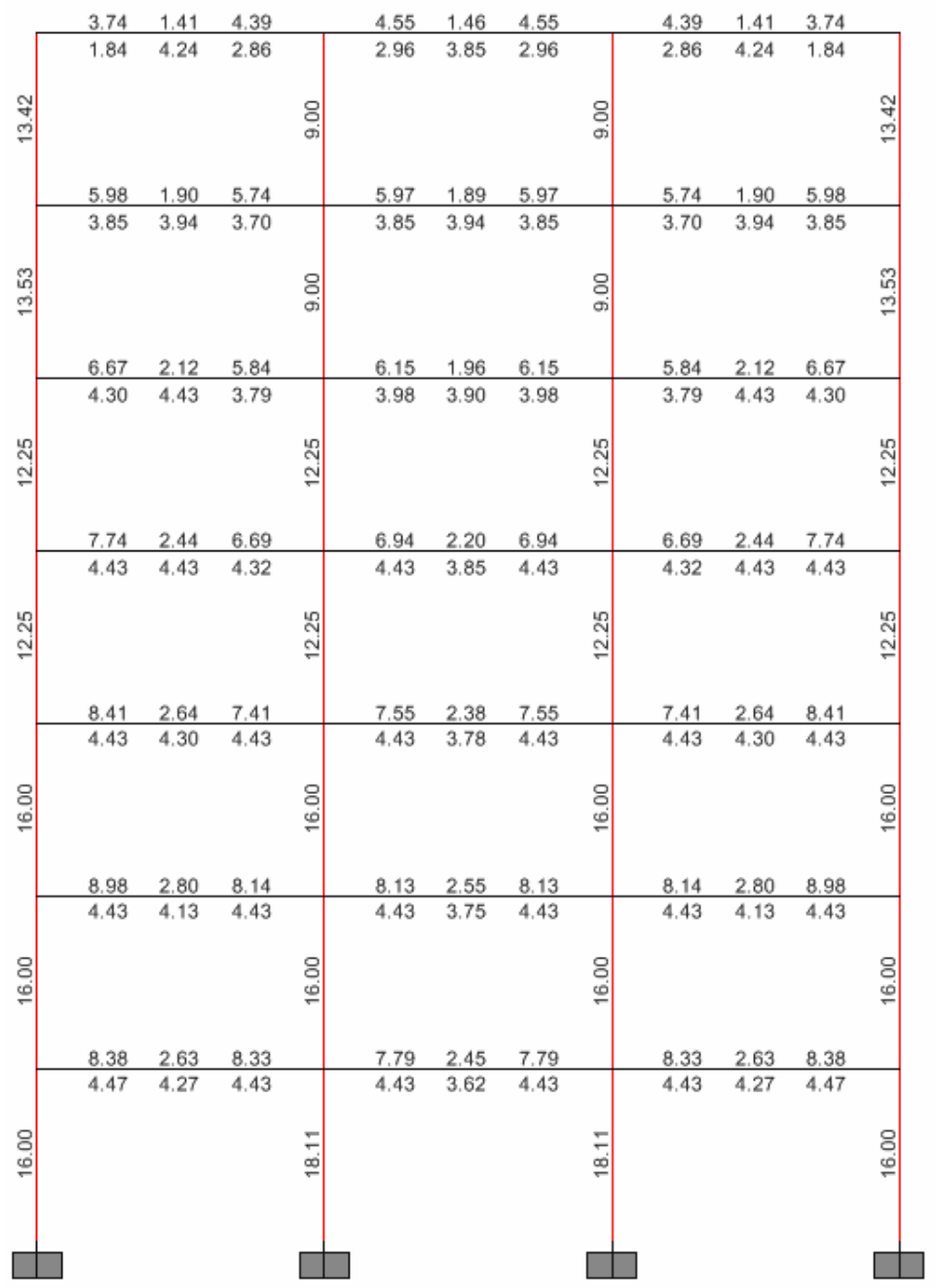

Figure A.17 Reinforcement areas in cm^2 for 7e1'

A.16 Model 7e2'

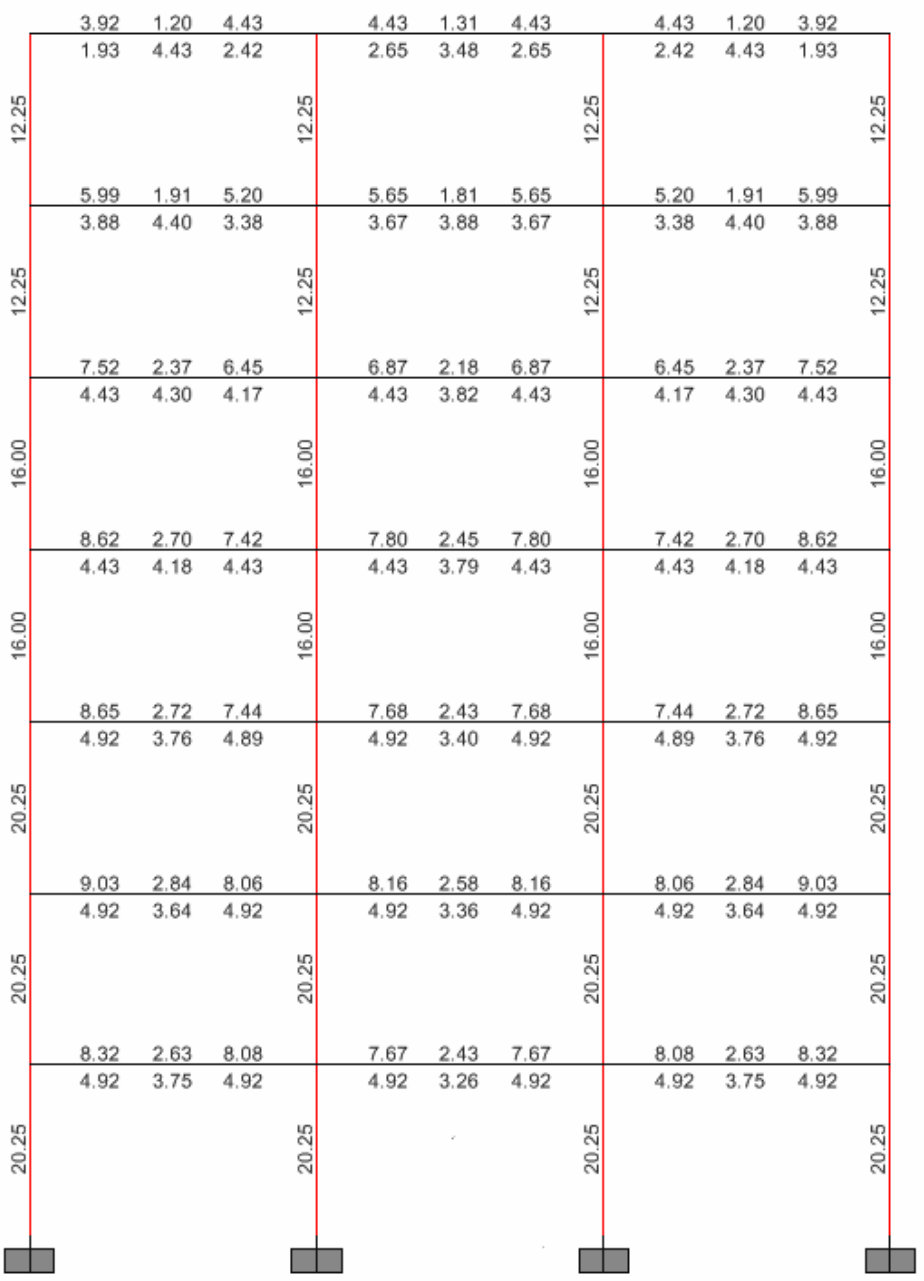

Figure A.18 Reinforcement areas in cm^2 for 7e2'

A.17 Model 9e1

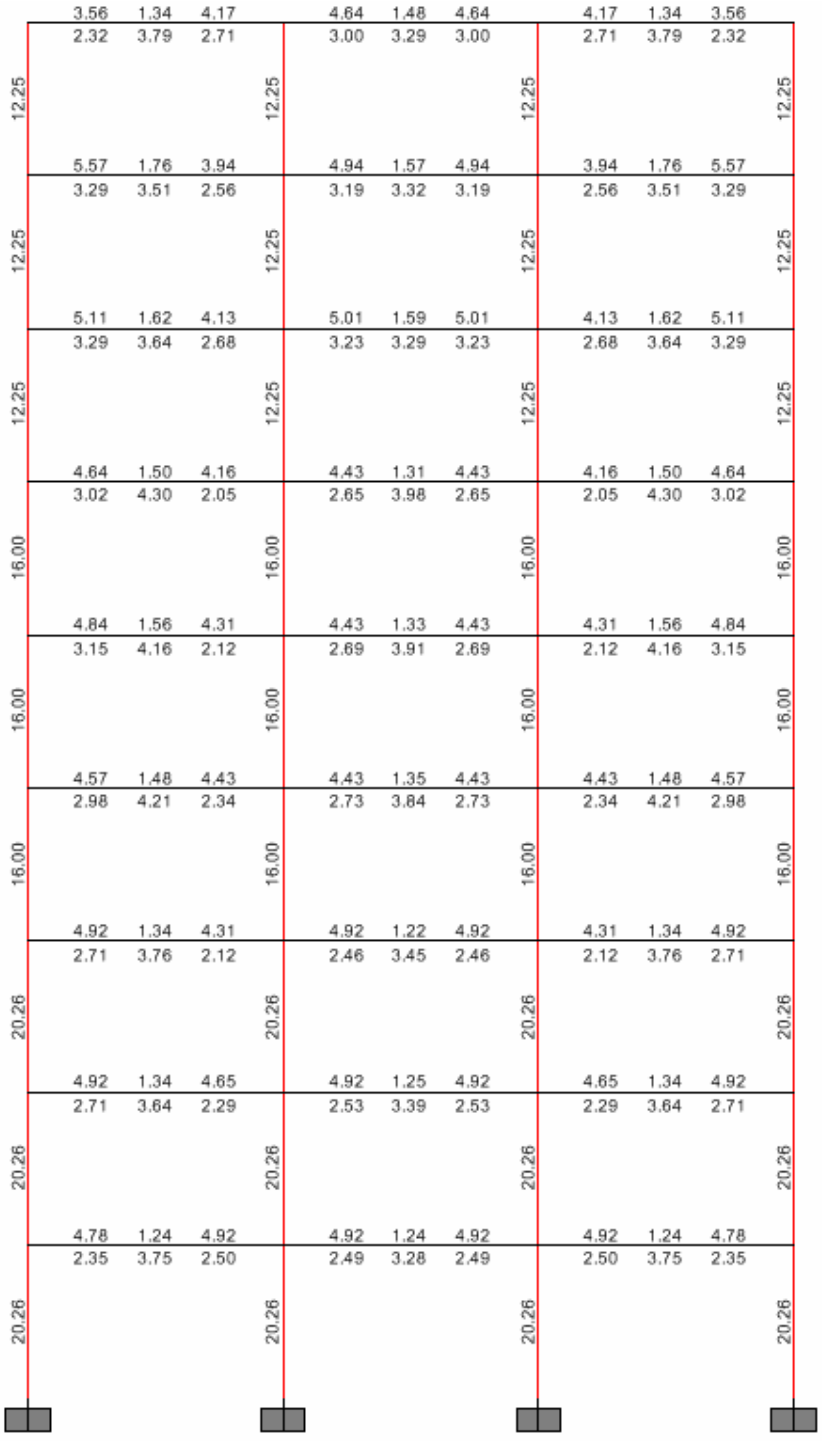

Figure A.19 Reinforcement areas in cm^2 for 9e1

A.18 Model 9e2

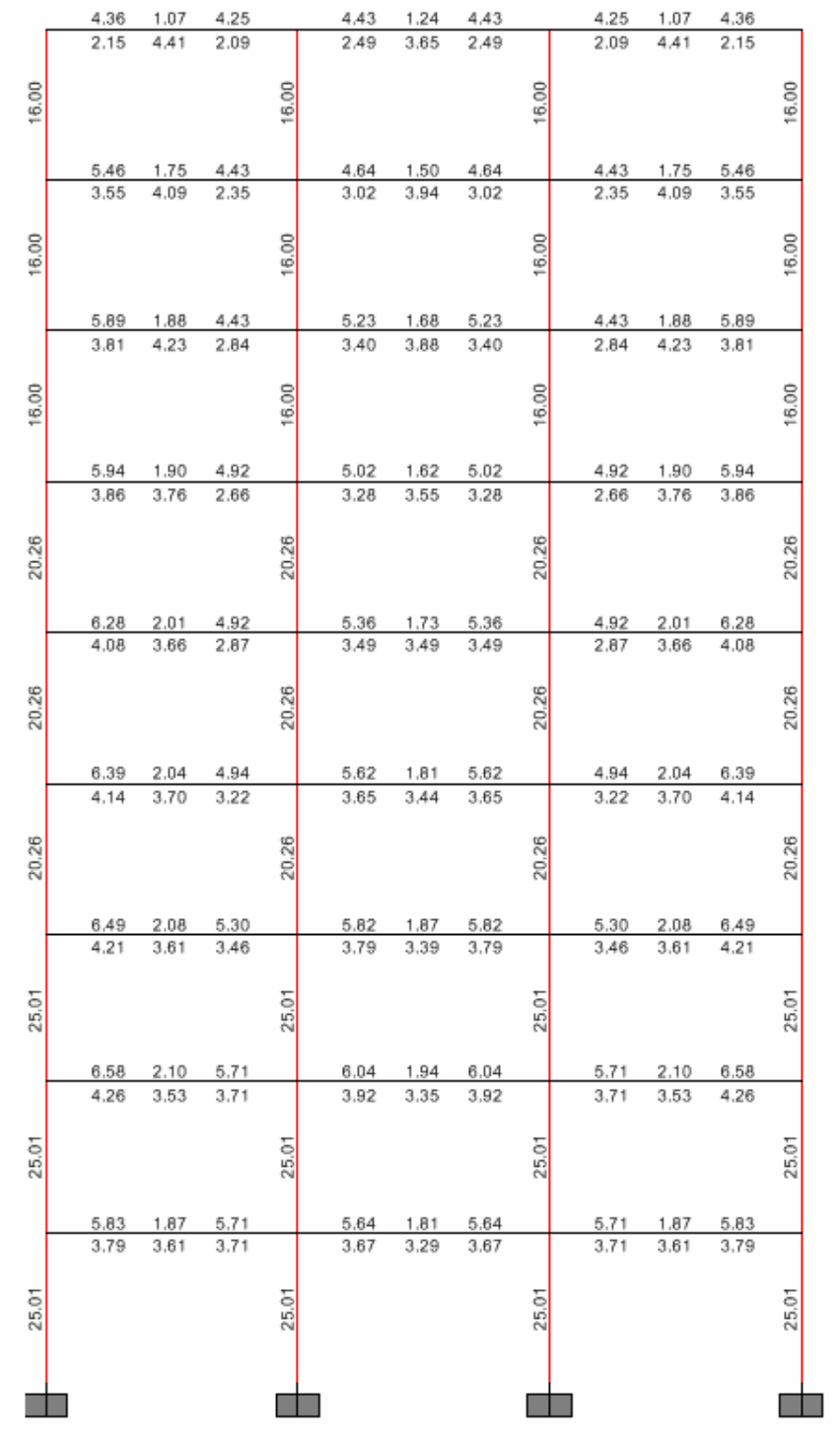

Figure A.20 Reinforcement areas in cm^2 for 9e2

A.19 Model 9e3

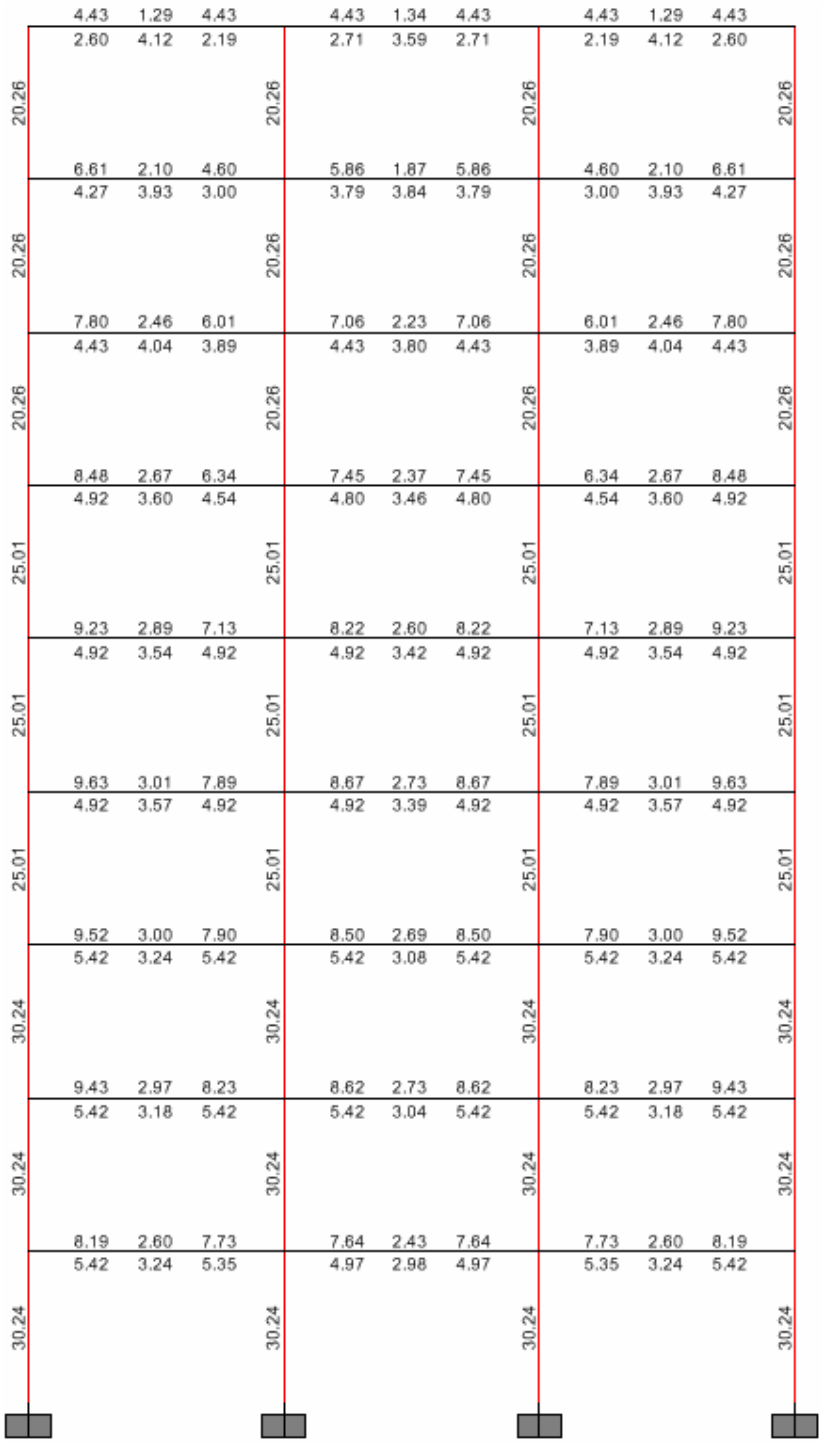

Figure A.21 Reinforcement areas in cm^2 for 9e3

A.20 Model 9e1'

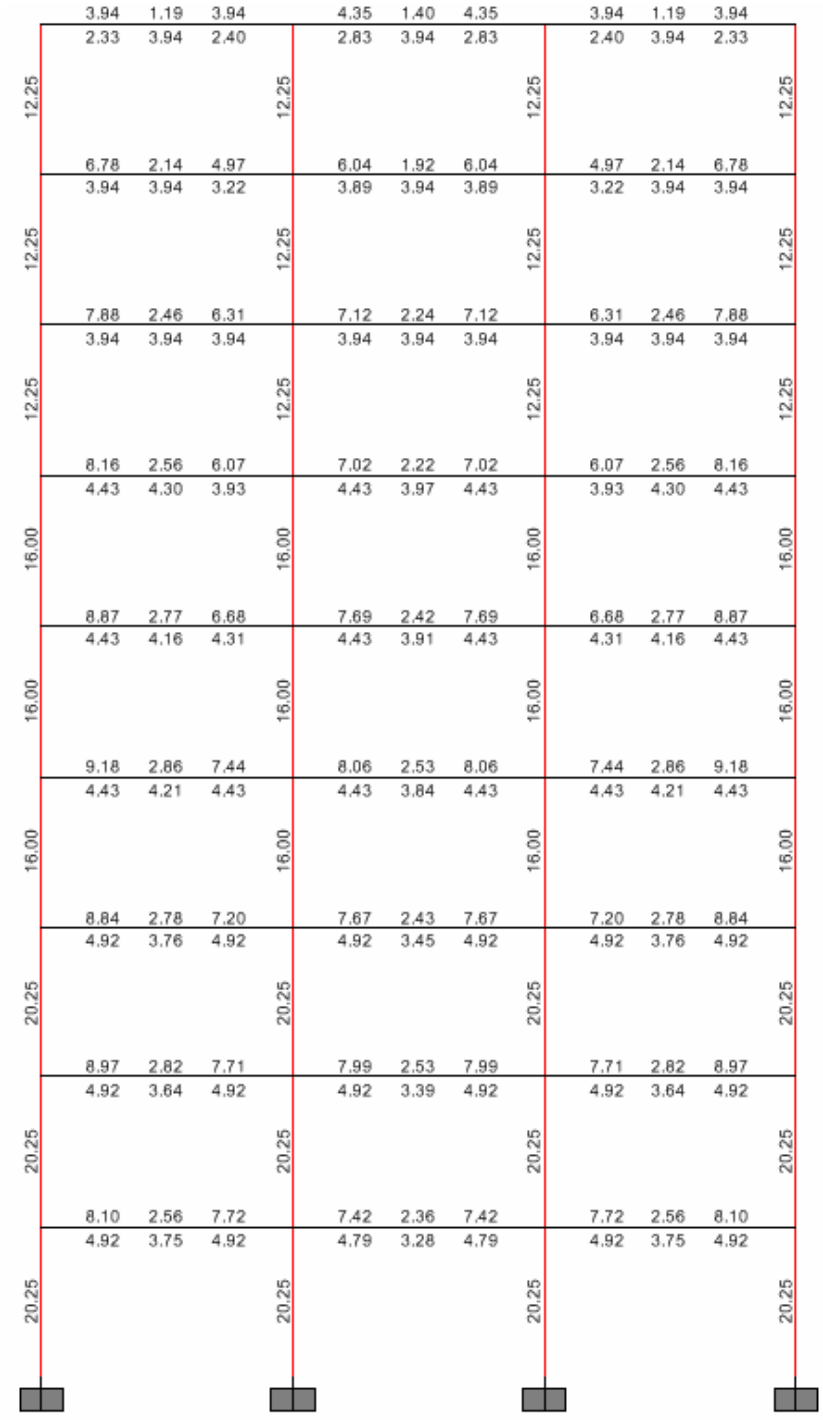

Figure A.22 Reinforcement areas in cm^2 for 9e1'

A.21 Model 9e2'

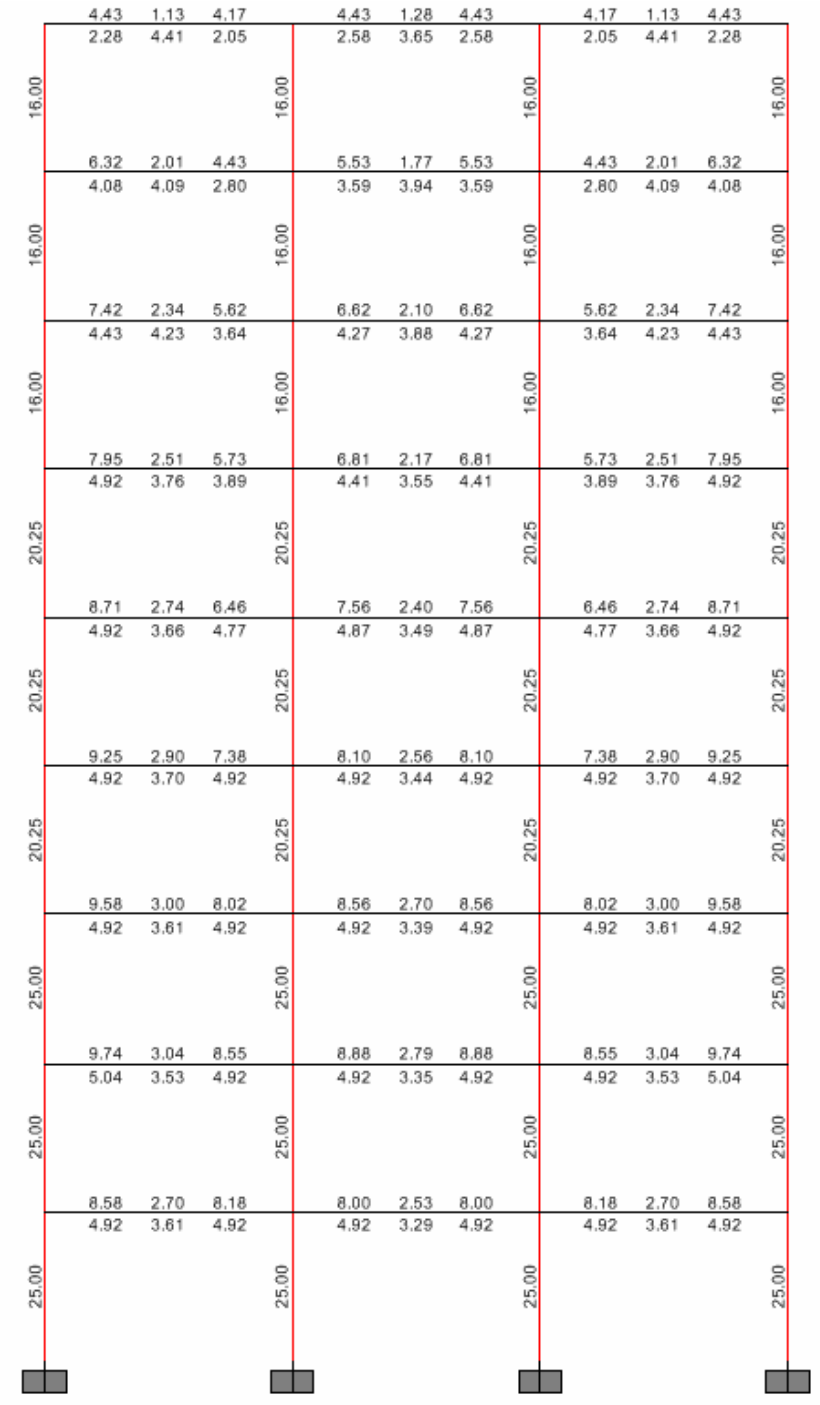

Figure A.23 Reinforcement areas in cm^2 for 9e2'

APPENDIX B

RELEVANT TABLES AND FIGURES OF CHAPTER 2

B.1 Dynamic properties of the models

Table B.1 Dynamic properties of e1, e2, e3, e1' and e2' models

Story	Mode	e1 models				e2 models				e3 models			
Σ mass		T(s)	Γ	Φ	% weight	T(s)	Γ	Φ	% weight	T(s)	Γ	Φ	% weight
3	1	0.733	0.820	1.517	89.062	0.586	0.816	1.537	88.029	0.412	0.805	1.578	85.805
(133t)	2	0.235	0.263	-1.231	9.135	0.182	0.272	-1.228	9.811	0.122	0.291	-1.215	11.222
	3	0.141	0.117	0.676	1.802	0.104	0.128	0.636	2.160	0.063	0.150	0.555	2.973
5	1	1.043	1.029	1.268	82.959	0.787	1.031	1.261	83.134	0.698	1.025	1.267	82.310
(224t)	2	0.357	0.373	-1.177	10.877	0.264	0.370	-1.177	10.720	0.226	0.371	-1.196	10.770
	3	0.197	0.212	0.976	3.528	0.145	0.216	0.964	3.645	0.121	0.228	0.946	4.069
	4	0.142	0.150	-0.563	1.759	0.102	0.145	-0.593	1.656	0.080	0.157	-0.565	1.924
	5	0.099	0.106	0.106	0.877	0.073	0.104	0.133	0.845	0.056	0.109	0.156	0.928
7	1	1.152	1.194	1.139	79.307	0.958	1.189	1.129	78.642	0.872	1.189	1.123	78.530
(315t)	2	0.425	0.455	-1.167	11.481	0.340	0.474	-1.079	12.464	0.300	0.469	-1.082	12.204
	3	0.245	0.287	0.905	4.577	0.193	-0.273	-0.960	4.148	0.167	-0.275	-0.980	4.209
	4	0.166	0.170	-0.813	1.602	0.128	-0.184	0.824	1.883	0.108	-0.200	0.780	2.222
	5	0.128	0.168	0.356	1.576	0.098	0.161	0.463	1.437	0.079	0.160	0.488	1.418
	6	0.097	0.126	-0.096	0.880	0.075	0.124	-0.141	0.855	0.059	0.120	-0.184	0.806
	7	0.072	0.102	0.009	0.578	0.054	0.101	0.015	0.571	0.044	0.105	0.025	0.611
9	1	1.296	1.330	1.033	76.192	1.121	1.354	0.987	78.944	0.989	1.336	1.011	76.931
(407t)	2	0.478	0.544	-1.029	12.741	0.391	0.503	-1.010	10.903	0.347	0.532	-1.014	12.173
	3	0.274	0.348	0.859	5.223	0.221	0.320	0.885	4.414	0.197	0.333	0.904	4.778
	4	0.186	0.212	-0.868	1.936	0.148	0.217	-0.857	2.027	0.129	0.223	-0.844	2.146
	5	0.136	-0.183	-0.622	1.450	0.109	-0.181	-0.654	1.414	0.092	0.189	0.636	1.532
	6	0.106	-0.136	0.483	0.796	0.082	-0.142	0.503	0.862	0.069	0.150	-0.465	0.968
	7	0.088	-0.139	-0.186	0.834	0.068	0.120	0.277	0.618	0.056	0.122	0.260	0.636
	8	0.070	-0.096	0.043	0.399	0.054	0.099	-0.064	0.422	0.044	0.099	-0.073	0.425
	9	0.055	0.100		0.429	0.043	0.096		0.395	0.035	0.097		0.409

Story	Mode	e1'				e2'			
Σ mass		T(s)	Γ	Φ	% weight	T(s)	Γ	Φ	% weight
3	1	0.674	0.809	1.560	86.658	0.567	0.809	1.556	86.623
(133t)	2	0.220	0.280	-1.236	10.377	0.177	0.283	-1.223	10.568
	3	0.130	0.150	0.559	2.966	0.102	0.146	0.597	2.809
5	1	1.016	1.025	1.275	82.190	0.779	1.029	1.265	82.845
(224t)	2	0.347	0.375	-1.188	10.991	0.262	0.371	-1.178	10.794
	3	0.192	0.219	0.967	3.748	0.144	0.217	0.964	3.693
	4	0.136	0.160	-0.537	2.010	0.101	0.149	-0.583	1.739
	5	0.097	0.116	0.110	1.061	0.072	0.109	0.128	0.929
7	1	1.140	1.195	1.139	79.313	0.951	1.189	1.130	78.625
(315t)	2	0.421	0.455	-1.168	11.531	0.339	0.474	-1.081	12.496
	3	0.243	0.286	0.908	4.559	0.193	-0.273	-0.959	4.150
	4	0.165	0.171	-0.804	1.621	0.128	-0.184	0.824	1.872
	5	0.126	0.167	0.361	1.550	0.098	0.161	0.460	1.439
	6	0.097	0.124	-0.102	0.855	0.075	0.124	-0.140	0.852
	7	0.071	0.101	0.010	0.570	0.054	0.101	0.014	0.567
9	1	1.283	1.330	1.034	76.168	1.113	1.353	0.988	78.912
(407t)	2	0.474	0.545	-1.031	12.786	0.389	0.504	-1.011	10.944
	3	0.272	0.348	0.861	5.229	0.220	0.320	0.886	4.419
	4	0.185	0.212	-0.867	1.932	0.148	0.217	-0.857	2.022
	5	0.135	-0.183	-0.619	1.442	0.108	-0.181	-0.652	1.411
	6	0.106	-0.135	0.480	0.787	0.082	-0.141	0.502	0.858
	7	0.088	-0.139	-0.182	0.838	0.068	0.120	0.275	0.619
	8	0.070	-0.096	0.042	0.395	0.054	0.099	-0.064	0.420
	9	0.054	0.099		0.425	0.043	0.096		0.394

B.2 Pushover curves and ADRS of the models

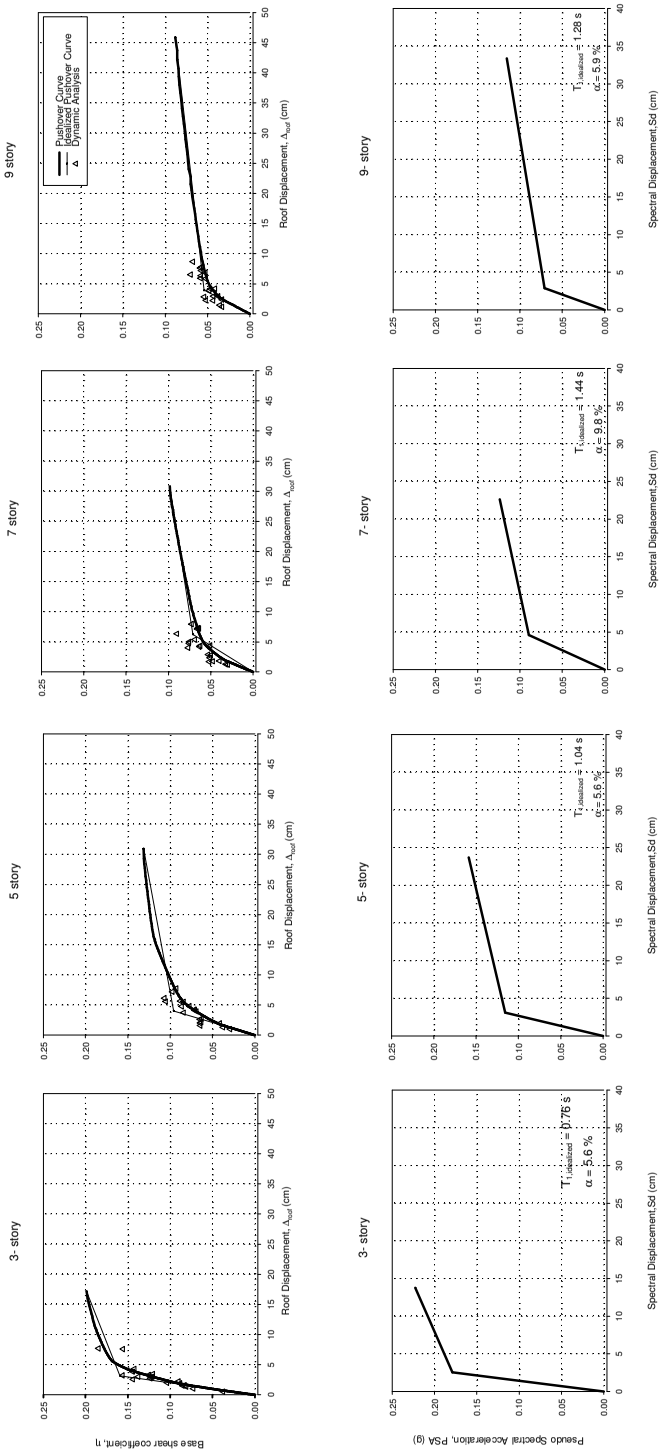

Figure B.1 Pushover curves and ADRS of e1 models for non degrading case

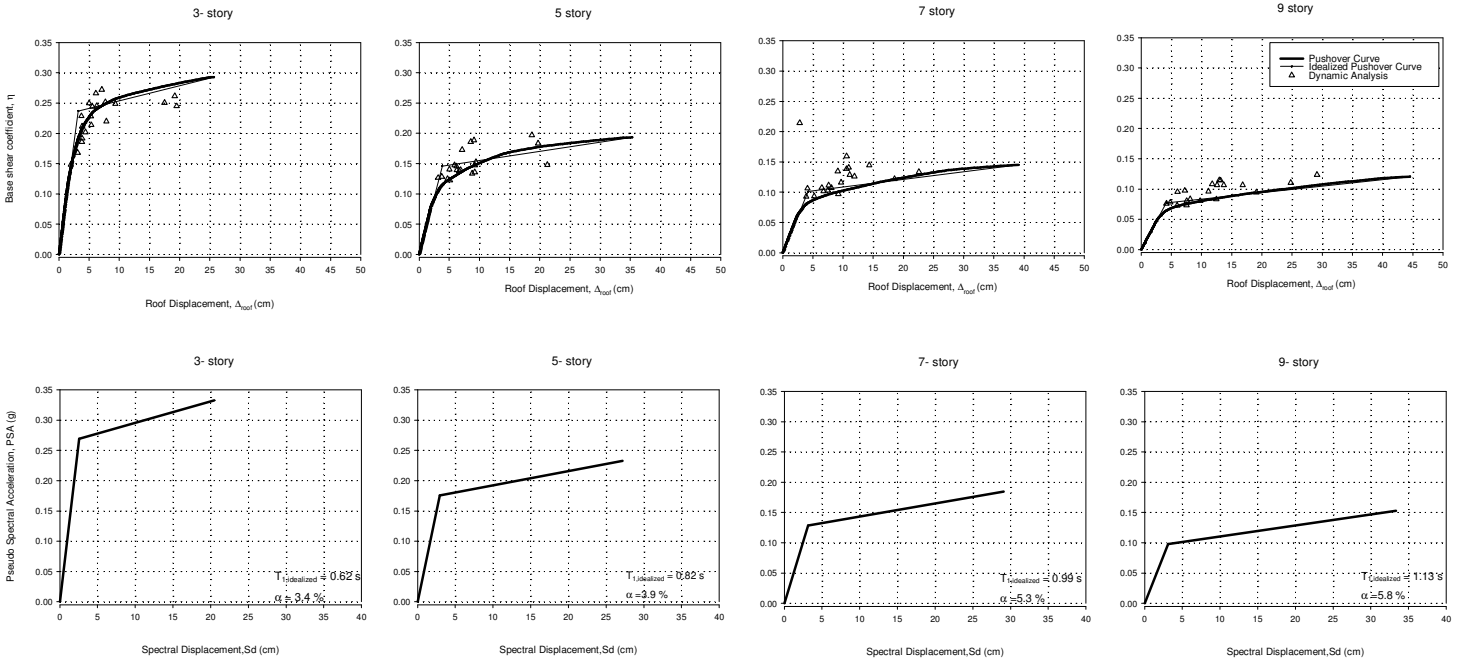

Figure B.2 Pushover curves and ADRS of e2 models for non degrading case

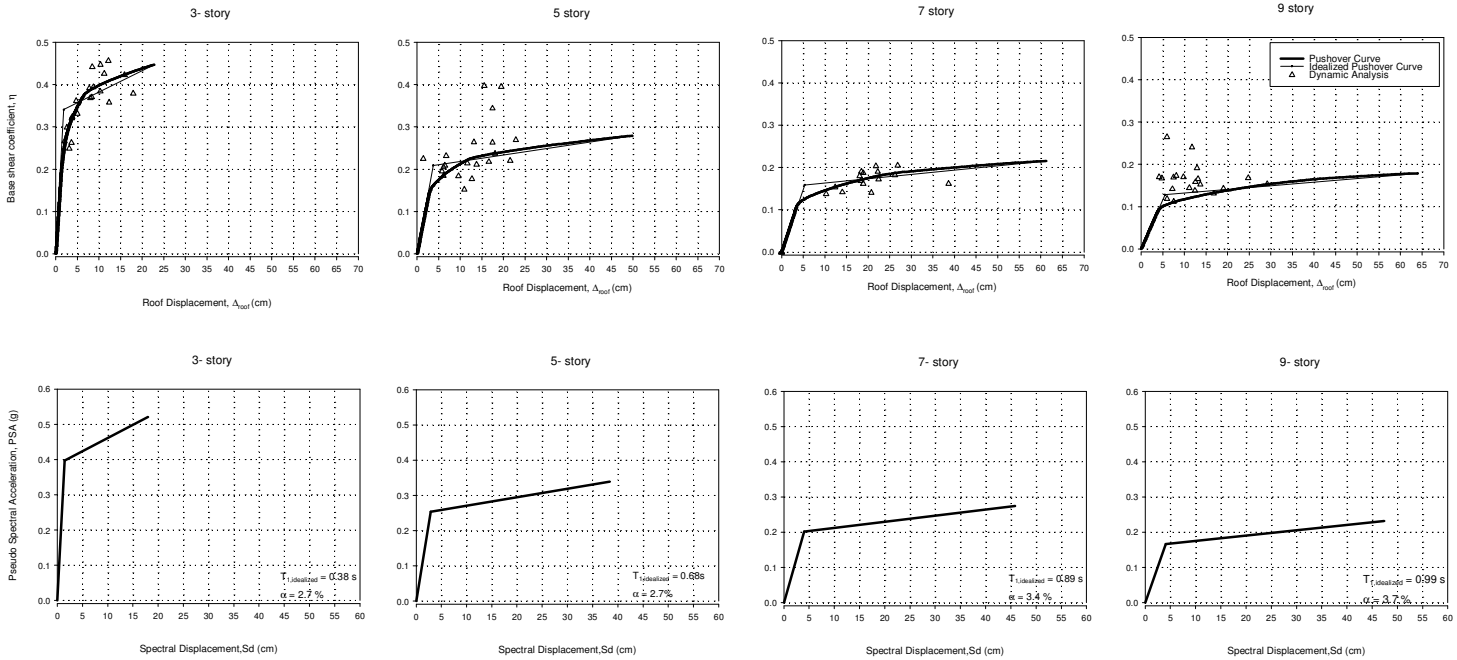

Figure B.3 Pushover curves and ADRS of e3 models for non degrading case

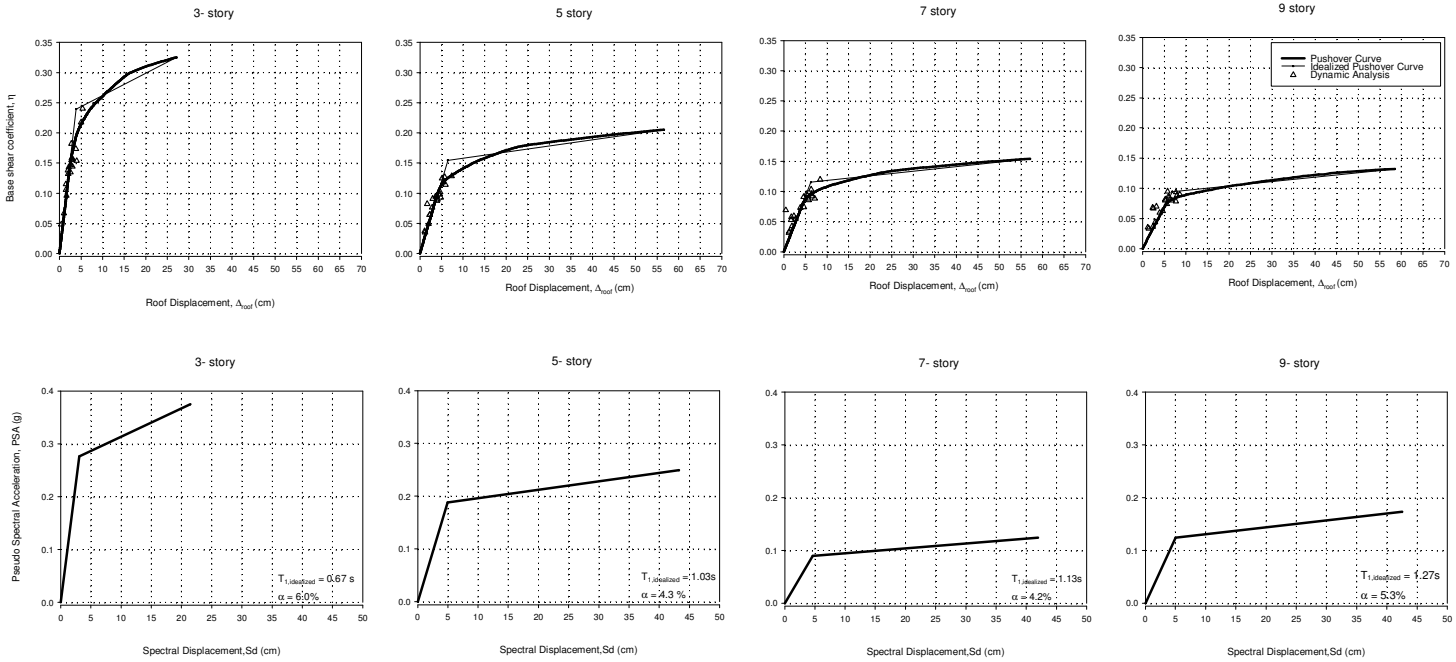

Figure B.4 Pushover curves and ADRS of e1' models for non degrading case

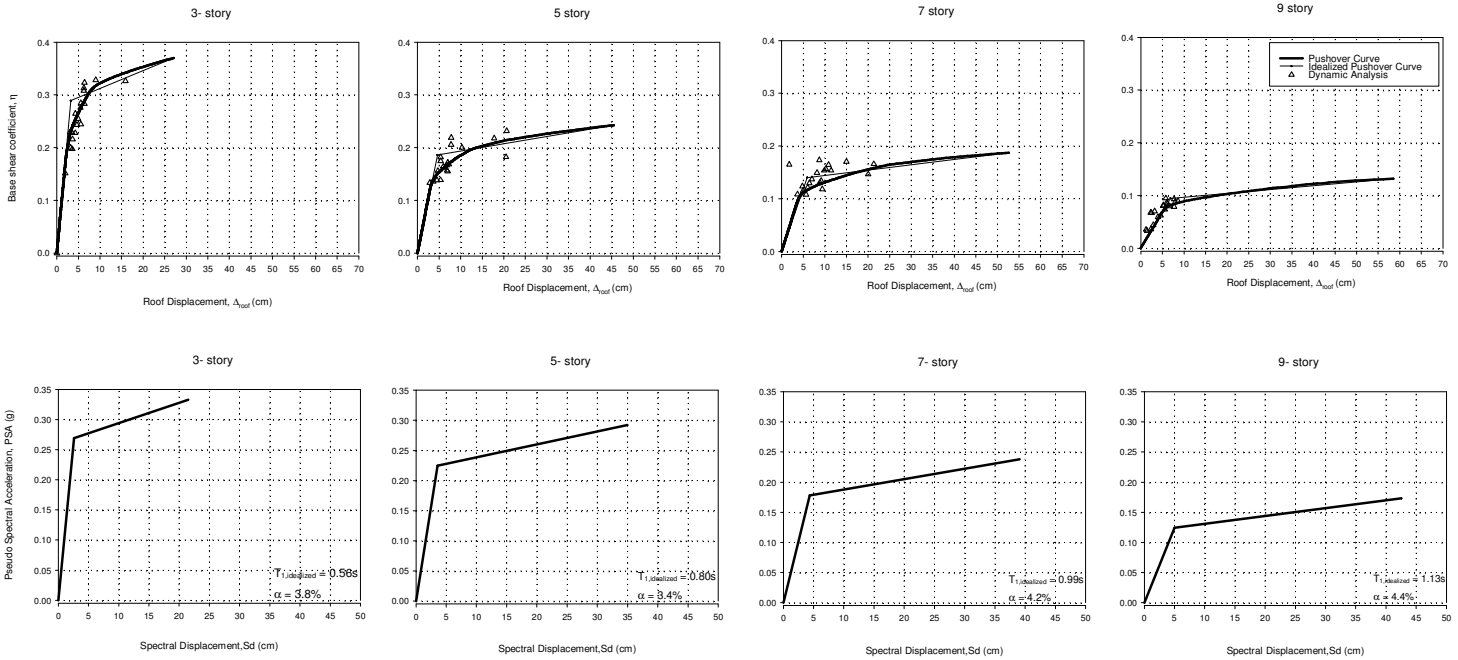

Figure B.5 Pushover curves and ADRS of e2' models for non degrading case

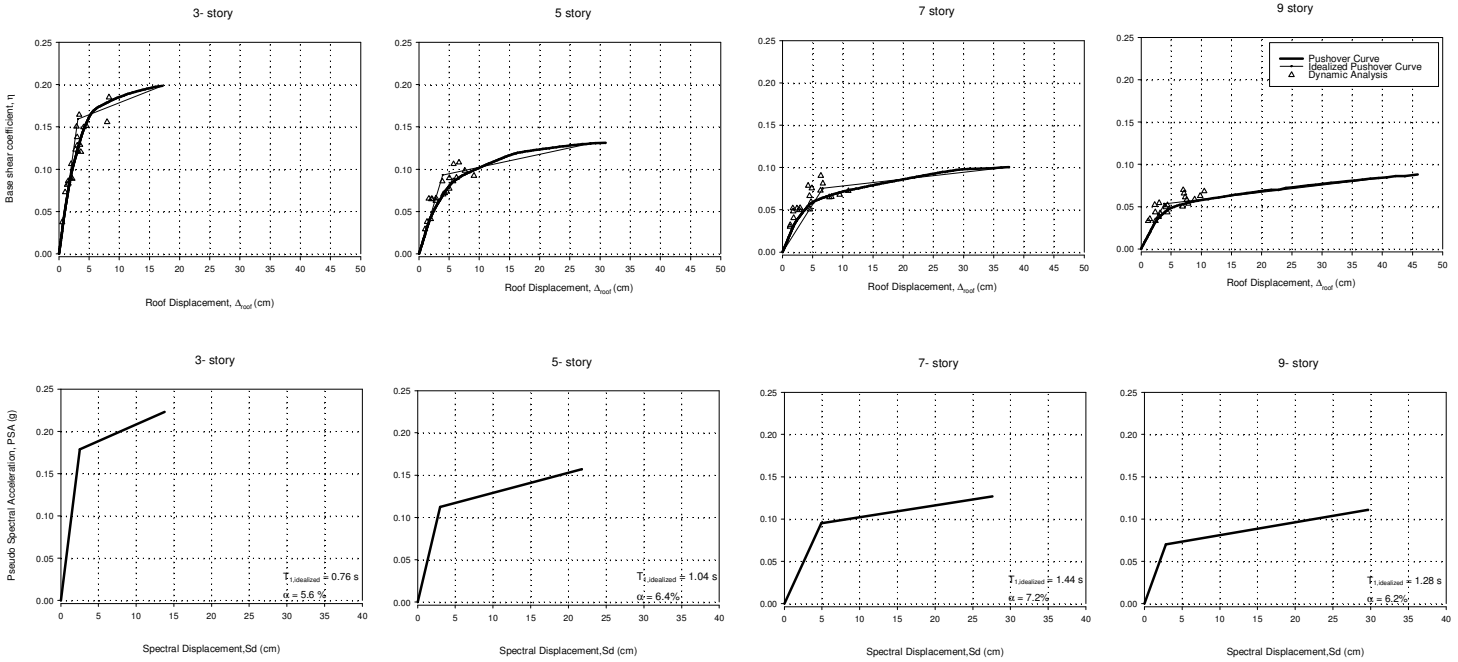

Figure B.6 Pushover curves and ADRS of e1 models for stiffness degrading case

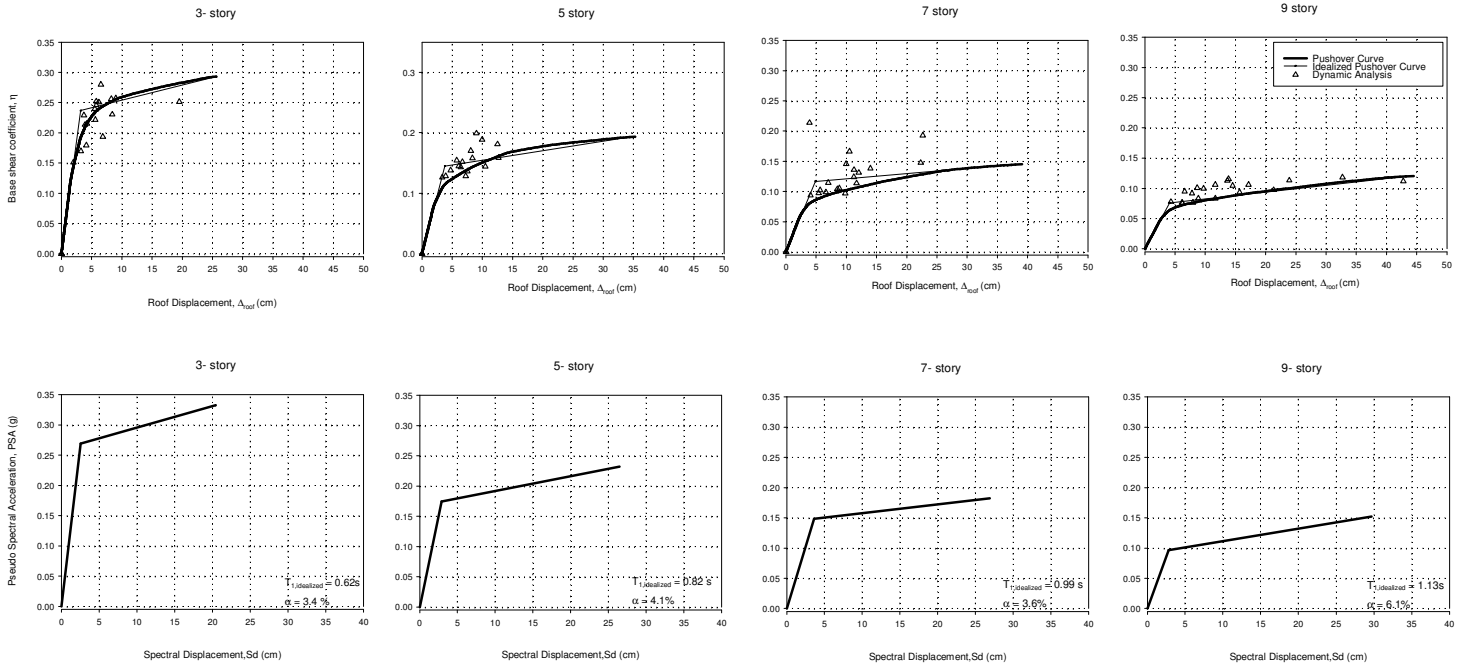

Figure B.7 Pushover curves and ADRS of e2 models for stiffness degrading case

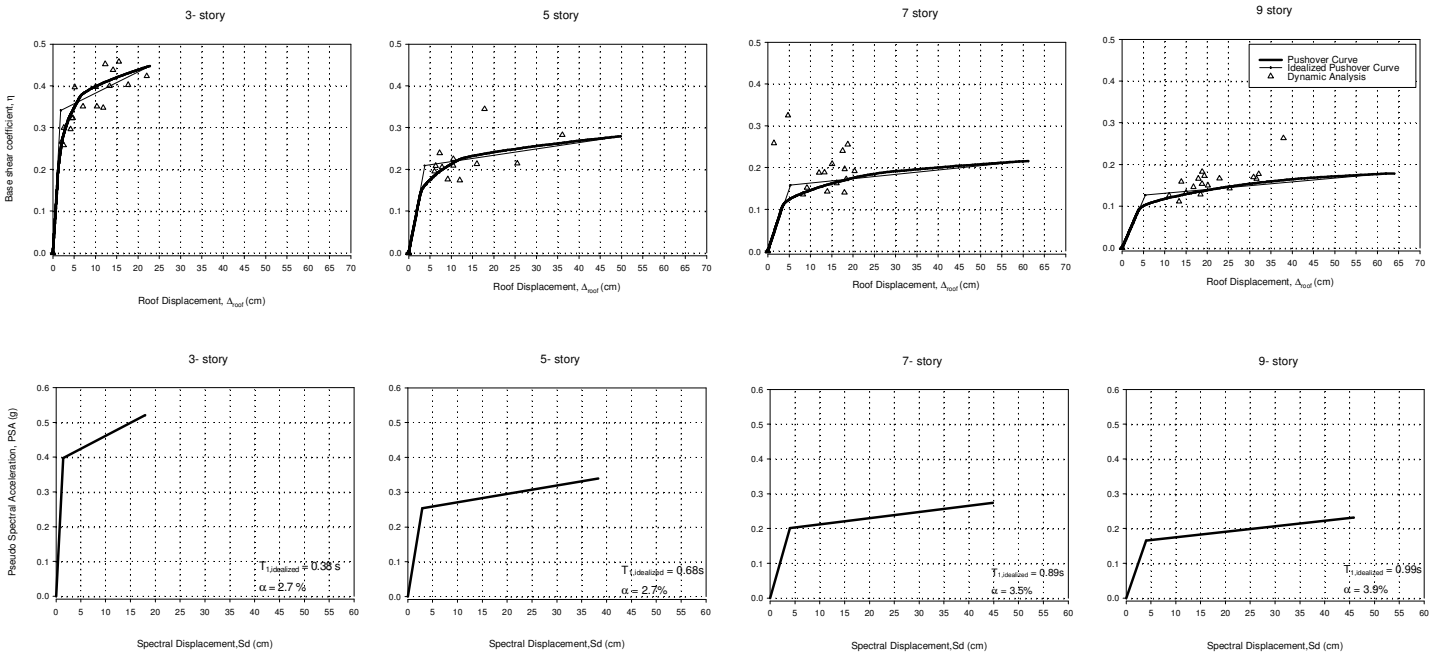

Figure B.8 Pushover curves and ADRS of e3 models for stiffness degrading case

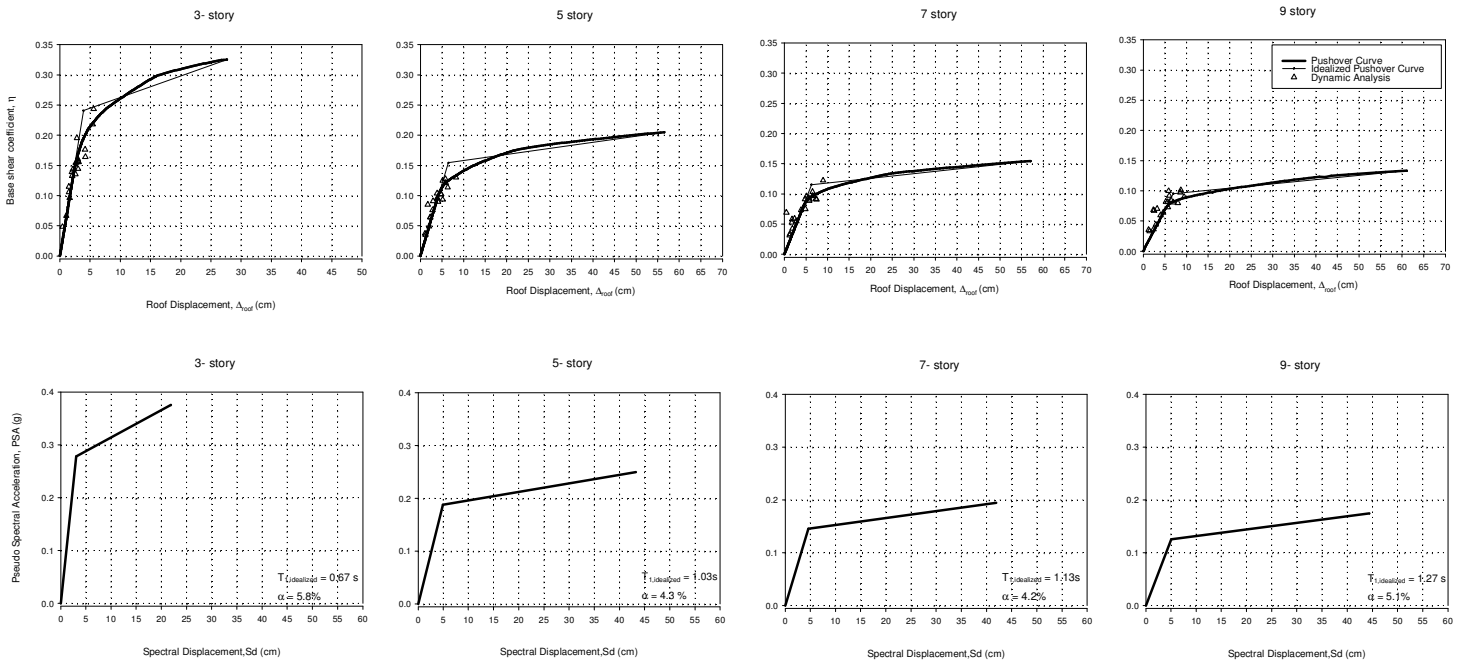

Figure B.9 Pushover curves and ADRS of e1' models for stiffness degrading case

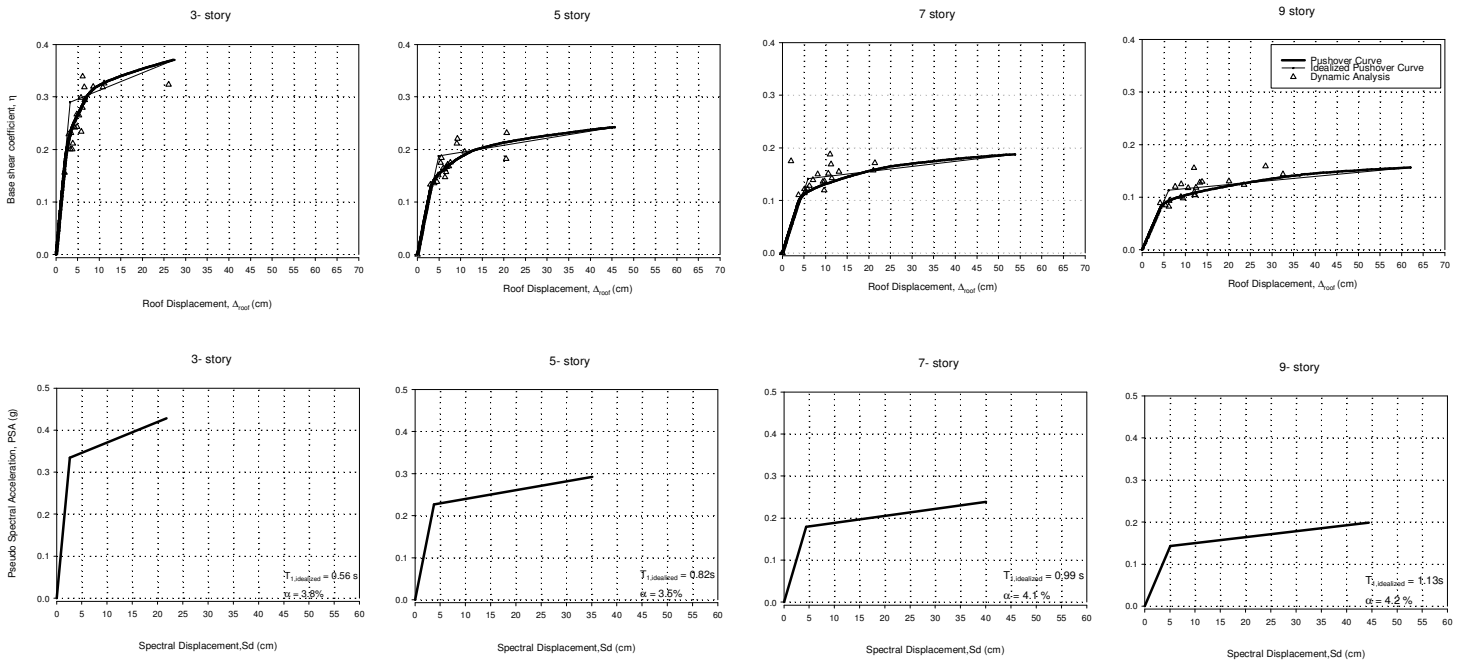

Figure B.10 Pushover curves and ADRS of e2' models for stiffness degrading case

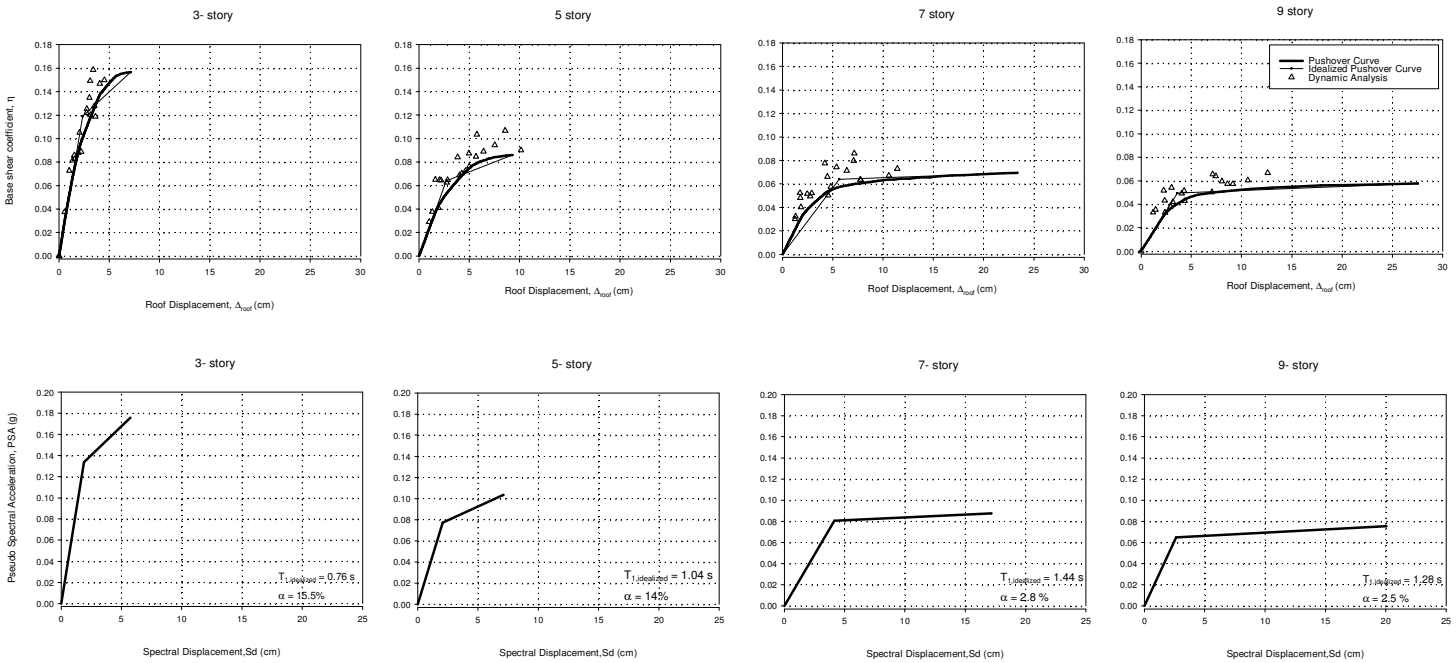

Figure B.11 Pushover curves and ADRS of e1 models for stiffness and strength degrading case

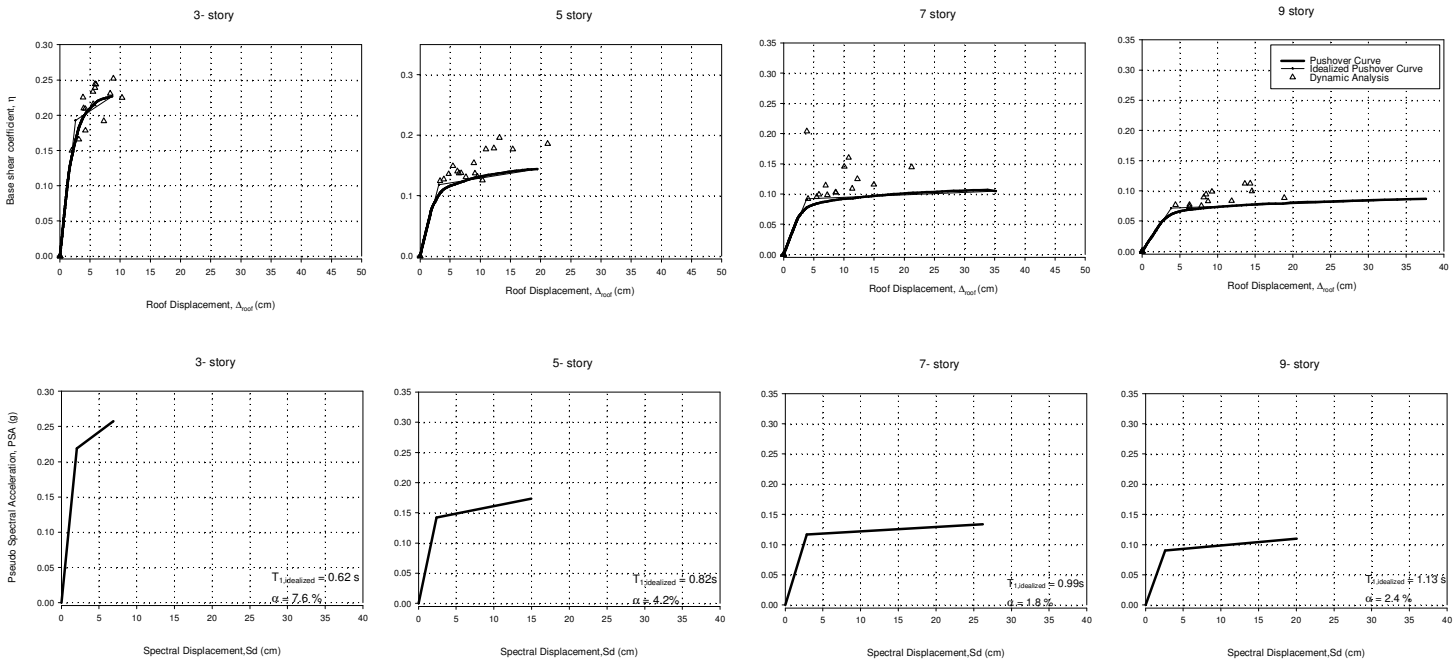

Figure B.12 Pushover curves and ADRS of e2 models for stiffness and strength degrading case

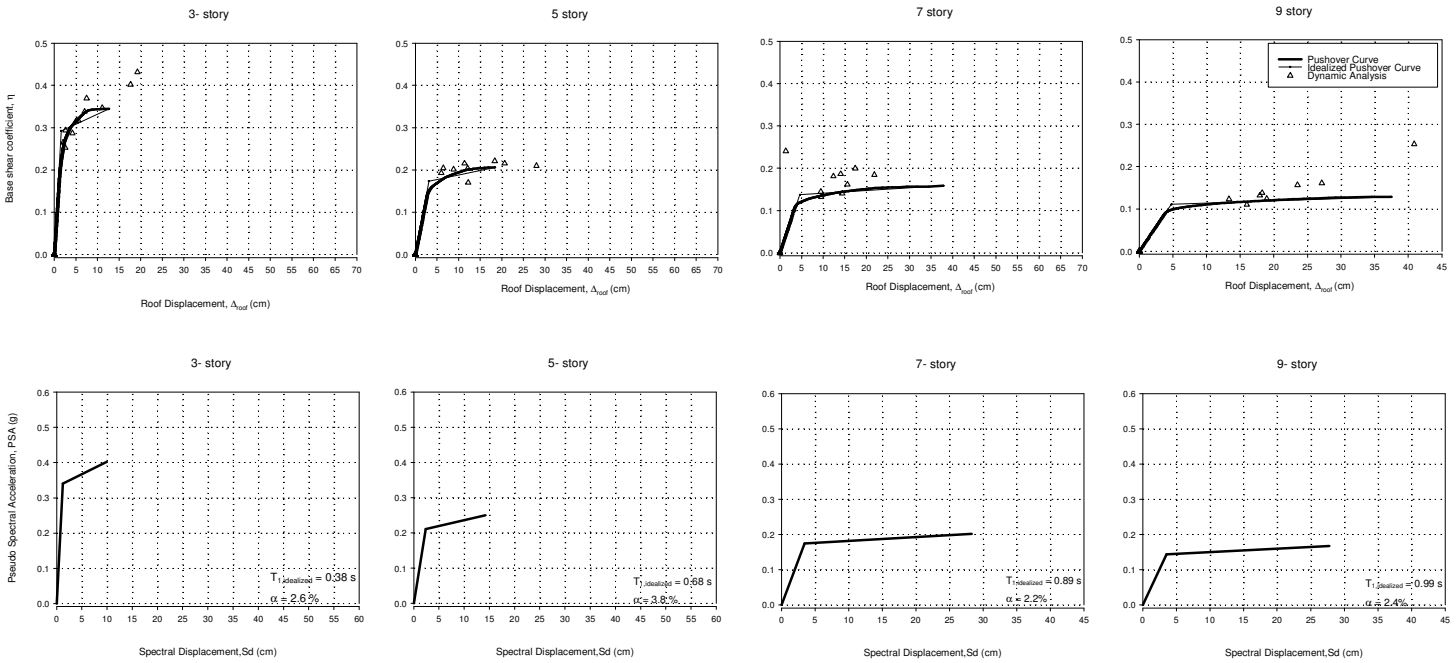

Figure B.13 Pushover curves and ADRS of e3 models for stiffness and strength degrading case

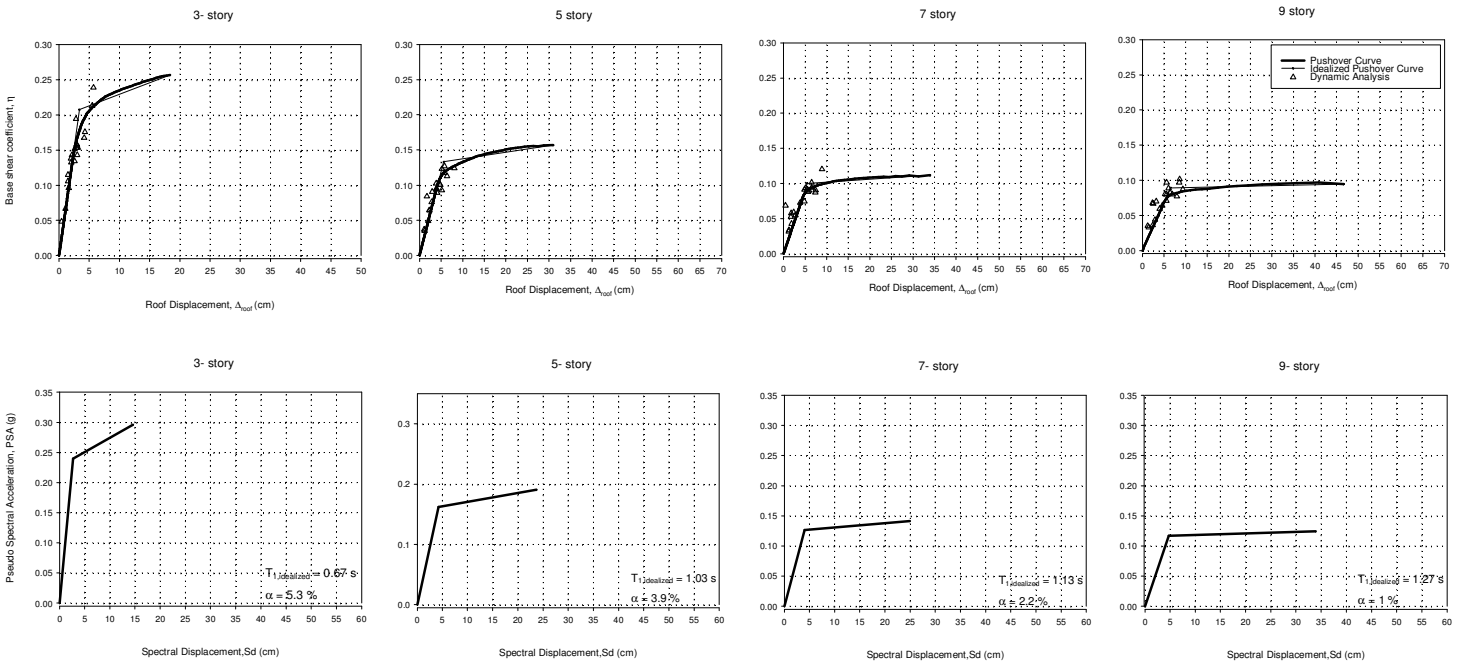

Figure B.14 Pushover curves and ADRS of e1' models for stiffness and strength degrading case

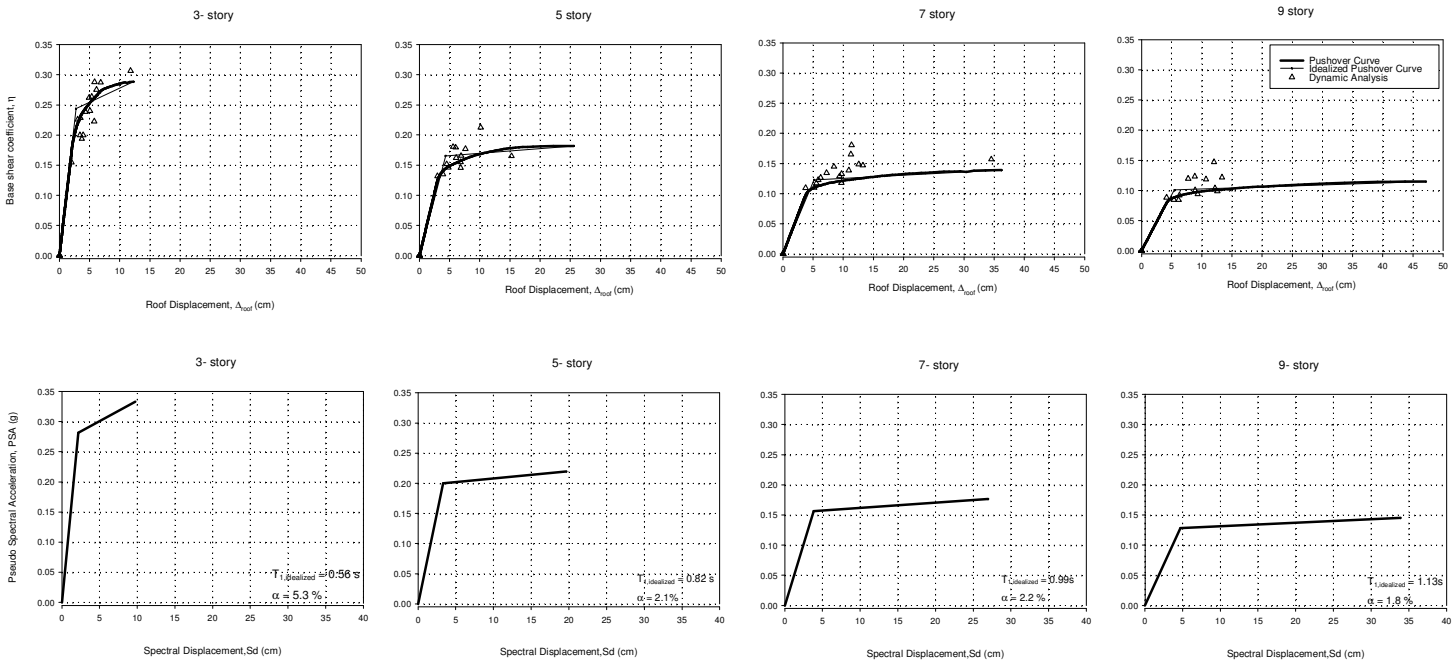

Figure B.15 Pushover curves and ADRS of e2' models for stiffness and strength degrading case

Table B.2 Idealized pushover curve parameters

Number of Story	Model	GM Used	Structural Behavior	Yield Base Shear Coefficient (V/W)	Yield Roof Displacement (cm)	Ultimate Base Shear Coef. (V/W)	Maximum Roof Displacement (cm)
3	e1	Bin 1	ND	0.159	3.153	0.199	17.124
			SD	0.159	3.152	0.199	17.124
			SSD	0.119	2.355	0.157	7.143
	e2	Bin 2	ND	0.237	3.197	0.293	25.672
			SD	0.237	3.196	0.293	25.628
			SSD	0.193	2.599	0.227	8.673
	e3	Bin 3	ND	0.341	1.841	0.447	22.782
			SD	0.341	1.840	0.447	22.764
			SSD	0.292	1.578	0.345	12.653
	e1'	Bin 1	ND	0.239	3.875	0.325	27.117
			SD	0.241	3.900	0.326	27.648
			SSD	0.208	3.362	0.257	18.361
	e2'	Bin 2	ND	0.289	3.251	0.370	27.086
			SD	0.290	3.259	0.370	27.387
			SSD	0.244	2.739	0.288	12.278
5	e1	Bin 1	ND	0.096	4.022	0.132	30.915
			SD	0.093	3.909	0.131	28.426
			SSD	0.064	2.690	0.086	9.272
	e2	Bin 2	ND	0.146	3.831	0.193	35.329
			SD	0.145	3.804	0.193	34.418
			SSD	0.118	3.102	0.144	19.426
	e3	Bin 3	ND	0.209	3.762	0.279	49.806
			SD	0.209	3.762	0.279	49.778
			SSD	0.174	3.123	0.206	18.370
	e1'	Bin 1	ND	0.154	6.481	0.205	56.542
			SD	0.154	6.480	0.205	56.517
			SSD	0.133	5.595	0.157	30.992
	e2'	Bin 2	ND	0.186	4.657	0.242	45.493
			SD	0.188	4.928	0.243	45.613
			SSD	0.165	4.341	0.182	25.568
7	e1	Bin 1	ND	0.071	6.265	0.098	30.748
			SD	0.075	6.653	0.101	37.547
			SSD	0.064	5.639	0.070	23.350
	e2	Bin 2	ND	0.101	4.238	0.145	39.080
			SD	0.117	4.894	0.143	36.102
			SSD	0.092	3.853	0.105	35.203
	e3	Bin 3	ND	0.159	5.330	0.216	61.189
			SD	0.158	5.300	0.215	59.874
			SSD	0.137	4.604	0.158	37.793
	e1'	Bin 1	ND	0.115	6.295	0.154	57.105
			SD	0.115	6.294	0.154	57.073
			SSD	0.100	5.467	0.112	33.958
	e2'	Bin 2	ND	0.140	5.877	0.187	52.588
			SD	0.141	5.914	0.188	53.820
			SSD	0.123	5.155	0.139	36.232
9	e1	Bin 1	ND	0.054	3.944	0.088	45.869
			SD	0.053	3.879	0.085	40.742
			SSD	0.049	3.598	0.058	27.532
	e2	Bin 2	ND	0.077	4.160	0.121	44.535
			SD	0.076	4.105	0.120	43.204
			SSD	0.071	3.850	0.087	37.627
	e3	Bin 3	ND	0.128	5.532	0.179	63.979
			SD	0.127	5.475	0.178	61.957
			SSD	0.111	4.773	0.129	37.467
	e1'	Bin 1	ND	0.094	6.883	0.132	58.509
			SD	0.095	6.945	0.133	61.028
			SSD	0.089	6.502	0.095	46.625
	e2'	Bin 2	ND	0.112	6.052	0.156	60.548
			SD	0.113	6.092	0.157	62.041
			SSD	0.101	5.450	0.115	47.143

APPENDIX C

PREDICTION EQUATIONS FOR GROUND MOTION AND ELASTIC SPECTRAL DISPLACEMENT

C.1 Prediction Equation for ground motion (Akkar and Bommer, 2007)

The prediction equation is derived by using the strong-motion database for seismically active areas of Europe and the Middle East only for *PGV*. The explanatory variables in the equation are magnitude, Joyner-Boore distance, site class and style-of-faulting. The functional form is provided in equation C.1.

$$\log(PGV_{xx}) = b_1 + b_2 M + b_3 M^2 + (b_4 + b_5 M)\log(\sqrt{R_{jb}^2 + b_6^2}) + b_7 S_s + b_8 S_A + b_9 F_N + b_{10} F_N \quad \text{(C.1)}$$

where M is magnitude; S_A and S_S are dummy variables representing the influence of site class, taking values of 1 for stiff and soft soil sites, respectively, and zero otherwise; F_N and F_R are dummy values of 1 for normal and reverse ruptures respectively, and zero otherwise. Subscript xx denotes either GM or max. Regression coefficients from b_1-b_{10} are given in Table C.1.

Table C.1 Regression coefficients of the prediction equation

Eq.	b_1	b_2	b_3	b_4	b_5	b_6	b_7	b_8	b_9	b_{10}
GM	-1.36	1.063	-0.079	-2.948	0.306	5.547	0.243	0.087	-0.057	0.0245
MAX	-1.26	1.103	-0.085	-3.103	0.327	5.504	0.226	0.079	-0.083	0.0116

C.2 Prediction Equation for ground motion (Boore and Atkinson, 2007)

This study covers the Ground-motion prediction equations for the average horizontal component of *PGA*, *PGV* and 5% damped *PSA* at spectral periods between 0.01s and 10s. They were derived by using strong-motion database compiled by the "PEER NGA" (Pasific Earthquake Engineering Research Center's Next Generation Attenuation Project). The equation has the following functional form :

$$\ln Y = F_M(\mathbf{M}) + F_D(R_{JB}, \mathbf{M}) + F_S(V_{S30}, R_{JB}, \mathbf{M}) + \varepsilon\sigma_T$$

Where F_M, F_D and F_S represent magnitude scaling, distance function and site amplification, respectively.

Magnitude scaling

(a) M≤M_h

$$F_M(\mathbf{M}) = e_1 U + e_2 SS + e_3 NS + e_4 RS + e_5(\mathbf{M} - \mathbf{M}_h) + e_6(\mathbf{M} - \mathbf{M}_h)^2$$

(b) M> M_h

$$F_M(\mathbf{M}) = e_1 U + e_2 SS + e_3 NS + e_4 RS + e_7(\mathbf{M} - \mathbf{M}_h)$$

Where *U*, *SS*, *NS* and *RS* are dummy variables used to denote unspecified, strike-slip, normal-slip and reverse-slip fault type respectively. M_h is the hinge magnitude for the shape of the magnitude scaling.

Distance function

$$F_D(R_{JB}, \mathbf{M}) = [c_1 + c_2(\mathbf{M} - \mathbf{M}_{ref})]\ln(R / R_{ref}) + c_3(R - R_{ref})$$

$$R = \sqrt{R_{JB}^{\ 2} + h^2}$$

R_{ref}=1.0 km

Site amplification function

$$F_S = F_{LIN} + F_{NL}$$

Linear term

$$F_{LIN} = b_{lin} \ln(V_{S30} / V_{ref})$$

Nonlinear term

a) $pga4nl \le a_1$:

$$F_{NL} = b_{nl} \ln(pga\_low / 0.1)$$

b) $a_1 < pga4nl \le a_2$:

$$F_{NL} = b_{nl} \ln(pga\_low / 0.1) + c[\ln(pga4nl / a_1)]^2 + d[\ln(pga4nl / a_1)]^3$$

c) $a_2 < pga4nl$:

$$F_{NL} = b_{nl} \ln(pga4nl / 0.1)$$

$$c = (3\Delta y - b_{nl}\Delta x) / \Delta x^2$$

$$d = -(2\Delta y - b_{nl}\Delta x) / \Delta x^3$$

$$\Delta x = \ln(a_2 / a_1) \qquad \Delta y = b_{nl} \ln(a_2 / pga\_low)$$

The details of the prediction equations can be seen in the related article Boore and Atkinson (2007).

C.3 Prediction Equation for spectral displacement (Akkar and Bommer, 2007b)

This empirical equation for the prediction of displacement response ordinates is derived using the strong motion databank from Europe and the Middle East. The functional form selected for the the equation is the same as that used by Akkar and Bommer (2007a) for the prediction of *PGV*.

$$\log[SD(T,\xi)] = b_1 + b_2 M + b_3 M^2 + (b_4 + b_5 M)\log\sqrt{R_{jb}^2 + b_6^2} + b_7 S_S + b_8 S_A + b_9 F_N + b_{10} F_R$$

Where M is moment magnitude, R_{jb} is the Joyner-Boore distance in kilometers, S_s and S_A are binary variables taking values 1 for soft and stiff soil sites, respectively (and zero otherwise) and F_N and F_R are similarly derived for normal and reverse faulting earthquakes.

Regression coefficients are provided for different period and damping values in the related article.